PLANT-POLLINATOR AERODYNAMICS

A Dissertation
Presented to
The Academic Faculty

By

Megan Matthews

In Partial Fulfillment
of the Requirements for the Degree
Doctor of Philosophy in the
School of Physics
Physics of Living Systems

Georgia Institute of Technology

December 2021

PLANT-POLLINATOR AERODYNAMICS

Thesis committee:

Dr. Simon Sponberg
Department of Physics
Georgia Institute of Technology

Dr. David Hu
Department of Mechanical Engineering
Georgia Institute of Technology

Dr. Michael Schatz
Department of Physics
Georgia Institute of Technology

Dr. Karen Mulleners
School of Engineering (STI)
Ecole polytechnique federale de Lausanne (EPFL)

Dr. Flavio Fenton
Department of Physics
Georgia Institute of Technology

Date approved: August 26, 2021

ACKNOWLEDGMENTS

TABLE OF CONTENTS

LIST OF FIGURES

SUMMARY

Interactions between plants and pollinators have adapted over long evolutionary timescales and fill a vital ecological role. For flying pollinators, the same coherent aerodynamic mechanisms are employed across the broad Reynolds number range of $10^2 - 10^4$. This thesis aims to understand some of the physics involved in plant-pollinator aerodynamics.

The main contributions of this work are: (1) natural environments for pollinators have steady, unsteady, and turbulent features and (2) external flow environments directly influence aerodynamic force through fluid-structure interactions. As expected, natural flow environments are complex, but within the turbulence, irregular periodic structures emerge suggesting pollinators must dynamically adapt to their local environment. Future work is needed to understand how the re-circulation zone and near-turbulence might be beneficial to flowering plants, possibly by assisting in pollen transport.

First, Chapter 2 establishes that the wake of an unsteady flower disrupts pollinator tracking performance, but also reveals the robustness of flower tracking from a dynamical systems perspective. Chapter 3 focuses on the aerodynamic effects of fluid-structure interaction between flexible insect wings and incoming airflow. Last, 2D particle image velocimetry (PIV) is used to capture the size dependent features of hawkmoth-pollinated flower wakes. The features in flower wakes and their consequences for pollinator flight forces are described in Chapter 4.

CHAPTER 1

INTRODUCTION

The intersection of physics and biology is rife with unanswered questions. Inherent complexities of biological systems make them challenging to describe with generalizable models, but carefully constrained questions and experiments help key features emerge from the details. Physics approaches are applied to biological systems at all scales [182, 265, 44, 327], but the ecological context of the system is usually neglected, resulting in an understanding of physics and behavior in a highly unrealistic environment [10]. Organisms not only interact with each other, but behaviors are also mediated by the surrounding environment (Figure 1.1), so it is crucial to explore the local dynamics a system encounters along with the organism itself. In plant-pollinator interactions, animals and plants perform coordinated behaviors to ensure pollen propagation (for the plant) and an energetic reward (for the pollinator). For flying pollinators, this is especially challenging due to the fluctuating air environment they must navigate to locate host plants. The work in this thesis acts as a starting point to understand the physics involved in the ecological interactions of plants and their pollinators. An interdisciplinary study of the unique wing kinematics of small wasps led to the identification of the clap-and-fling mechanism, a then unknown real-world example of 2D inviscid vortex formation [32, 170]. Following a similar philosophy, this thesis studies how well-known aerodynamic mechanisms enable flapping flight in unsteady and biologically-relevant conditions.

Aerodynamics of insect flight

For decades, the high lift achieved by flying insects could not be captured using conventional aerodynamic airfoil theories [176]. Since insect wings are airfoils with sharp leading edges, incoming flow is separated resulting in a bound leading-edge vortex (LEV), simi-
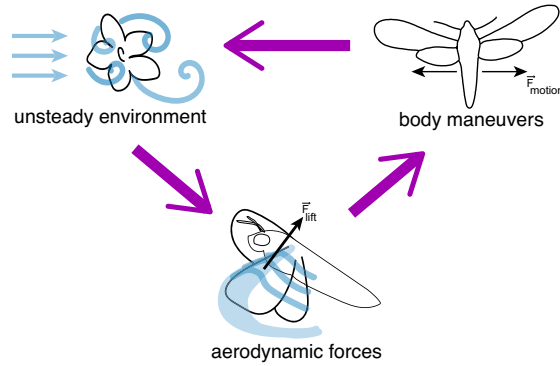
Figure 1.1: Three way interaction between pollinators, plants, and their environment.

lar to that found on delta wings. The inclusion of vortex flow (rotational) effects resolved the lift enhancement for steadily moving delta wings [283], but the build-up of circulation contributing to lift takes time, which is limited during the short wingstrokes used by many insects (flapping frequencies ranging from 25 Hz-400 Hz) [51]. To resolve this, new aerodynamic mechanisms were proposed that attribute rapid circulation build-up to rapid wing rotation and separation at stroke reversal [32, 170]. In larger insects that fly around $Re \sim 10^3$, additional lift enhancement was identified due to the formation of coherent leading edge vortices that remained bound to the wing until stroke reversal, when the initial LEV is shed and a new one is formed [41, 172, 277].

The flapping flight of insects relies on unsteady mechanisms, such as the LEV, to generate lift during the steady periods of the wingstroke. However, use of this mechanism is only possible because of the unsteady aerodynamics and wing motion at each stroke reversal. Despite this knowledge, our ability to control flight at these scales (with engineered systems) is limited and far from the adaptability displayed in biology. This suggests that something fundamental is lacking in our understanding of these unsteady mechanisms and requires systematic exploration of the link between wing motion and aerodynamics.

In potential flow ($\nabla \times v = 0 \implies v = -\nabla\Phi$, where v is the flow velocity), interaction with the leading-edge (LE) of an airfoil results in a suction force component parallel to the airfoil chord [283, 277] (Figure 1.2). For flow to remain attached as it is accelerated

around the leading-edge, pressure forces are induced perpendicular to the flow direction (and parallel to the LE). When the LE is sharp (as described above), flow separates into a spiral vortex sheet which re-attaches to the wing upper surface [283, 277]. Analogous to a rounded leading edge, with finite radius, this generates a suction (pressure) force as a balance to the centrifugal force necessary to accelerate the vortex flow. Since the vortex re-attaches along the upper surface, the resultant force is redirected perpendicular to the wing chord, enhancing lift for angles of attack up to $\alpha = 25°$. Unlike delta wing aircrafts,
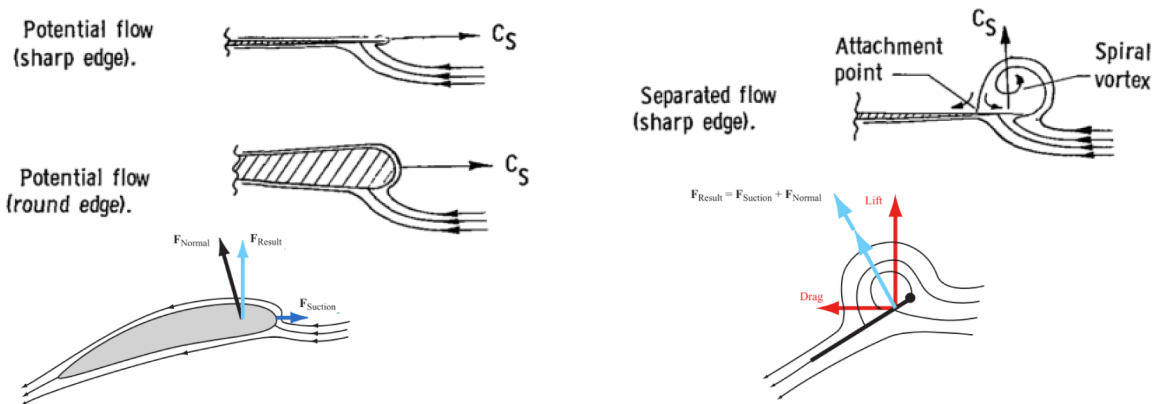
Figure 1.2: Polhamus leading-edge suction analogy. Figure modified from [283] and [277].

flying insects adopt high angles of attack ($\alpha > 25°$), yet they rely on similar aerodynamic mechanisms to hover. Differences between insect and delta wings arise in the length of time necessary for LEV formation and growth (stability). Formation of the leading-edge vortex relies on the build-up of circulation, but many insects are able to generate bound circulation nearly instantaneously during rapid wing rotations at the end of each half-wingstroke [32]. Each 'flip' at the end of the upstroke (pronation) and downstroke (supination), generates an LEV on the upper surface of the wing that remains stable during the steady wing motion in the upstroke and downstroke (Figure 1.2).

The LEV on insect wings was first thought to follow the same delayed stall mechanism as larger delta wings, with spanwise flow through the (conical) vortex core stabilizing growth. This was based on qualitative flow visualization of tethered hawkmoths and a mechanical flapper [172]. However, experiments with a dynamically-scaled *Drosophila*

flapper later showed that disrupting spanwise flow in the LEV had no detectable effect on LEV stability [116]. The differences in LEVs between different species of insects (and across the Reynolds number range $10^2 < Re < 10^4$), can be classified according to flow features and spanwise flow at critical points. Different classes of LEV show that insects use the same mechanism in different ways, with most variation arising due to differences in morphological parameters and kinematics.

For larger insects, like the hawkmoth *Manduca sexta*, the leading-edge vortex (LEV) maintains a constant diameter across the wingspan, continuous from tip to tip, and persists for most of the wingstroke [6].

Although the LEV should grow in size throughout the downstroke, it only continues to increase during the steady portion of the wing motion. At stroke reversal, a 'flip' is performed resetting the bound circulation around each wing. If stroke reversal is reached before the LEV grows large enough to become unstable, then strong spanwise flow is irrelevant. This suggests two non-mutually exclusive hypotheses for vortex stability. (1) Vortex stability is related to LEV size, maintianed through spanwise flow along the wing (from root to tip), either through the LEV core or behind the re-attachment point [172, 116]. (2) Strouhal number restricts the timescale of LEV growth to be stable during the steady up- and downstrokes [160, 6, 200].

$$St_{wing} = \frac{f_{wb}\phi}{U_{wing}} \tag{1.1}$$

where f_{wb} is wingbeat frequency, ϕ is stroke amplitude, and U_{wing} is forward speed, measured at the wing tip.

Even if we assume that the LEV adheres to our current knowledge of vortex dynamics once formed on the wing, how LEV formation depends on other unsteady mechanisms during the wingstroke is still unknown. Insects use various aerodynamic mechanisms that are explicitly linked to wingstroke kinematics during the unsteady portions of each wingstroke

[200] (Figure 1.3). When the wing starts from rest and at each stroke reversal the fluid surrounding the wing is accelerating, inducing added mass effects (increased pressure acting on the wing surface). Wing rotations during pronation and supination are also responsible for generating circulation in the air around the wing. Depending upon when the wing 'flip' occurs relative to stroke reversal, this circulation can either enhance or reduce lift. If insects were only concerned with hovering, they could tune wing rotation to always maximize lift and increase flight efficiency. However, survival in nature requires many behaviors, so maximizing lift may not always be beneficial.
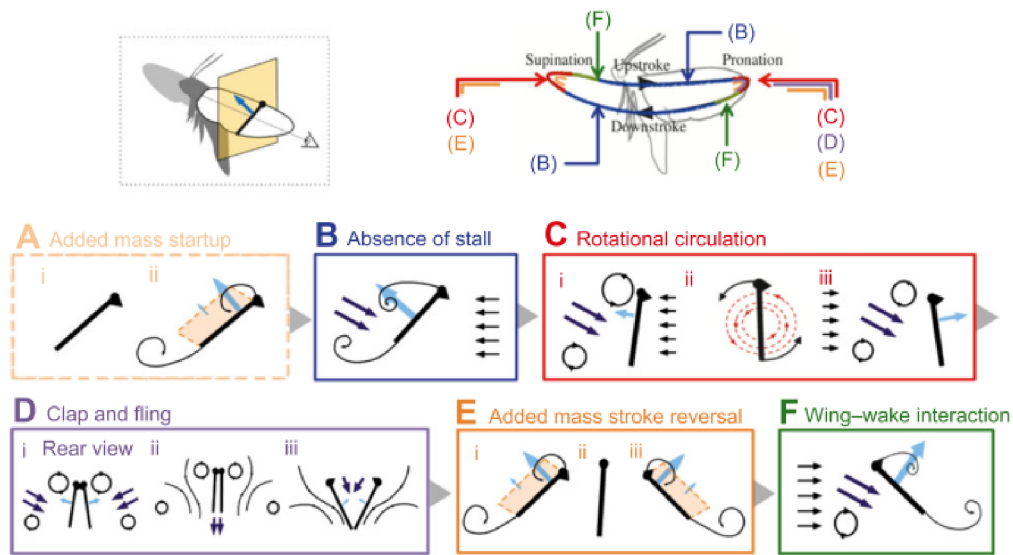
Figure 1.3: Aerodynamic mechanisms throughout the wingstroke. Figure reproduced from [200].

The leading edge vortex (LEV) is established as the dominant high-lift generating mechanism is insect flight. We know that wing kinematics change during maneuvers and in response to unsteady flow, but is the combined effect sufficient to change the aerodynamics? Alternatively, animals may choose to shift their behavior in a way that maintains stable aerodynamic mechanisms. However, this introduces a conflict between maneuvering and hovering performance, the dual roles of the wing system.

Over the past two decades, a consensus has emerged that LEVs are necessary structures for small flapping systems to stay aloft [172], but the LEVs of insects have only been visu-

alized in steady flow [6]. In nature and lab settings [6, 179, 14, 137] hawkmoths (*Manduca sexta*) feed from flowers while hovering in unsteady, windy environments. Although studies of insect flight in steady flow emphasize the necessity of LEVs, it is still unknown how these structures interact with unsteady environments as well as how this affects the flight dynamics of the animal. In an unsteady wake, flow separation at the leading edge of the wing will be multidirectional, which may inhibit the ability of each wing to generate bound vortices of opposing circulation [170].

Biology of flight in unsteady environments

Effects of unsteady flow on aerodynamic mechanisms and behavior [202, 191, 298] have been explored separately, but the combined study of how both change in response to unsteady flow interactions has received less attention. Understanding how animals maintian stability in unsteady environments requires coupled investigation of interactions between environmental and aerodynamic flow structures and the subsequent impact on a complex behavior.

It remains an open question whether shifts in body dynamics due to a turbulent environment are consequences of limitations on flight control or increased power costs and reduced lift production. Numerical simulations of bumblebees in turbulence revealed that the roll axis was most sensitive to perturbations, resulting in casting motions [230]. Despite these changes in body dynamics, the structure and average lift force of the LEV was approximately the same in laminar and turbulent conditions. However, maintenance of lift while maneuvering results in increased aerodynamic costs due to compensation for re-direction of the force vector [63]. Theoretical estimates, flapper experiments, and numerical simulations confirmed these costs arise after a roll maneuver which tilts the force vector. This re-direction reduces the lift force which is often corrected by altering wing kinematics. An increase in wingbeat frequency and/or stroke amplitude acts to increase force production.

Bumblebees are known to forage in wind conditions that can be replicated in wind

6

tunnel experiments (Figure 1.4 [126]). For median wind speeds and turbulence intensity of 1 m/s and 0.28, respectively, bees compensated with small changes to wingbeat frequency and stroke amplitude, including increased asymmetry between left and right wingstroke amplitude [126].
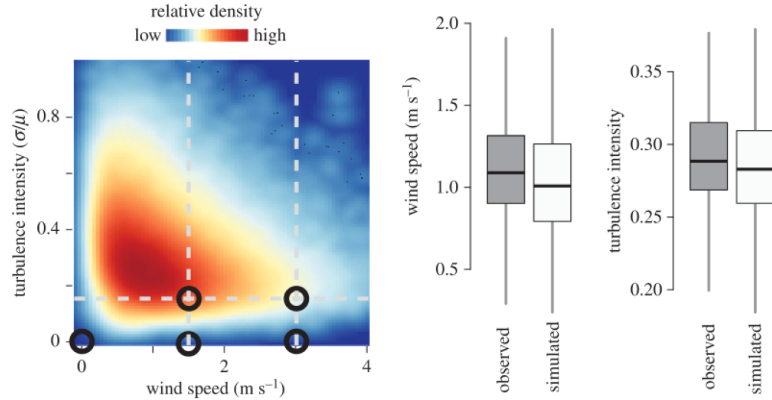
Figure 1.4: Observed (natural) and simulated wind conditions during bumblebee (*Bombus impatiens*) foraging. Reproduced from [126].

At the scale of hummingbirds ($Re \sim \mathcal{O}\left(10^4\right)$), mechanical flapper experiments suggested that freestream turbulence may reduce the effective angle of attack potentially suppressing LEV stability and force production [113]. Larger insects, like hawkmoths, may also encounter environments on this scale, so control over angle of attack will also be necessary for flight stability. Interactions with specific features of the unsteady environment cause these behavioral changes, but it is unclear which flow interactions cause each shift in dynamics.

Although freestream turbulence may be a better approximation for nature, the use of structured unsteady flow allows for easy identification of flow features as they affect in flight dynamics. Additionally, in the near wake of objects in nature (such as flowers) animals may encounter alternating vortices of a consistent size due to the shape and structure of the flower. This environment is often approximated with a von Karman vortex street shed from a circular cylinder. Since these vortices are shed at a constant frequency and size (relative to downstream distance), we can easily quantify if flight behavior synchronizes with

unsteady flow and which spatiotemporal scales are most destabilizing. Combined experiments and numerical simulations for bumblebees in a vortex street showed flight responses consistent with forward flight through freestream turbulence [264]. The bees were most susceptible to lateral perturbations and relied on casting (roll) maneuvers.

Hawkmoths hovering at a feeder in a cylinder wake synchronized their yaw oscillations to the vortex shedding frequency regardless of wind speed and vortex size, but varied coupling to other rotational axes [179]. While smaller vortices also affected pitch stabilization, larger unsteady flow structures destabilized the moths along the roll axis. Since small vortices only interact with one wing, compensatory flight behavior can be maintained on the unperturbed wing. One known example is flapping counter torque (FCT) which compensates for asymmetries in wing forces during body rotations [13]. However, if flow structures interact with both wings, asymmetry between wing velocities isn't possible which changes the effect of FCT, potentially leading to the coupling between yaw and roll oscillations. The extreme limit of this situation could be considered as a whirlwind vortex enclosing the moth and feeder. Hawkmoths compensate for environments that challenge both wings simultaneously with symmetric and asymmetric variations in wing kinematics [14]. Body oscillations around yaw and pitch axes were also used to stabilize position at the feeder, but this may be a reaction to wing variation that re-orients the force vector. Left and right wings were found to use asymmetric angles of attack, but symmetric stroke amplitudes and stroke plane angles. Due to the velocity gradient imposed by the whirlwind, the combination of asymmetric angle of attack and symmetric stroke plane angle could re-establish FCT as a flight control mechanism.

Combined interaction between plants, pollinators, and their environment

Successful maneuvers in nature require insects to vary the forces they generate as they navigate through obstacles and interact with unsteady winds. Not only will added mass effects change due to pre-existing fluid velocity, but circulation build-up around each wing may re-

quire more or less power depending upon the initial circulation present in the environment. Even in a steady flow environment, the wing may be able to 'capture' energy from previously shed vortices in the wake, enhancing force production [288, 73, 301]. Wing-wake interactions may also occur as the animal moves through an unsteady flow environment, potentially increasing flight efficiency. However, perturbations due to the environment also incur corrective body maneuvers and alter flight behavior. The combination of these effects could lead to additional aerodynamic costs. The details of these costs have been explored for normal hovering and some flight maneuvers [179, 40, 63].

Flower tracking in hawkmoths is an ideal flight behavior to study the interaction between aerodynamic mechanisms, behavior, and the environment (Figure 1.1). By causing flowers to wiggle, wind introduces environmental challenges that are overcome with specific biomechanical adaptations [46, 260]. The influence of flower morphology on the wake are unknown as are any potential functionality from the flower's perspective. However, the animals themselves are also perturbed by interaction with windy surroundings, leading to additional changes in wing and body kinematics. If interaction with an unsteady environment disrupts the LEV, then the animal must rely on other unsteady aerodynamic mechanisms to maneuver in nature. Systematically investigating how LEV stability changes in response to unsteady flow may reveal the importance of under-appreciated mechanisms, such as wake-capture. The persistence of the LEV across unsteady environments would emphasize its robustness as a lift-generating mechanism and show gaps in our understanding of how the LEV interations with surrounding airflow.

CHAPTER 2

HAWKMOTH FLIGHT IN THE UNSTEADY WAKES OF FLOWERS

This chapter is reproduced from published work in the Journal of Experimental Biology [293]. The authors contributing to this work are myself and Simon Sponberg.

Introduction

Flying animals rely on maneuverability to survive in unsteady environments whether evading predators, finding mates, or foraging for food [256, 17, 109]. As these animals actively move through their environments, locomotion depends on interactions between their body and the surrounding fluid to produce necessary forces and torques. Changing fluid environments naturally manifest unsteady airflow. Animals must respond to perturbations due to wind gusts and wakes shed from flowers and other objects [277, 40]. Successful flight control requires managing the impact of unsteady flow on body maneuvers and wing aerodynamic forces (Figure 2.1). Since biological systems are driven by sensing and feedback, changes to wing forces may also induce body motion and vice versa.

How unsteady flow influences flight has been explored for hovering and forward flight [179, 36, 14, 114, 318, 141, 233]. However, we still do not know how an unsteady environment impacts the full dynamic range of maneuvers exhibited by flapping fliers. Nor do we know if fundamental aerodynamic mechanisms present in hovering flight persist when an animal must maneuver in flow that is already unsteady. A system identification approach can reveal how flight maneuvers are changed in wind and whether this generalizes across environments [328, 80].

Hawkmoths must maneuver in unsteady flow while hovering to feed in the wakes of flowers. They must quickly respond to environmental perturbations and changes in flower position [217, 17, 87, 137, 19]. Using precisely coordinated wing and body kinematics
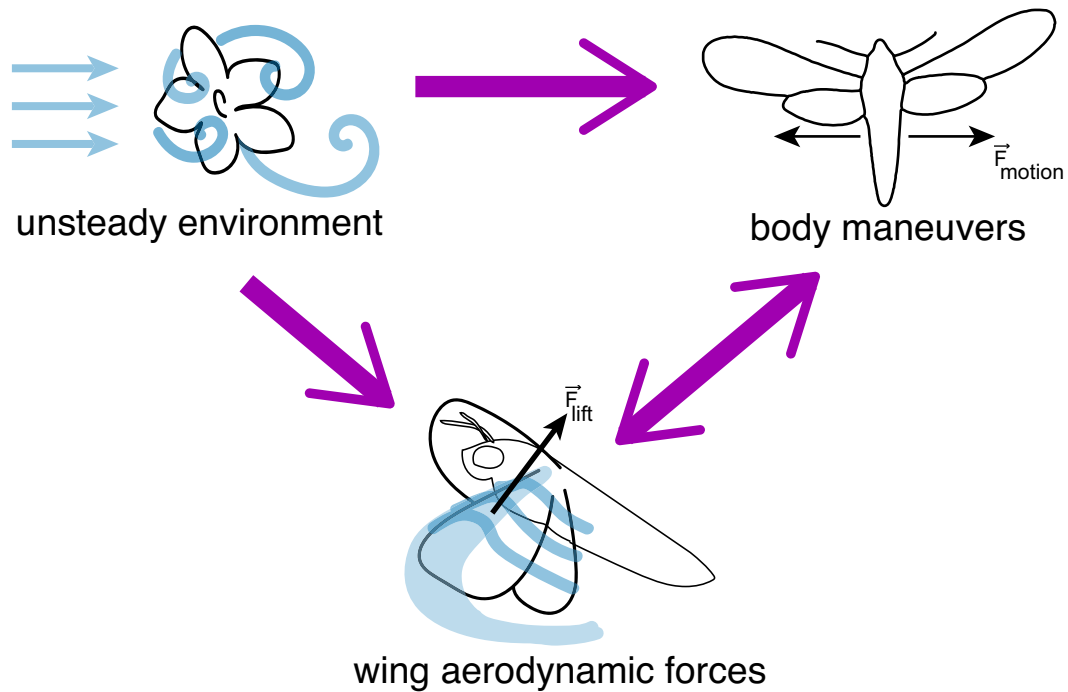
Figure 2.1: **Components for flight success.** Insects flying in natural environments must (often simultaneously) (1) interact with unsteady wind, (2) generate stable lift forces through aerodynamic mechanisms, such as the leading edge vortex (LEV), and (3) perform complex body maneuvers to complete tasks. Kinematic variation can arise when the environment pushes the moth or if the moth senses the wake and responds (top arrow). Biological systems are inherently feedback controlled so body maneuvers may also shift if wing aerodynamic forces are changed (double arrow).

[297], the agile hawkmoth *Manduca sexta*, has adapted robust mechanisms to shift the balance between stability and maneuverability depending on the desired behavior [246, 93]. Hawkmoths modulate their kinematics to track flower motion up to 14 Hz, well above what they encounter in nature, albeit with poor performance at high frequencies [137].

Coordinated wing and body kinematics are also responsible for lift production through unsteady aerodynamic mechanisms [32, 170]. One mechanism, the ubiquitous leading edge vortex (LEV), is thought to contribute to the high lift achieved in insect flight [172, 277, 86, 200]. The LEV has been visualized both qualitatively and quantitatively revealing the basic vortex structure, its dynamics throughout a wingstroke, and vortex stabilization for many insect species (e.g. [291, 6, 115]). However, the LEV on the animal has only been visualized in steady flow [41, 228, 26, 193]. Moths may need to alter wing motion to maintain lift generation in unsteady flow which could disrupt the quasi-steady LEV. LEV disruption is visualized as vortex bursting, which can occur when increased momentum deflects flow through the vortex core. The deflected flow alters the LEV structure and attachment to the wing [116]. At the Reynolds numbers for hawkmoth flight, $Re \sim 10^3$, LEVs on dynamically-scaled flappers burst at high angles of attack [153]. However, LEV bursting has not been observed on freely flying or tethered hawkmoths in steady flow [6, 167, 138]. Although we understand how the LEV generates lift, it is not known how vortex structure and stability are affected by flow in the environment that is already unsteady.

For the hawkmoth, one way unsteady flow is generated in the environment when natural winds encounter flowers. As wind moves around the flower shape, vortices are shed into the wake. Foraging moths feeding from these flowers must interact with these vortices. Feeding in a flower wake introduces two challenges: (1) steady freestream wind and (2) unsteady vortex shedding. In nature, these effects are inseparable and both could have consequences for moth tracking behaviors. The unsteady wake can potentially disrupt tracking maneuvers and the structure of the LEV. LEV bursting and changes to lift production could result in changes to body maneuvers and vice versa (Figure 2.1). How do flower wake

interactions lead to changes in tracking maneuvers? And how does the LEV interact with unsteady flow already in the environment? In order to address these two questions, we must investigate the interplay between maneuvering, aerodynamics (specifically the LEV), and unsteady flow.

To do this we have moths track robotic flowers in a wind tunnel, where we can control the flow environment. In wind, we also visualize the unsteady wake around the robotic flower, natural flowers, and the moth to reveal impacts on the LEV structure.

If flower tracking performance decreases in wind, then moths must balance reactions to unsteady flow (i.e. the flower wake) with foraging maneuvers. In this case, we predict that moths will react to unsteady flow by matching the dominant vortex shedding frequencies in the flower wake. Consequently, foraging maneuvers used to track the flower will suffer the most at these frequencies.

If the leading edge vortex is disrupted in the flower wake, then we expect to observe LEV growth and bursting around mid-wing during mid-stroke. If no vortex bursting is observed, then we can determine whether LEV structure is altered in the flower wake by visualizing flow over the thorax. The presence of a vortex over the thorax suggests that the LEV is continuous across the full wingspan, rather than conical and rooted on the wings [6].

Methods

<u>Wind tunnel characteristics</u>

We performed experiments using an open-circuit Eiffel-type wind tunnel (ELD, Inc.). The 150 cm working section consisted of two interchangeable test sections with 60.96 cm symmetric cross-sections (schematic drawing in Figure 2.2A). The fan is driven by a 3HP induction motor (belt-driven, ODP, 208/230VAC) and generates continuously variable wind speeds from 0.25 - 10 ms^{-1} with less than $\pm 2\%$ variation of the mean. Based on the maximum free stream velocity, stream-wise turbulence should not exceed 0.5%. Air is drawn
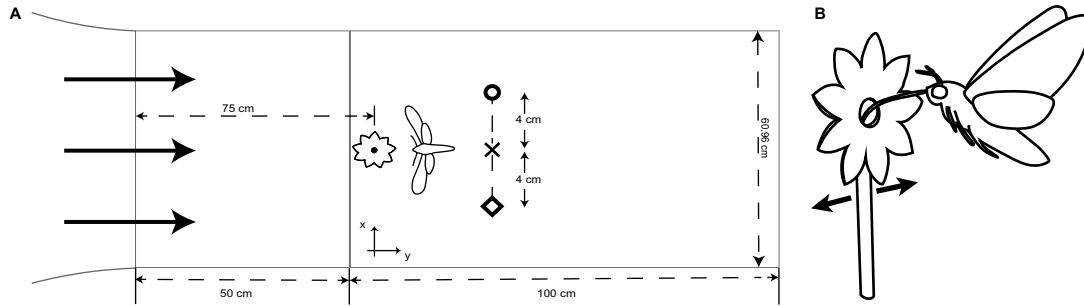
Figure 2.2: **Experimental set-up and conditions.** (A) Schematic diagram of the wind tunnel test section. The robotic flower is placed approximately 75 cm downstream (y-direction) of where flow enters and the moth feeds 2-5 cm downstream of the flower. Wind speed measurements were taken at multiple lateral positions (4 cm apart, marked by symbols) with and without the flower (Fig. S1). (B) Sketch of the hawkmoth feeding from the robotic flower. The moth hovers without landing and tracks as the flower laterally oscillates.

into the elliptical inlet and passes through a honeycomb mesh to condition the flow, which is subsequently contracted and accelerated through to the test section. To regain static pressure, the air then passes through a diffuser before traveling through the fan and back into the room. The entire wind tunnel is supported by structural steel frames positioned on fitted leveling pads. To prevent vibrations of the fan and room from interfering with the air flow, the wind tunnel sections and supporting frames are isolated with rubber-shear-in mounts and flexible coupling.

Wind tunnel flow ducts, test section, and fan motors

The ducts are a composite of fiberglass and reinforced plastic with a molded balsa wood core. The inlet of the settling chamber and flow ducts has 1.61 m lateral clearance to the walls and 0.23 m vertical clearance to the ceiling. Prior to the contraction section, air passes first through a settling chamber and then through a tensioned, hexagonal-cell aluminum honeycomb grid. Before air enters the test section, it flows through a duct fitted with flow straighteners to maximize laminar flow into the test section. The contraction section has a 6.25:1 area ratio with a symmetric cross-section. The inlet and exit areas of this section have static pressure taps.

14

Moths were flown in the test section which is joined to the diffuser and contraction sections via aluminum angle flanges. The test section is 1.37 m from the walls of the room and can (optionally) be divided into two separate, but continuous sections. The primary section (100 cm) is double the length of the secondary test section (50 cm). Test sections are accessible by way of portholes in the panels. The floor, ceiling, and sidewalls of the primary section are made of 13 mm thick soda lime glass. Sidewalls are secured with toggle clamps and can be removed and replaced with custom panels depending on experimental needs. On the operator side of the test section, the sidewall panel has a pneumatic opening door for easy access to the test section. The ceiling, floor, and sidewalls of the secondary section are made of 19.1 mm thick, clear, GM grade acrylic. There are 34M stainless steel, high porosity (60%), tensioned catch screens in place on either side of the test section to prevent the moths from flying into other components of the wind tunnel.

Air flows out from the test section into the diffuser which expands with a total angle of 4.6° and is separated from the fan by an air gap. This air gap (13.9 cm in width and 2.43 m circular cross-section diameter) acts as a vibration isolator. The diffuser contains a highly porous perforated plate to decelerate the flow before it exits into the room and protects the fan.

The fan is 2.13 m from the door and controlled by a transistor inverter variable frequency speed controller (60 Hz/30 Amp). The fan is equipped with a fusible disconnect to protect the motor and controller. A remote control operator station is located downstream of the test section, near the upstream end of the diffuser.

Flow characteristics

We placed a 3D-printed robotic flower [137] at the front of the secondary test section, 75-80 cm downstream from the upstream mesh and at the approximate lateral midpoint (Figure 2.2, x symbol). The flower is actuated by a bipolar stepper motor (57STH56 NEMA23 with 1067 controller; Phidgets, Inc.) using a 14.5 cm moment arm and the center of the

flower face is 20 cm above the bottom panel of the test section.

Wind speed measurements were made at multiple points along the centerline of the working section using an air velocity transducer (TSI Alnor) both with and without the robotic flower present. Measurements were taken at seven downstream points and three lateral positions (Figure 2.2A,S1B). The 0.7 ms^{-1} freestream velocity is chosen to replicate what hawkmoths experience in their natural habitat. Anemometer recordings of average wind speeds around six different species of hawkmoth-pollinated flowers all included 0.7 ms^{-1} [137].

Experimental set-up and procedure

Animals

The hawkmoths used were shipped as pupae from a colony maintained at the University of Washington on a diet that contains retinoic acid [137]. Prior to experiments, the moths were kept on a 12:12 day:night cycle with foraging/feeding time ("dusk") set around noon EST. Tracking experiments were performed with 5 male and 5 female moths (m=1.87 $\pm$ 0.54 g, mean $\pm$ s.d.) and still flower experiments with 5 male and 5 female moths (m=1.70 $\pm$ 0.32 g, mean $\pm$ s.d.); each moth was only used for a single trial, 2-5 days post-ecolsion, and was not exposed to the artificial flower prior to the experiments. For all trials, naive moths were dark-adapted to the experiment room for a minimum of 30 minutes. Temperature during experiments was maintained between 24-26°C. A seven-component flower scent (mimicking *Datura wrightii*) is applied to the robotic flower to encourage foraging behavior [263].

Prior to experiments, moths were marked with a dot of white paint (1:1 ratio of tempera and acrylic paint) on the ventral side of the thorax for tracking. Only the thorax point was used since head tracking is not significantly different [292]. Once the moth was feeding (Fig. 2B), we recorded the positions of both the moth and flower throughout the 20 second tracking run. Moths were removed from the flight chamber if feeding was not initiated

within 5 minutes.

Robotic flower

The robotic flower consists of a 3D-printed flower face (5 cm tip-to-tip diameter) and 2 mL glass nectary attached to the stepper motor. Flower motion is prescribed as a sum of 20 sinusoids (SoS), each with a different driving frequency and randomized phase, and controlled through MATLAB. The stimulus is designed to broadly sample the frequency range and minimize potential learning effects [178]. A dot of white acrylic paint is applied to the nectary to allow for tracking of the flower motion. The digitized time series verifies that the robotic flower reproduces the designed trajectory (green line, Figure 2.3). To limit potential harmonic overlap, the prescribed driving frequencies are logarithmically-spaced prime multiples (0.2-19.9 Hz) [178, 93, 80]. To prevent the moths from reaching the saturation limit of their muscle output at the higher frequencies, the velocity amplitude of the flower motion is scaled to be constant at all frequencies [80].

Video recordings

We recorded all flights from below (ventral view) using a Photron UX100 with a 50 mm lens operating at 125 frames per second (fps). Moths were illuminated with two 850 nm IR lights (Larson Electronics) as well as a "moon light" (Neewer CW-126) used to make the flower face visible and set background luminance [137]. Color temperature, based on a blackbody radiation spectrum, was 5400 K. The moon light was equipped with neutral density filters to reduce the measured illuminance to approximately 0.3 ± 0.1 lx (measured in front and to each side of the flower face) for all trials, which is the preferred foraging light level for *M. sexta* [253].

For smoke-wire visualization an additional Photron UX100 (50 mm lens, 125 fps) was used to record the side view of the animal. The ventral view was used to confirm the horizontal position of the smoke plane relative to either the wingspan or the flower. Addi-

tionally, the moon light was increased approximately 0.1 lx to enhance smoke visibility in the ventral camera.

Smoke-wire visualization

Smoke visualization [249] was performed with a nickel chromium (nichrome) wire aligned with the center of the flower face and approximately 10-20 cm upstream. The 0.25 mm wire was double-coiled and coated with Protosmoke train smoke oil (MTH Trains). After running a current through the wire, the oil condenses into droplets along the length of the wire which are then vaporized into smoke trails as the wire is heated.

Data analysis

Frequency response and tracking performance

After digitizing the flower and moth motions using DLT tracking software [261], the individual time series (Fig. S5) were detrended and then Fourier transformed to be analyzed in the frequency domain (in MATLAB). Flower tracking has been previously shown to be a linear response [137, 19]. Using a sum of sinusoids probes a wide dynamic range of behavior, but linearity allows us to generalize to other stimuli. We can characterize the broad frequency response of the system by the gain and phase, (G, ϕ), at each unique driving frequency (Figure 2.3D,E insets). First, we Fourier transform the individual time series data for each trial,

$$
\begin{aligned}
x_{flower}\left(t\right) \to X_{flower}\left(i\omega\right) &= \int_{-\infty}^{\infty} x_{flower}\left(t\right)e^{-i\omega t}dt = A_F\left(i\omega\right)e^{i(\omega t+\phi)} \\
x_{moth}\left(t\right) \to X_{moth}\left(i\omega\right) &= \int_{-\infty}^{\infty} x_{moth}\left(t\right)e^{-i\omega t}dt = A_M\left(i\omega\right)e^{i(\omega t+\phi)}
\end{aligned}
\tag{2.1}
$$

We then use the complex ratio of the Fourier transformed moth and flower motion to define gain (G) as the absolute value of the complex ratio

$$G\left(i\omega\right) = \left| \frac{X_{moth}\left(i\omega\right)}{X_{flower}\left(i\omega\right)} \right| \tag{2.2}$$

and phase (ϕ) as the angle between the real and imaginary parts of the complex response ratio

$$\phi\left(i\omega\right) = \tan^{-1}\left[\frac{\text{Im}\left(\frac{X_{moth}(i\omega)}{X_{flower}(i\omega)} \right)}{\text{Re}\left(\frac{X_{moth}(i\omega)}{X_{flower}(i\omega)} \right)} \right] \tag{2.3}$$

Respectively, these quantities represent the relative position and timing differences between flower and moth. This frequency response can be represented in the (polar) complex plane by ordered pairs (G, ϕ) where gain corresponds to the radial distance and phase to the angle measured counterclockwise from the horizontal. In this representation, perfect flower tracking occurs at (1,0). To explore how tracking performance (measured here using gain and phase) varies with frequency, we plot gain and phase separately, but both are necessary to describe the behavior of the system across all frequency bands.

Tracking error

Instead of separating the real and imaginary components of the frequency response, we can also use the distance from perfect tracking, (1,0), in the complex plane (Figure 2.3F, inset) to assess tracking performance.

$$\varepsilon = \|(1 + 0i) - (G + \phi i)\| \tag{2.4}$$

As tracking improves, tracking error approaches zero. Tracking error above 1 indicates that the moth would achieve better performance by remaining stationary at that frequency [178, 137].

Mechanical (and inertial) power

To assess how body maneuvers specific to flower tracking change due to wind, we restrict our analysis to inertial COM mechanical power. Following previous methods [17], we calculate the inertial power required to laterally accelerate the center of mass during flower tracking. The moth's response to the summed sinusoid motion of the robotic flower can be written as

$$\boldsymbol{x}\left(t\right) = \sum_{k=1}^{20} A_k \sin\left(2\pi f_k t + \phi_k\right) \hat{\boldsymbol{x}} \tag{2.5}$$

where the indices k correspond to the 20 driving frequencies. Lateral oscillations dominate during flower tracking, so we neglect contributions from vertical and looming motion (Fig. S5). Previous experiments with horizontal flower motion also showed that downstream distance from the flower (looming axis) and hovering position (vertical axis) remained fairly constant during tracking, which supports our assumptions [17]. Inertial power (changes in kinetic energy) for the 1D lateral component of tracking motion is given by

$$\dot{E} = ma\left(t\right)v\left(t\right) \tag{2.6}$$

with

$$v\left(t\right) = 2\pi \sum_k \left(f_k A_k\right) \cos\left(2\pi f_k t + \phi_k\right)$$
$$a\left(t\right) = -\left(2\pi\right)^2 \sum_k \left(f_k^2 A_k\right) \sin\left(2\pi f_k t + \phi_k\right) \tag{2.7}$$

as the lateral components of velocity and acceleration. Then, the inertial power needed for

lateral tracking becomes

$$\dot{E} = -m\left(2\pi\right)^3 \sum_k f_k^3 A_k^2 \sin\left(2\pi f_k t + \phi_k\right) \cos\left(2\pi f_k t + \phi_k\right) \qquad (2.8)$$

Flower motion is periodic, so the time-averaged tracking power is either positive or negative during each half-period. Since power cycles twice as fast as the underlying driving frequency, we average over a quarter period of flower motion,

$$\dot{E} = \left(4 f_k\right) \left[m\left(2\pi\right)^3 f_k^3 A_k^2\right] \left| \int_0^{1/4 f_k} -\sin\left(2\pi f_k t + \phi_k\right) \cos\left(2\pi f_k t + \phi_k\right) \; dt \right| \qquad (2.9)$$

$$\dot{E} = 8m\pi^2 \sum_k f_k^3 A_k^2. \qquad (2.10)$$

As an upper bound, we calculate inertial power assuming that all changes in kinetic energy must be actively generated. Then, both positive and negative work contribute equally and we take the absolute value to get an upper bound for tracking power [17]. If only positive work must be generated by the animal and energy is dissipated by the environment (e.g. aerodynamic damping [13]), then the inertial power is exactly half the value in Eqn. 2.10, which gives a lower bound for inertial power requirements,

$$\dot{E}_{pos} = 4m\pi^2 \sum_k f_k^3 A_k^2. \qquad (2.11)$$

By comparing the inertial COM power for tracking in wind and still air, we can reveal how flower wake interactions affect body maneuvers. Interacting with the unsteady flower wake

could alter total mechanical power requirements compared to tracking in still air. Total mechanical power in insect flight combines contributions from multiple sources including profile and induced power, which refer to drag effects on the wings, and parasite and inertial power, corresponding to body drag and acceleration effects [246]. While inertial power contains costs for accelerating the wing mass (and added mass), it also includes costs due to accelerations of the body (center of mass, COM) required for flight maneuvers, such as tracking. Body inertial power can be thought of as the added cost to maneuver assuming all other metabolic costs remain constant during maneuvering (e.g. wing inertial power, aerodynamic power, and muscle efficiency [17]).

Statistics

Statistically significant tracking was assessed at each driving frequency using a coherence threshold [178, 80] and Fisher's exact g test for periodicity (±0.5 Hz frequency bands around each driving frequency were tested with a confidence threshold of 0.05 [290, 137]). Additionally, all averaging and variance estimation were performed in the complex plane [178]. These values were comparable to results for averaging log gain and using circular statistics to average phase [19]. Error bars are 95% confidence intervals of the mean unless otherwise noted.

Gain, phase, and tracking error were all tested for significance using two-factor ANOVA (with wind and frequency as our factors). This test was also used to determine significant differences in inertial power within specific frequency bands.

Results

Tracking performance decreases in an unsteady flower wake

In unsteady air, all moths successfully tracked for the full 20 seconds with significant tracking at least up to 6.1 Hz with 0.90 coherence [178, 137] (Figure 2.3B, gray line). Most moths (70%) were able to significantly track up to 11.3 Hz, but few moths (30% or less)

were able to track any higher frequencies. This is lower than in still air, where half of the moths significantly tracked flower motion up to 13.7 Hz.

Comparisons between the frequency responses for tracking in wind and still air are best interpreted by examining specific frequency bands: (i) 0.2-1.7 Hz, (ii) 1.7-5.3 Hz, and (iii) 5.3-11.3 Hz. The first band corresponds to the range at which natural hawkmoth-pollinated flowers oscillate [137, 292], the second captures the range with the largest overshoot in position (Figure 2.3B), and the third describes how the moths modulate tracking as they fail.

Low frequency response: Moths track best at natural flower oscillation frequencies

The effect of wind on moth dynamics is very small at the lowest frequencies. In wind, moths track nearly perfectly ($G = 1; \phi = 0$) across low frequencies up to 0.7 Hz, revealing only minor differences with tracking in still air (gain and phase difference at 0.7 Hz: 0.15 and 2.8°, Figure 2.3D,E). Across all low frequencies, 0.2-1.7 Hz, the moth's gain was higher in windy conditions than in still air, increasing by 14% at 1.7 Hz (gain for 0.2-1.7 Hz: *F=30.25, dF=1, P¡0.05*). However, there were no distinguishable differences in the phase response (0.2-1.7 Hz: *F=0.6, dF=1, P=0.4393*).

Higher gain does not necessarily indicate improved tracking performance. Because the moth was overshooting the flower in windy conditions, the tracking error was larger than in still air (0.7-1.7 Hz, *F=11.14, dF=1, P=0.0012*, Figure 2.3F, blue line).

Intermediate frequency response: Interaction with wind decreases tracking performance

As in still air, moths tracking in wind have a distinct region of overshoot ($G > 1$) in the intermediate frequency range (Figure 2.3D). However overshoot is both more pronounced and persists over a greater range of frequencies in wind (peak $G = 2.17 \pm 0.16$, $\phi =109.9°$ $\pm 5.9°$ at 2.9 Hz). Overall, tracking in wind between 1.7-5.3 Hz results in a nearly 40% higher peak overshoot (gain: *F=79.52, dF=1, P¡0.05*). Tracking in wind also removes the
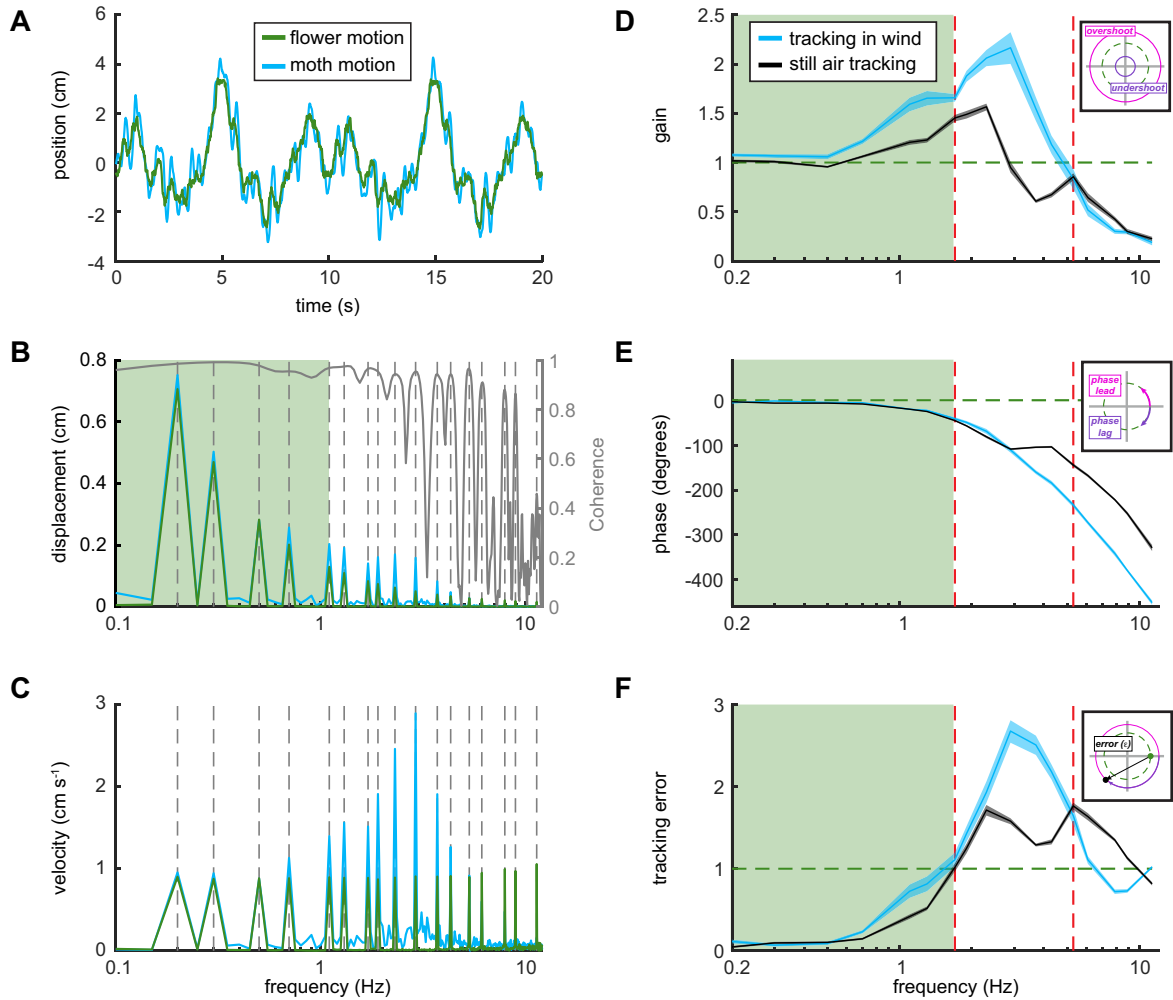
Figure 2.3: **Frequency response comparison for tracking with and without wind.** All still air data (black) previously collected in Sponberg et al (2015). (A) Example raw time series data for one trial of tracking in wind. The moth (blue) overshoots the flower (green) throughout the trial. (B) (left axis) Amplitude (position) in the frequency domain (after Fourier transform of data from A). Peaks correspond to prescribed flower driving frequencies. (right axis) Coherence threshold shows significant tracking drops below 0.9 above 6 Hz. (C) Velocity in the frequency domain. (D, E) Frequency responses (mean±95% CI of the mean, two-way ANOVA) for the same tracking task in still (black) and unsteady (blue) air. Responses are categorized into three frequency bands, separated by (red) dashed lines at 1.7 Hz and 5.3 Hz. Gain (D) describes the relative amplitude difference between moth and flower while phase (E) characterizes timing differences. The insets graphically show how gain, phase and tracking error are interpreted in the complex plane. (F) Gain and phase are combined and used to calculate tracking error, the distance from perfect tracking in the complex plane. The green box marks the frequency range below 1.7 Hz matching the range of oscillations exhibited by natural hawkmoth-pollinated flowers.

plateau in the phase response, producing a monotonic roll off not seen in still air (phase: *F=5.57, dF=1, P=0.0201*).

Tracking error throughout this frequency band is large due to a combination of gains above 1 and phase lags greater than 90°. Maximum tracking error in windy conditions is higher than in still air, with a 70% increase at 2.9 Hz. Tracking error in wind steadily increases until the maximum of 2.68 ± 0.14 at 2.9 Hz (Figure 2.3E, blue line) and then decreases until it falls just below the maximum of still air tracking error (1.65 ± 0.11 at 5.3 Hz), resulting in a statistically significant difference with and without wind (*F=58.62, dF=1, P¡0.05*). In both cases, but especially with wind, the moth would track these intermediate frequencies better if it stayed stationary ($G = 0; \phi = 0; \epsilon = 1$).

High frequency response: Moths show similar failure dynamics while tracking with and without wind

Despite the large overshoot in wind at the mid-range frequencies, moths tracking with and without wind fail similarly as flower motion frequency increases towards the saturation limit of the moths' flight system.

Although few moths were able to successfully track above 11.3 Hz in wind, the decrease in gain leading up to this frequency is similar to the response in still air, with no significant difference (*F=3.19, dF=1, P=0.0773*). The approximately 90° difference in phase lag between wind and still air grows until exceeding a 100° difference at 11.3 Hz (Figure 2.3D,E). Above this frequency the moth lags the flower by a full cycle. The continuous phase roll off at high frequency is likely due to an inescapable delay inherent in all real biological systems. Since tracking error is a distance in the complex plane and phases of 0° and ±360° are equivalent, the increased phase lag for tracking in wind reduces tracking error back toward a value of 1. This results in a maximum difference of 0.63 ± 0.03 between tracking in wind and in still air (*F=36.31, dF=1, P¡0.05*).

These differences for tracking with and without wind lead to the differences in tracking

error (Figure 2.3F). In wind and still air, moths fail by undershooting and lagging behind the flower at higher frequencies until, at the highest frequencies, they are effectively non-responsive ($G = 0; \phi = 0$). As tracking gain approaches zero, the tracking error necessarily approaches 1.

Flower tracking in wind manifests simpler dynamics

The change in the transfer function (frequency response, Figure 2.3D,E and Fig. S2) suggests that windy conditions simplify tracking maneuvers. Tracking in wind can be described by a reduced-order dynamical system, compared to still air. While the low frequency behavior is maintained, the response at high frequencies is diminished. The transfer function describing still air tracking includes a simple delay term [137, 19, 292] and a minimum of four poles and three zeroes to capture the double peak in gain, but more importantly, the plateau in phase between 3-5 Hz. In wind, the phase plateau is removed and gain has a single peak, so tracking can be described by a lower-order transfer function with only two poles. This order reduction suggests that wind acts as an environmental filter that modifies tracking dynamics at and above the range of vortex shedding. The second gain peak in still air represents a removed pole between 4.3-6.1 Hz, which overlaps the end of the range of vortex shedding frequencies.

Dominant vortex shedding frequencies of unsteady flower wakes coincide with specific frequency bands

Roboflower sheds vortices in the intermediate frequency range, matching the frequency band of overshoot

To explore the temporal dynamics of the unsteady flow around the moth we imaged the wake of the stationary robotic flower. Using smoke-wire visualization, we observed that the dominant vortex structures in the flower wake are irregular, but mostly within the intermediate frequency band of 1.7 to 5.3 Hz. The vortex shedding frequency was determined

by observing the number of vortices (rotating in the same direction) over 300 frames, approximately 5-10 cm downstream of the flower face (Figure 2.4A, red box). Averaging across four videos, the vortex shedding frequency from the top petals was 2.16 Hz $\pm$ 0.25 Hz (mean $\pm$ s.d.). Flow around the nectary shed vortices at 0.95 Hz $\pm$ 0.17 Hz (mean $\pm$ s.d.). However, this is a lower bound of the vortex shedding frequency because the flower sheds vortices that rotate in multiple directions with one or more arriving at the same downstream location simultaneously (Movie S1).

While the streaklines had a slight upward drift due to higher temperature than surrounding air, the flower wake structure is distinct from the undisturbed streaklines above the flower. As the wake develops downstream the shed vortex structures interact with one another. Some vortices cluster (multiple vortices, Figure 2.4B), appear distinct (single vortex, Figure 2.4C), or merge with counter-rotating, neighboring vortices (diffuse streaklines, Figure 2.4D). These overlapping vortices (Figure 2.4B,D) potentially double the number of vortices, raising the estimated dominant vortex shedding frequency up to 4.33 Hz $\pm$ 0.49 Hz (mean $\pm$ s.d.) from the top petals and 1.90 Hz $\pm$ 0.34 Hz (mean $\pm$ s.d.) from the nectary. While the moth feeds in a relatively low flow region (approximately 5 cm downstream), the wingspan extends past the face of the flower so structures shed from the perimeter interact directly with both wings. The vortex shedding frequencies range from 2-5 Hz, overlapping the region of increased overshoot (Figure 2.3D).
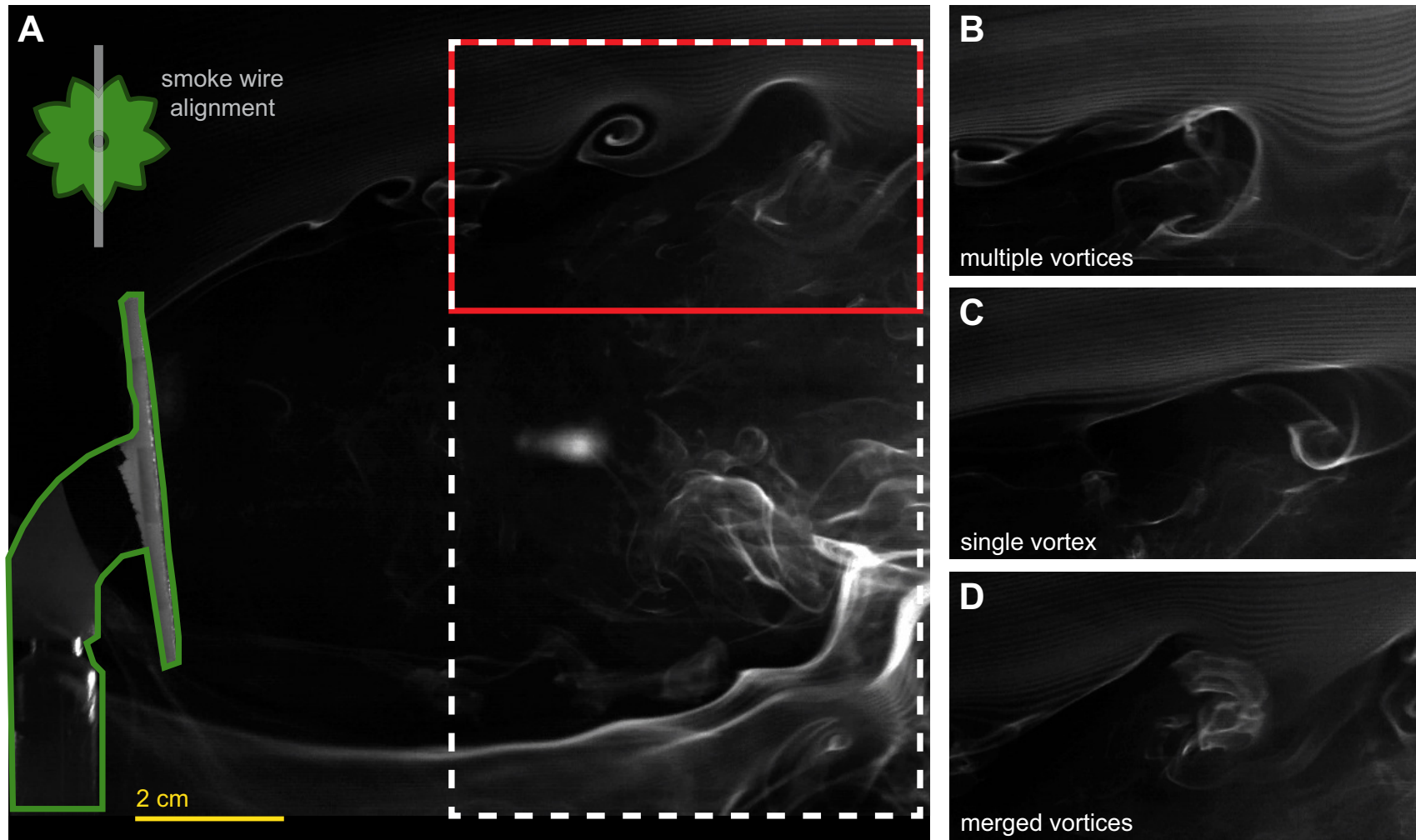
Figure 2.4: **Smoke visualization of the robotic flower wake.** (A) Full frame view of flower wake. Inset shows smoke wire lateral alignment with the flower face. The moth primarily feeds in the relatively low flow region approximately 2-5 cm downstream of the flower. Vortices were most distinguishable around 5 cm downstream (white dashed box) and vortex shedding frequency was measured at this location (red box). (B) Snapshot of flower wake (from red boxed region) showing multiple vortices, rotating in multiple directions, passing through the same location. (C) Snapshot of a single vortex. (D) Snapshot of diffuse streaklines due to merging vortices. Level adjustments were made to highlight the smoke lines using Photoshop with a mask over the robotic flower, shown in green.

Real hawkmoth-pollinated flowers shed unsteady wakes at low frequencies

Size and material differences between our robotic flower and natural flowers could lead to different unsteady wakes. Hawkmoths forage from flowers of various sizes, from 1-2 cm up to 10 cm [87, 137] and natural flowers are more flexible than the 3D-printed roboflower. Using the same visualization method, we observed the wakes shed from fully bloomed *Datura sp.* (tip-to-tip, flower face diameter: 9 cm, Figure 2.5A) and *Petunia sp.* flowers (tip-to-tip, flower face diameter: 7 cm, Figure 2.5B) attached to the same rigid support used for the robotic flower. Larger *Datura* flowers shed vortices 2-3 cm further downstream than *Petunia*. This includes the feeding position of the moth (Figure 2.5A). Fewer vortices appear in the measurement region (Figure 2.5, red box) resulting in a lower frequency of structures shed off the flower petals, (lower bound: 0.43 Hz $\pm$ 0.06 Hz; upper bound: 0.87 Hz $\pm$ 0.12 Hz). The vortex shedding frequency around the nectary was similar to the roboflower since the same support structure was used (bottom wake structure, Figure 2.5A). Averaging over three *Datura* videos gives a lower bound of 0.88 Hz $\pm$ 0.26 Hz and an upper bound of 1.77 Hz $\pm$ 0.51 Hz. For *Petunia*, these vortices are partially disrupted due to interactions with the lower set of petals, which did not allow for measurement of vortex shedding in this region (Figure 2.5B). Based on three different *Petunia*, and averaged over four videos, the vortex shedding frequency is 0.95 Hz $\pm$ 0.18 Hz. Unlike the robotic flower wake, *Petunia* showed fewer overlapping vortices, but vortices were still multi-directional, so while an upper bound of 1.90 Hz $\pm$ 0.36 Hz is unlikely, some structures are shed at frequencies above 1 Hz.
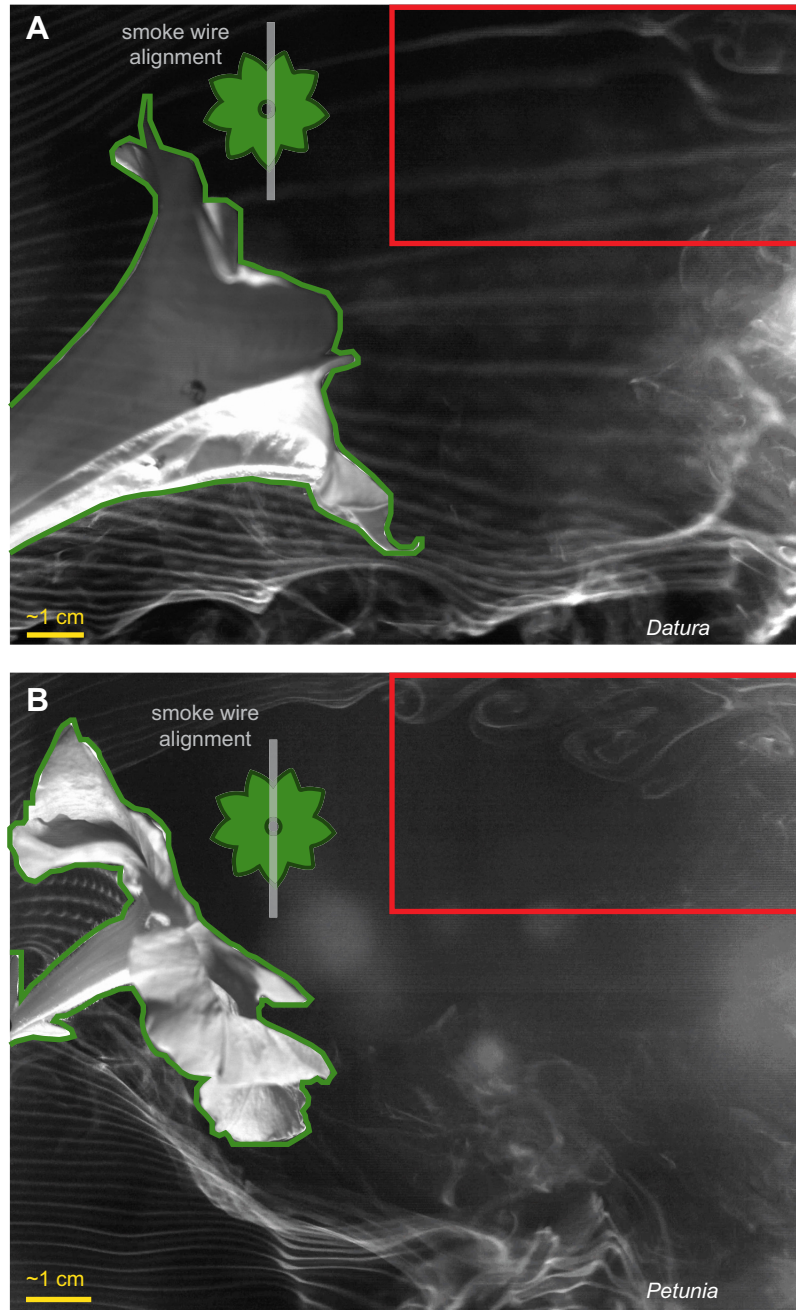
Figure 2.5: **Smoke visualization of natural flower wakes.** (A) Snapshot of Datura sp. wake. (B) Snapshot of Petunia sp. wake. Inset shows smoke wire lateral alignment with the flower face. For both flowers, vortices similar to those shed by the robotic flower are seen coming from the top petals, with fewer passing through the measurement region for Datura (red box). The wake structure from the bottom petals is disrupted by the rigid support rod. Global adjustments were made to brightness, contrast, and gamma, within the Photron software (PFV). Additional level adjustments were made to highlight the smoke lines using Photoshop with a mask over the flower, shown in green.

Inertial power comparisons quantitatively confirm consistency of flower wake and reveal nonlinearity

To test if flower tracking in wind (case 1) is a linear superposition of stationary hovering in wind (case 2, Figure 2.6A,B) and tracking in still air (case 3), we compared the mechanical power utilized during these maneuvers. For the two tracking cases, (1) and (3), moths exhibit inertial COM power peaks at each of the driving frequencies and minimal power at the non-driving frequencies (Figure 2.6C). When the flower is held stationary in wind (case 2), we expect that power requirements should only increase in the frequency band corresponding to vortex shedding. A stationary flower would result in a stationary moth and therefore low inertial COM power. Then, inertial COM power for hover-feeding in wind (case 2) reveals the maneuvers induced by flower wake interactions (Figure 2.6D). Agreement between tracking (case 1) and hover-feeding (case 2) in wind at the non-driving frequencies suggests that the flower motion at various frequencies does not significantly change the vortex shedding frequency. The sum of the moth's inertial power for hover-feeding in wind (case 2) and tracking in still air (case 3), give a linear prediction for the power needed to track in wind (case 1).

$$\widehat{\dot{E}}^{wind}_{tracking} = \dot{E}^{still}_{tracking} + \dot{E}^{wind}_{hovering}. \tag{2.12}$$

The linear sum $\left(\widehat{\dot{E}}\right)$ over-predicts the measured response $\left(\dot{E}^{wind}_{tracking}\right)$ for tracking in wind at all non-driving frequencies (Figure 2.6E). The response at the lowest driving frequencies is well-captured by a linear combination of still air tracking and hover-feeding in wind. However, at the mid-range driving frequencies (1.7-5.3 Hz), the linear sum consistently under-predicts the actual response by a minimum of 11.4 W kg^{-1} (at 5.3 Hz) and a maximum of 92.1 W kg^{-1} (at 2.9 Hz). Although there is a slight increase in inertial power

between hover-feeding (case 2) and tracking in wind (case 3), the over-prediction by the linear sum, especially between 2-5 Hz (Figure 2.6E), is too large to be explained by differences in flower wake characteristics alone.

Key features of the leading edge vortex are maintained in wind

Since the flower wake significantly decreases tracking performance, we next used smoke visualization to see if the leading edge vortex bursts in wind. Bursting is expected to occur along mid-span during the middle of the wingstroke. In the absence of bursting, the LEV may maintain the same structure observed in steady air with a relatively constant diameter extending across the full wingspan during mid-wingstroke [6].

With the smoke wire aligned at mid-wing, we observe a single LEV that reattaches without bursting (Figure 2.7A), consistent with LEV structure in steady air conditions [172, 6]. During each downstroke, the mid-wing LEV grows until it is shed prior to the beginning of the upstroke. The stable LEV is most visible at mid-downstroke (Figure 2.7A and Movie S2). Although the freestream velocity in our experiments was slightly lower than in previous studies [172, 6], the mid-wing LEV is qualitatively similar in size (relative to the wing chord) and shape to their results. Other features of the LEV structure, such as trailing-edge (Figure 2.7B, white arrow) and tip vortices (Figure 2.7A, yellow arrow) are also visible on some wingstrokes, but the full vortex loop structure cannot be resolved with smoke-wire visualization alone.

The LEV structure is continuous across the thorax in the absence of vortex bursting. Over the thorax, the LEV forms during stroke reversal and grows during the upstroke (Figure 2.8B and Movie S3), consistent with observations in steady air [6]. However, a transient LEV was sometimes present during the downstroke (Figure 2.8A), so LEV structure may not be conserved from wingbeat to wingbeat. Despite possible inter-wingbeat variation,

32
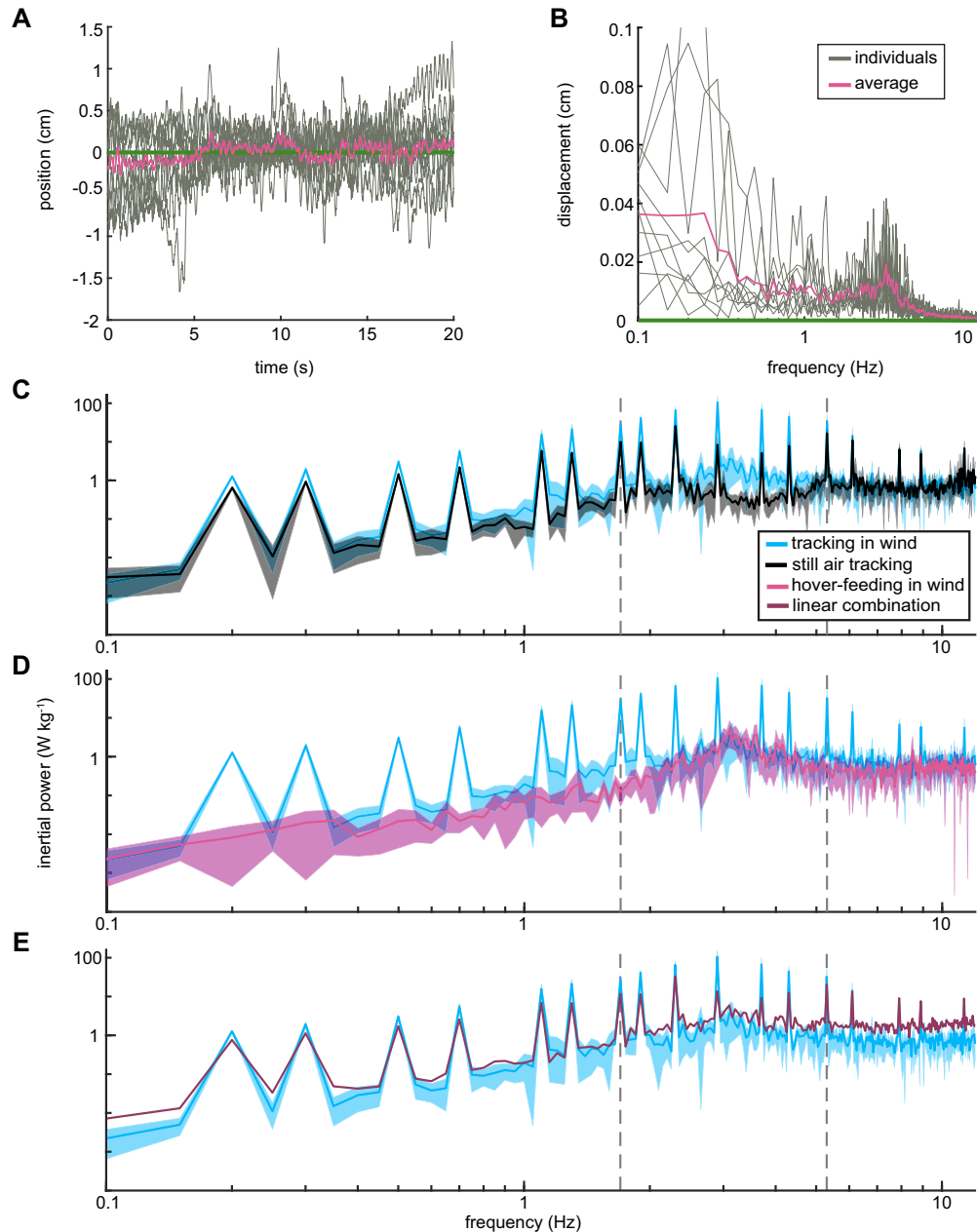
Figure 2.6: **Effects of unsteady wake on inertial power.** (A) Example time series data for hover-feeding trials in the wind tunnel. The flower (green) remains stationary while the moth oscillates and tries to maintain a stable position with 0.7 m s-1 freestream wind. Traces showing trajectories of all sampled moths (grey) and the mean (pink) show high variation between individuals. (B) Fourier transform of data (from A). Each individual trial was transformed and then averaged. Despite individual variation, all moths display large amplitude oscillations below 1.7 Hz with an additional (smaller) peak occurring between 2-5 Hz. (C) Inertial (COM) power comparison (mean±95% CI) for tracking in wind (blue) and in still air (black). Power peaks at the driving frequencies for both tracking cases, but peaks are higher for tracking in wind. (D) Comparison for tracking in wind (blue) and hover-feeding in wind (pink). Power peaks at the driving frequencies for tracking in wind, but both traces show agreement in non-driving frequencies between 1.7-5.3 Hz. (E) Comparison between measured tracking in wind (blue) and the linear combination of still air tracking ([137]) and hover-feeding in wind (dark purple). While the linear combination agrees fairly well with the response at the lowest frequencies, it under-predicts the response between 1.7-5.3 Hz and over-predicts at the highest frequencies.
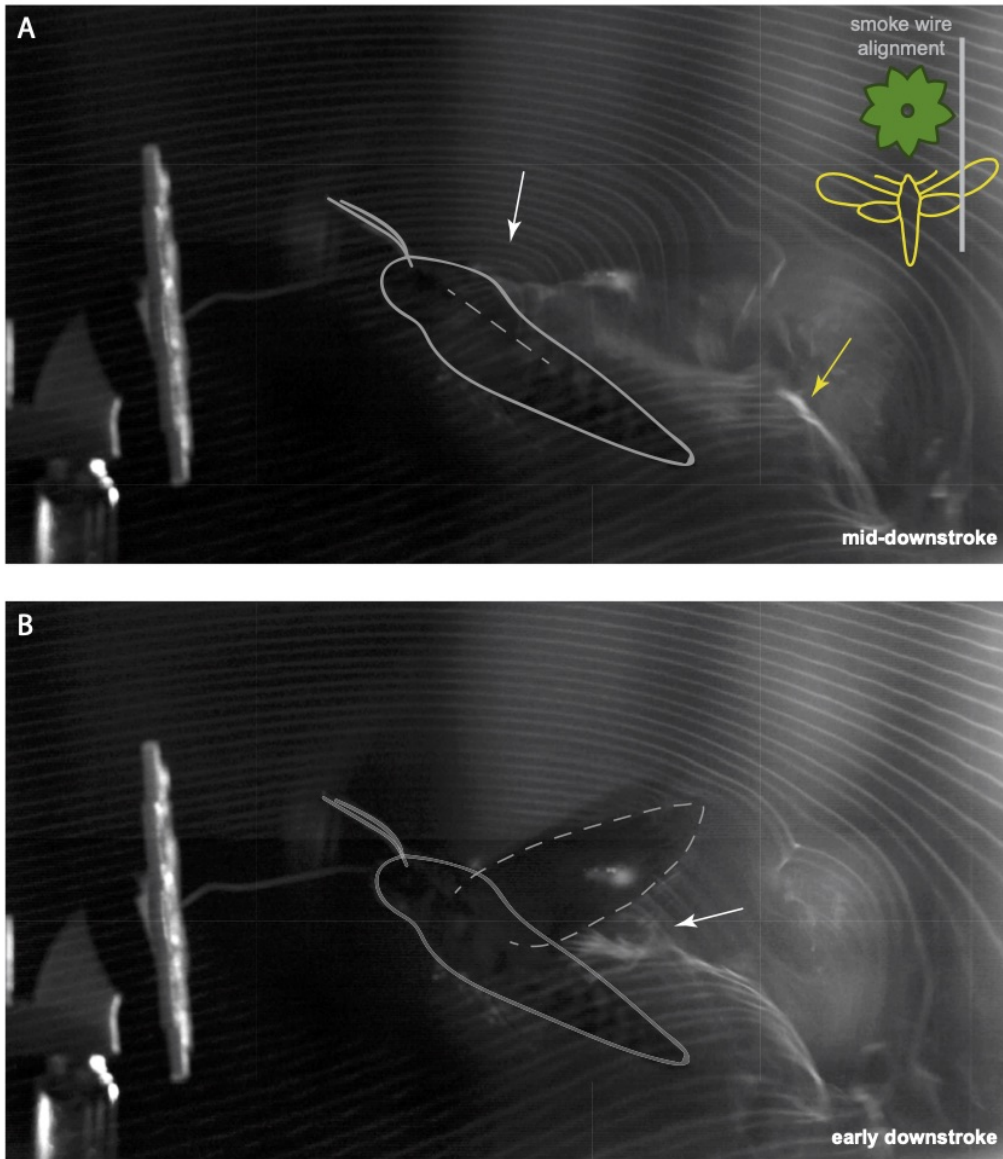
Figure 2.7: **Smoke visualization of the leading edge vortex at the mid-wing position.**
Free-flying moths ($n = 2$) maintaining a stable position while feeding from the robotic
flower in wind. Outline of moth added for clarity. (A) Mid-downstroke. Separated flow
region of LEV (white arrow) and roll up of the tip vortex (yellow arrow). The LEV during
the mid to late downstroke resembles what has been seen previously for tethered Manduca
in steady air (compare to [6]), but the tip vortex (yellow arrow) shows a down and backward
trajectory, rather than back and upwards. (B) Early downstroke. A possible trailing edge
vortex (TEV) indicated by a white arrow. Level adjustments were made to highlight the
smoke lines using Photoshop. Inset shows smoke wire lateral alignment with the moth and
flower face.

moths appear to use an unburst LEV with and without wind.

Discussion

Wake interactions shift tracking performance within vortex shedding frequency range

Although performance declines, moths maintain near perfect tracking in the flower wake within the range of flower oscillations they encounter in nature. Outside of this range, moths face significant challenges from vortices shed in the flower wake. Gain overshoot, tracking error, and inertial power, all peak within 2-5 Hz and are higher than in still air (Figure 2.3D,F and Figure 2.6C,D,E). Hawkmoths [179], bumblebees [264], and fish [**Liao2003a**, 202, 191, 298] have all demonstrated an ability to stabilize perturbations at vortex shedding frequencies when maintaining a position. We found that shed vortices also impact active maneuvers, like flower tracking. Despite changes in underlying tracking dynamics, the flower wake does not lead to tracking failure. Aerodynamic interactions challenge tracking maneuvers, but moths still successfully feed and maintain comparable positional errors (Fig. S4).

Responses to the flower wake are consistent across all non-driving frequencies, regardless of whether the flower is moving or not. Wakes of oscillating cylinders exhibit increased vortex strength [64] and varied modes of vortex shedding depending on the frequency of oscillation [81, 305, 49]. When the cylinder oscillates at the natural vortex shedding frequency of the still cylinder, a "lock-in" condition can be reached where the motion of the cylinder can drive vortex shedding away from the natural frequency [186]. Although the mean inertial power for moving and still flowers in wind differs slightly at non-driving frequencies outside of the vortex shedding range, the confidence intervals maintain overlap (Figure 2.6D). The consistent overlap across non-driving frequencies in wind suggests that the vortex shedding in the flower wake occurs between 2-5 Hz whether the flower is moving or not (Figure 2.6D). Separation between vortex shedding frequencies and flower motion frequencies may allow the moth to decouple tracking maneuvers and perturbation

responses.

In nature, even wind speeds below 5 cm s^{-1} induce small amplitude oscillations (approximately 0.5 cm, peak-to-peak) in hawkmoth pollinated flowers (*Phlox*) and higher wind speeds result in larger lateral than longitudinal oscillations [241]. Frequency analysis of multiple flower species showed that most hawkmoth-pollinated flowers oscillate below 5 Hz [87] with over 90% of flower power (power spectral density or oscillation energy at each frequency) contained below 1.7 Hz [137]. In addition to oscillating within this low frequency band (0.1-1.7 Hz), we found that natural hawkmoth-pollinated flowers shed wake structures at these frequencies (Figure 2.5). Because the frequencies of flower oscillation and vortex shedding overlap, natural flower wakes could pose challenges to tracking in nature. Alternatively, if the passive response to wind is in the same direction as tracking motion, then moths might exploit this phenomenon to "surf" on flower wakes.

Nonlinear inertial power response indicates nonlinear tracking dynamics biased to low frequency motion

Tracking performance is reduced in the flower wake with a larger effect at vortex shedding frequencies. More motion than predicted is seen at the driving frequencies, especially at frequencies (2-5 Hz) where the flower sheds vortices (Figure 2.4 and 6Figure 2.6). Moths do not combine tracking and perturbation responses as a simple superposition. Hawkmoths have a high roll moment of inertia and are known to rely on passive damping mechanisms in response to roll perturbations [13, 203, 162]. Although the moment of inertia is lower around the yaw and pitch axes, similar passive mechanisms could be employed to stabilize position in the flower wake. Reliance on passive damping could explain the large overshoot and tracking error between 2-5 Hz (Figure 2.3D,F), if the moth only actively tracks outside this frequency range. The addition of unsteady flow emphasizes that best tracking performance is biased to low frequencies matching natural flower oscillations.

Moths are perturbed by wind, but they may correct for this through feedback. Both

experiments and numerical simulations showed that bumblebees in von Karman streets respond to perturbations with passive, drag-based mechanisms [13, 159], but must also use active flight control to maintain stability as wake perturbation effects increase over time [233]. In addition, we know the abdomen responds actively to visual motion stimuli to stabilize body pitch over multiple wingstrokes [93]. Hawkmoths maneuvering in wind could adjust abdomen position either to increase drag and stabilize against perturbations or tilt their aerodynamic force vector without changing wing kinematics.

Measurements of energetic costs of tracking showed that maneuvering does increase COM inertial power, but the increase is small compared to the energy required for hovering alone [17]. At our freestream velocity, 0.7 ms^{-1}, the moths are in slow forward flight, however wing kinematics and body pitch are comparable to hovering [41]. We only consider power due to lateral motion. Contributions from wing aerodynamic power could also change in wind and it is not clear how changes in wing kinematics would influence aerodynamic power. At higher wind speeds, hawkmoths pitch down and adopt a figure 8 wing path [193]. Adding the unsteady wake on top of higher speed steady wind could exaggerate these adjustments. Although the flower wake could increase the total energy needed to hover, increased inertial power requirements for motion may not be accompanied by increased power output (or metabolic) demands. Rainbow trout adopt a Karman gait to slalom though unsteady wakes and reduce costs of locomotion [202]. Moths could similarly slalom through the flower wake to track flower motion [301, 288, 73]. If so, they may reduce control against perturbations occurring at the driving frequencies, even if this results in increased overshoot (Figure 2.3D). Energy from the flower wake disrupts tracking maneuvers, but vortices are thought to first interact with the moth aerodynamically. Then, the flower wake should first disrupt the LEV, which we can identify with smoke visualization of vortex bursting.

We see no evidence of vortex bursting due to interaction with the flower wake. Instead we observe a continuous LEV across the wings and thorax. In wind, the flower sheds vortices in multiple directions causing multidirectional flow separation at the leading edge of the wing, which may inhibit the ability of each wing to stabilize bound vortices, such as the LEV. To maintain LEV structure and size, energy must be dissipated or the vortex would continue to grow in size and strength until it is shed off of the wing into the wake of the insect. Interactions with the flower wake could alter spanwise flow [116] and potentially induce vortex bursting. However, additional energy from the flower wake is successfully dissipated out of the LEV. The lack of vortex bursting suggests that the leading edge vortex is robust to interactions with vortex structures at the spatiotemporal scale of the robotic flower.

Stability of the LEV in wind could be due to the small size of vortex structures (Figure 2.4), suggesting they may not be energetic enough to cause disruption. The comparable size of vortices in natural flower wakes (Figure 2.5) also implies that vortex size is not a challenge to the LEV in nature. The temporal range of vortex shedding frequencies (2-5 Hz) lies well below the wingbeat frequency of the moth during hovering and tracking (approximately 25 Hz). We found that while interacting with wind at these frequencies moths still maintain the timescale of the wingbeat (Fig. S3). Therefore the timescale of LEV growth is also maintained in the unsteady flower wake. Nonetheless, wakes do affect tracking. Quantitative flow visualization of LEV strength and development throughout the wingstroke could reveal if lift forces are affected by interactions with wind although the LEV structure appears not to change.

Although LEV structure is qualitatively maintained, moths produce reduced-order dynamics for tracking in wind compared to still air. Interaction with the flower wake removes the

bimodal response in both gain and phase within the range of vortex shedding frequencies (Figure 2.3D,E). The wake could be considered a disturbance, but if the unsteady flow also alters force generation of the wings, then the underlying tracking dynamics have changed. In other words, the filter that transforms kinematics to forces is likely changed in the flower wake. Counterintuitively, this environmental filter simplifies tracking dynamics within 2-5 Hz. With lower frequency disturbances, such as the flower wake, moths may actively prioritize responses to lower frequencies and ignore the higher frequency flower motions. This is one way adding the flower wake could filter the tracking response of the moth. Electric fish vary opposing thrust and drag forces to remain stable in different flow speeds [273]. Passive responses to vortices in the flower wake could also counteract higher-order tracking maneuvers at certain frequencies, even if the moth does not deliberately control against these perturbations.

Contradiction in wake impact on maneuvering and aerodynamics

Hawkmoths employ a stable leading edge vortex to produce lift despite changing how well they track flowers in still and windy conditions. Since vortices in the flower wake are relatively small, interactions between these structures and the LEV may result in vorticity or lift magnitude differences, but not cause the overall LEV to burst or change structure along the wingspan. LEVs have been classified for many different insects based on the qualitative structure of the vortex across the wingspan and a quantitative understanding of how energy is dissipated to maintain LEV stability [6]. Hawkmoths rely on a continuous, actively generated LEV in steady air [41] and operate in the Reynolds number range of vortex bursting. Our results show that moths continue to use the same class of LEV with no obvious evidence of vortex bursting.

While smoke visualization can identify LEV bursting, it cannot quantify changes in spanwise flow, either through the vortex core or towards the trailing-edge of the wing. We conclude that any changes in spanwise flow due to the flower wake are not large enough to

burst the LEV or change its class.

Consequences for flight control

Freely behaving animals rely on feedback systems to control locomotion and encode information about both the environment and their state within that environment. Fish swimming through von Karman cylinder wakes largely maintain position through visual feedback [191]. The foraging task studied here was previously shown to rely on redundant visual and mechanosensory (from the proboscis-nectary interaction) pathways [19]. The addition of mechanosensory feedback may help moths stabilize in wakes even if their vision is compromised. *M. sexta* also has a longer proboscis than some other hawkmoths, *D. elpenor* or *M. stellatarum* [30], which has been proposed to increase mechanosensory feedback during tracking since more of the proboscis is in contact with the nectary [292]. A longer proboscis could also cause the moth to interact with vortices that develop further downstream from the flower, requiring the LEV to also be stable to the wakes of a wide range of flowers from *Petunia* to larger *Datura* (Figure 2.5).

As they maneuver in nature, insects may need to encode both the environment around them and the forces they are able to produce through interactions with that environment. Campaniform sensilla present along the dorsal and ventral side of the hawkmoth forewing are sensitive to inertial forces on a timescale 80x smaller than the wingbeat period [239, 192]. In unsteady flow, aerodynamic interactions change local flow along the wing and lead to LEV bursting. Aerodynamic forces are not thought to influence overall wing motions, but they may locally strain the wing if changes in flow are large. If the boundary layer is disrupted, wind may also deflect hair sensilla on thorax. Encoding local strains could be a mechanosensory feedback mechanism for LEV stability.

Although performance suffers, the forces and torques fundamental to successful flower tracking at natural flower oscillation frequencies are maintained in wind. Features of the environment are sensed and integrated by multiple neural pathways to achieve a desired

motion. Variation in the environment then shifts behavior away from ideal locomotion, but not far enough to cause failure. Animals in nature may depend on sensing subtle changes in force-generating mechanisms, such as the LEV, to balance body maneuvers and lift production in an unsteady environment.

Acknowledgements
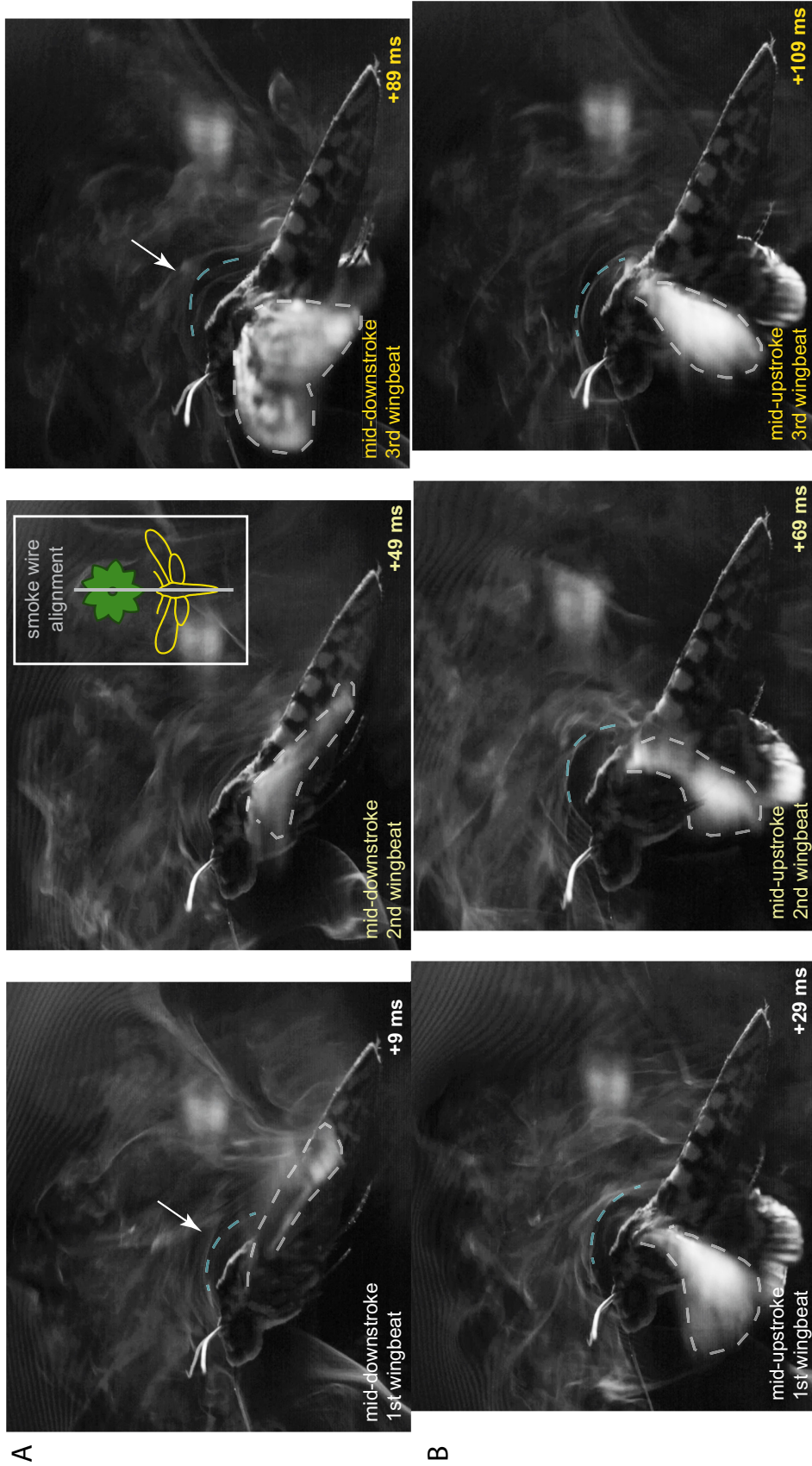
Figure 2.8: **Smoke visualization of the leading edge vortex over the thorax (centerline).** Flow is attached over the thorax at the late downstroke (for most wingstrokes), separates at stroke reversal, and then the LEV grows throughout the upstroke. Snapshots from three successive wingbeats for one moth show (A) a transient down-stroke LEV over the thorax and (B) the persistent thorax LEV at mid-upstroke. Relative time throughout each wingbeat is shown based on the approximately 25 Hz (or 40 ms) wingbeat frequency (Fig. S2). When present (white arrow and blue dashed outline), the downstroke LEV is comparable in size to the upstroke LEV. The wing is outlined in gray. Inset shows smoke wire lateral alignment with the moth and flower.

CHAPTER 3

WING FLEXIBILITY AND LEV STRUCTURE

This chapter is formatted for future publication in a physics/fluids journal (e.g. Experiments in fluids). The authors contributing to this work are myself, Marc Guasch, Alexander Gehrke, Jules Richeux, Karen Mulleners, and Simon Sponberg.

Introduction

Leading-edge vortices (LEVs) are widely encountered in airfoil fluid-structure interactions across biological and engineered systems. At high Reynolds numbers ($\mathcal{O}(10^5 - 10^6)$), LEVs are responsible for lift on delta wing aircrafts [237] and helicopter blades [92] as well as on the wings of predatory birds [200, 133]. The time evolution of the LEV depends on the kinematics of the airfoil. For pure translation, the LEV grows as circulation builds up on the wing, but sheds after a few chord lengths of travel [48]. On steadily revolving and reciprocating (or flapping) wings, the LEV still grows due to circulation build up, but it is balanced by Coriolis forces such that the vortex remains attached to the wing throughout the rotation. The same aerodynamic principles apply at the intermediate Reynolds numbers of centimeter-scale flight, but the dynamics of LEV stability are different for engineered and biological wings.

Studies on aerodynamics of LEVs on rotating rigid, flat plates indicate that the vortex structure undergoes bursting for Reynolds numbers $\mathcal{O}(10^3)$ [116, 156]. Bursting is characterized as a local stagnation of the spanwise flow through the LEV core leading to a disruption in the coherence of the LEV along the wingspan. Although the LEV remains attached to the wing, bursting can decrease lift and/or circulation by 10% [28]. During bursting LEV diameter rapidly increases and the loss of coherence causes a reduction in vortex strength. Lower vorticity within the LEV leads to a drop in lift at 90°-100° through the wing sweep.

Despite repeated observation of LEV bursting in engineered systems, losses in LEV coherence have not been observed in biological systems operating at $Re \sim \mathcal{O}(10^3)$, including the hawkmoth *Manduca sexta* [6, 167]. The Reynolds number for hawkmoth flight is between 5000-6000 for many species, but both the aerodynamics and flight behaviors of *M. sexta* are particularly well-established [321, 26, 193, 196, 13, 173]. *M. sexta* also has a wing sweep angle of around $100°$, suggesting that LEV bursting could occur only towards the end of the wingstroke, but biological systems may avoid LEV bursting to ensure robustness across flight behaviors and the difference remains. A 10% reduction in force may seem small, but the loss in lift could be significant for a flying insect if they are operating at a biological extreme, such as maneuvering or evading a predator. Burst LEVs could also impact other aspects of performance, such as the ability to effectively modulate forces or control or the aerodynamic power required per unit of aerodynamic force. Ultimately however, LEVs on hawkmoth wings are not observed to burst under the conditions of prior studies whereas rigid plate wings do have burst LEVs and so there is a gap in our understanding of aerodynamics for centimeter-scale flapping flight.

This incongruence raises several possible hypotheses for the differences in biological and engineered wings. First, flapping insects employ complex three-dimensional wing kinematics to generate flight forces [26]. Wingtips trace out figure-8s along the stroke plane with significant deviation from a pure sweep. The wing sweep can be decomposed into up- and downstrokes. During the majority of the wingstroke, insects maintain the angle of attack until stroke reversal when the wings are rapidly flipped and the direction of wing sweep is reversed. To study aerodynamic effects in engineered systems, wing kinematics are reduced to either steady revolution or idealized reciprocation. While these simplified wing motions produce LEVs similar to those observed on hawkmoth wings, the vortices now undergo bursting. We do not know if hawkmoth wings moving with idealized wingstroke kinematics would also display LEV bursting.

Second, unlike the flat plates used in most aerodynamic experiments, insect wings have

a textured surface due to scales. Surface patterns and texturing have been shown to impact aerodynamics in both biological and engineered systems [326, 275] and the scales on butterfly wings are thought to be beneficial for climbing flight [323]. On experiments with grooved plates, designed to mimic butterfly scales, secondary vorticity was generated within the grooves which enhanced strength of the primary LEV on the wing [69]. Scales on hawkmoth wings could potentially influence micro-airflow near the wing surface preventing the stagnation of flow through the LEV core to avoid LEV bursting.

Finally, in addition to complex kinematics and surface features, hawkmoth wings are also highly flexible. Wing bending and camber during a wingstroke are primarily driven by inertial-elastic forces [104, 238]. Recent work on flexible wings showed that the distribution of flexural stiffness along the wing contributes to force enhancement [244], but we do not know how LEV structure is affected. Experiments quantifying LEV bursting were performed with rigid plates [28, 140] which removes effects due to wing flexibility. Flexible hawkmoth wings may achieve more aerodynamically favorable camber or angle of attack during a wingstroke, compared to rigid wings. Changes in camber lead to changes in the effective angle of attack of the wing, which has a direct impact on LEV formation and force production. Hawkmoths may rely on passive wing bending to prevent LEV bursting during flight. There are two possible, non-mutually exclusive mechanisms for flexibility influencing LEV stability: 1) the deformable wing material allows the wing to adopt a static and aerodynamically favorable wing shape or 2) the dynamic flexing (aeroelasticity) of the wing membrane helps stabilize LEV structure.

To observe if LEVs burst on insect wings even with simplified kinematics, we constructed a 1D rotating flapper that could mimic the flow conditions used in previous bursting experiments on rigid plates [28], but used natural hawkmoth wings instead of a rigid, rectangular wing. We also repeated experiments at the flow conditions relevant for *Manduca sexta* hawkmoth flight to test whether LEV bursting could impact freely behaving animals.

Surface texturing and wing flexibility may both impact LEV structure, but we separate these effects by measuring LEVs on scaled and descaled wings. If scales influence LEV structure, we expect vortices to change size after removing scales. To understand how wing flexibility impacts the LEV, we compare fresh and aged wings. Aging wings results in higher spanwise flexural stiffness which may result in restricted wing deformation during a wingstroke. If stiffer wings promote LEV instability, we expect to measure larger LEVs on aged wings. By comparing wing shapes in fresh and aged states, we can determine how changes in flexibility affect aerodynamic performance of hawkmoths.

To separate the role of shape change change due to differences in flexibility and the dynamics of aeroelasticity we created 3D-printed wing models based on the static shape of the wing at the same instant as LEV bursting. On rigid wings that adjusted pitch angle throughout the wingstroke, it was found that wings with higher aerodynamic efficiency adopted lower angles of attack and high-lift generating wings had higher angles of attack [262]. Hawkmoths are known to use high angles of attack during flight, but wing flexibility allows the geometric angle of attack to vary along the wingspan. By measuring lift forces on statically deformed wing models we can neglect aeroelastic effects and only ask how quasi-static wing shape (quantified by camber and geometric angle of attack) impacts lift production.

Methods and Materials

<u>Animal and wing preparation</u>

We measured leading edge vortex size and spanwise flexural stiffness on hawkmoth (*Manduca sexta*) forewings in two states: fresh and aged. Wings were removed from moths 1-3 days post-eclosion and used in either smoke visualization or flexural stiffness measurements. Fresh wings were used within 1 hour of removal and then left to age (and dry) for 3 hours before repeating the experiment. While wings naturally dessicate with age in moths, preliminary observations and prior research [199] showed that they do so much

more rapidly when removed from the animal. During aging, the wings dry and stiffen causing the mass of aged wings to be lower than fresh wings. We correct for loss of mass by applying spray paint to the ventral side of the wings.

We also performed smoke visualization on fresh *M. sexta* wings with scales removed. After removing the wing from an animal, scales were removed from the dorsal surface using lens paper. Since removing wing scales also reduces wing mass, we apply spray paint to the ventral wing surface to match the original mass of the wing.

Spanwise flexural stiffness (*EI*) measurements

We used the same method as Mountcastle2009 to measure flexural stiffness at mid-span (50%) and 75% span. Fresh and aged wings were paired for all spanwise flexural stiffness measurements. At each spanwise position we calculate *EI* using

$$EI = \frac{FL^3}{3\delta} = \frac{(mg)L^3}{3\delta} \tag{3.1}$$

where m is mass recorded during wing deflection, g is the gravitational constant, L is the distance from the wing root to the point of deflection, and δ is the amount of deflection.

Smoke visualization of the leading edge vortex (LEV)

We visualized the LEV on isolated hawkmoth wings using a smoke-wire in a low-speed wind tunnel. High speed video was recorded at 500 fps (exposure time of $1\mu s$) using two Photron UX100 cameras (equipped with Navitar 50 mm lenses). One camera was placed laterally to capture a side view of the wing and LEV during a wingstroke and the other was mounted above the wind tunnel at approx. $45°$ to visualize wing shape. Overall, 20 wings were used to measure LEV size. Paired experiments were performed for 10 fresh and aged wings and LEVs on 10 descaled wings were measured separately.

For all wings, two experimental flow regimes were tested. The first was designed to match flow conditions known to produce LEV bursting on a flat plate in previous work

Medina2016 with Reynolds number $Re \sim 2500$, advance ratio $J = 0.21$, and aspect ratio $AR = R/c = 2$. Advance ratio is defined as the ratio between the freestream flow speed and the rotational speed of the motor. The second flow regime matches the flight conditions for *M. sexta* with Reynolds number $Re \sim 5000$, advance ratio $J = 0.11$, and aspect ratio $AR = R/c = 2$. Both the freestream wind speed in the tunnel and the rotation speed of the motor are adjusted to switch between flow conditions because of constraints on maintaining Re with sufficient translational flow to pass the smoke over the wing.

Wings were rigidly mounted to a stepper motor centered in the tunnel. The 3D-printed wing mount prescribed the geometric angle of attack (AoA) at the wing root as 40°, the expected AoA for hawkmoths during mid-wingstroke when the wing angle is constant [228]. Smoke visualization of the LEV was captured at four spanwise positions along each wing (30%, 40%, 50%, and 60%) during a simplified wingstroke using a double-coiled 0.25 mm nickel chromium (nichrome) wire coated with Protosmoke train smoke oil (MTH Trains). The smoke-wire was mounted on a frame with a micromanipulator, so the horizontal position of the smoke plane could be aligned with different points along the wingspan. Two halogen lamps illuminated the streaklines over the wing, with one lamp in a forward-scattering arrangement for the lateral camera and the other using back-scattering for the overhead view.

The wingstroke matched the trapezoidal velocity profile used in [28] with the rotation speed adjusted for motion in air. The addition of forward air velocity due to the freestream wind tunnel speed allows for Reynolds number matching at wing revolution frequencies below the natural wingbeat frequency of *M. sexta* (i.e. below 25 Hz). In both flow conditions, LEVs were visualized at 90° through the wingstroke, where LEV bursting was observed previously on rigid wings.

<u>3D wing shape extraction</u>

To quantify differences in flexibility between fresh and aged wings, the 3D shape of each wing was extracted using XMALab [299] and defined by tracking 10 points on each wing:, the wing root, wingtip, and 4 points along the leading and trailing edges. Wing shape was extracted from the same frame as LEV visualization to capture the static deformation associated with the observed vortex size and structure. Extracted wing shapes are used to quantify the changes in deformation for fresh and aged wings and generate 3D models of wings for force measurement.

The 3D-printed wing mount, included a rigid plane at the prescribed angle of attack of the wings was also tracked in XMALab as a reference plane.

Changes in wing shape were quantified using geometric angle of attack (AoA) and camber, defined as the distance between a rigid chord line and the wing surface at each spanwise position. Since AoA is set to $40°$ by the 3D-printed wing mount we examined how the angle changes along wingspan from root to tip.

<u>Force and circulation measurements</u>

Extracted 3D wing shapes were sent to collaborators in the Unsteady Flow Diagnostics lab (UNFoLD) at the Swiss Federal Institute of Technology Lausanne (EPFL). The wing shapes were 3D-printed and used to measure differences in force (in a fluid channel) and circulation between fresh and aged wings.

Results

<u>Wing spanwise flexural stiffness increases with wing aging</u>

We found spanwise flexural stiffness $EI \sim \mathcal{O}(10^{-5})$ (Nm^2) for *M. sexta* wings, which is consistent with previous results with wings aged for 12-24 hours [199]. Across all 10 wings, flexural stiffness increases after aging, but the differences are smaller than previ-
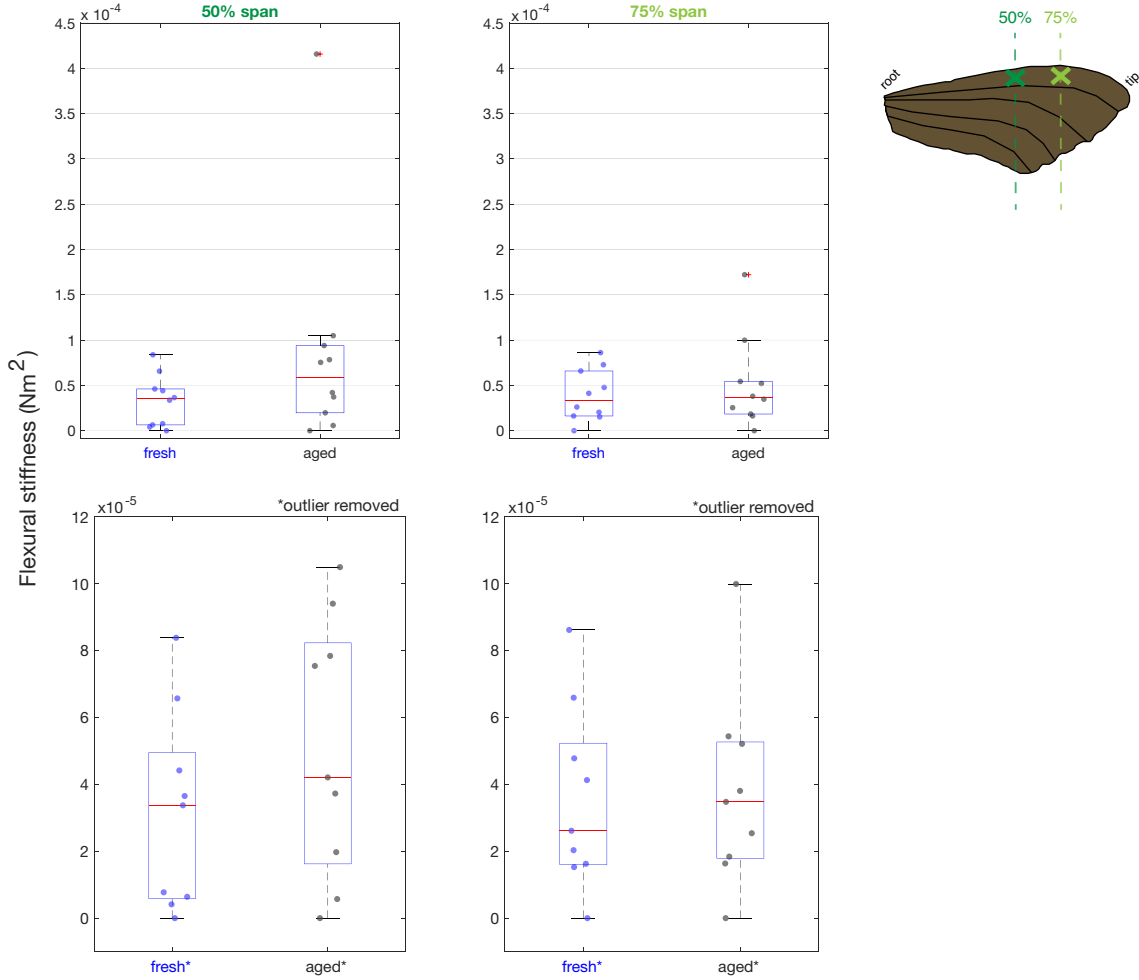
Figure 3.1: Flexural stiffness measured at 50% span and 75% span.

ously found due to shorter aging times in our experiment. At 75% along the wingspan, mean *EI* increases by 30.8% from 3.9 x 10^{-5} for fresh wings to 5.1 x 10^{-5} for aged wings (Figure 3.1, right), but the change is not statistically significant using a paired Student's t-test ($t = -0.9401; P = 0.3717$). Following the approach of [199], we performed paired t-tests for individual wings and EI at 75% span increased significantly for six out of ten wings ($t = -6.2219, -8.1743, -6.9365, 3.2715, 4.6851, -8.0006; P = 0.0084, 0.0038, 0.0061, 0.0467, 0.0184, 0.0041$). [199] found statistically significant increases in EI, but only measured values from three hawkmoth wings, suggesting our results may be muddled from including a broader range of biological variation.

At 50% span mean *EI* more than doubles after aging from 3.3 x 10^{-5} to 8.7 x 10^{-5},

a 163.6% increase in stiffness (Figure 3.1, left) that is not statistically significant ($t = -1.5315; P = 0.1600$). After removing one outlier wing, the change in EI at 50% span becomes statistically significant (Figure 3.1, lower plots, $t = -0.2446; P = 0.0249$). Flexural stiffness varied for individual wings with four out of ten wings showing a significant increase in EI at 50% span ($t = -5.2091, -4.0080, -9.0072, -16.4137; P = 0.0138, 0.0279, 0.0029, 10^{-4}$).

LEVs burst on hawkmoth wings, with simplified kinematics
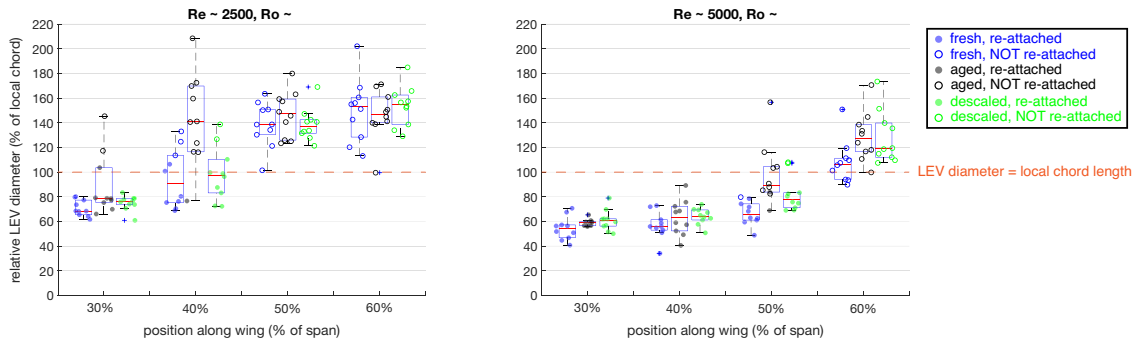
Figure 3.2: Smoke visualization of relative LEV diameter across span for all wing conditions: fresh (blue dots), aged (black dots), descaled (green dots). Points filled in indicate the re-attachment streakline was present and un-filled points indicate re-attachment was lost.

Previous smoke visualization and 2D PIV results suggested that leading-edge vortices (LEVs) on hawkmoth wings do not burst at 50% span [6]. At 30% along the wingspan, all LEVs included a distinct re-attachment streakline and relative LEV diameter was less than the local chord length. For $Re \sim 2500$, relative LEV diameter was between 50%-100% of the local chord length and for $Re \sim 5000$, LEV diameter remained between 50%-60% of chord length at 30% span (Figure 3.2).

Further out along the wing our results show that for both $Re \sim 2500$ and $Re \sim 5000$ the LEVs on hakwmoth wings are burst. No re-attachment streaklines are discernable at 60% span and relative LEV diameter also exceeds the local chord length for all wings (Figure 3.2).

Additionally, LEV structure is not affected by scales on hawkmoth wings. For both flow conditions, the LEVs formed on descaled wings match LEVs found on fresh wings with scales (Figure 3.2). Relative LEV diameter is consistent across span with and without scales.

LEV re-attachment point moves rootward on the wingspan for aged wings

At the higher Reynolds number, fresh wing LEVs have a distinct re-attachment streakline out to mid-span in all wings but one (wing #9). Excluding wing #9, after the wings stiffen with age the re-attachment streakline is only distinct out to 40% span (Figure 3.3, bar plots, right). The loss of a re-attachment streakline is a qualitative indicator of where the LEV core flow is stagnating along the wingspan. Drying and aging of the wings causes the stagnation point of the LEV to move rootward along the wingspan by at most 10%.

In the second condition, ($Re \sim 2500$ and $J = 0.21$), fresh wing LEVs have a distinct re-attachment streakline out to 40% span in most wings, but three wings only have re-attachment at 30% span. For the wings with re-attached LEVs at 40%, the streakline is lost after aging (Figure 3.3, bar plots, left). For the majority of wings, the same trend holds that aging the wings forces the stagnation point towards the wing root. Unlike the hawkmoth flight condition, LEVs at the lower Re and higher J are decoherent across 60%-70% of the wingspan.

The difference in relative LEV diameter between fresh and aged wings shows an overall increase in LEV size, especially at the spanwise position where re-attachment is lost (Figure 3.3, top row). When re-attachment was lost, LEV diameter was measured to a visible inflection point in the streakline where the LEV merges with the trailing-edge vortex (TEV). At $Re \sim 2500$, matching conditions from [28], aged wings lose LEV re-attachment by 40% span and LEV relative diameter also increases by 40%-60% on average (Figure 3.3, left). For the hawkmoth condition ($Re \sim 5000$), LEV re-attachment is lost at 50% span on aged wings and mean relative LEV diameter also increases by about 40% (Figure 3.3,

right). Although aging time and conditions were controlled during experiments, wings experienced differential drying due to biological variation in initial wing stiffness and other possible effects. The spread in the LEV size data reflects that all wings did not dry and age identically.

Aged wings show changes in camber and geometric angle of attack (AoA)

Across all wings, maximum AoA occurs between 50%-60% span and the peak is affected by wing aging. For half the data, wings show a reduction in AoA at midspan after aging, but this trend is reversed in the other half of the data (Figure 3.4, top two rows). While there are distinct differences in shape between fresh and aged wings, geometric angle of attack is not the dominant effect because results do not generalize across individual wings. Since aging the wings produces variable shape results, we next focused on one particular wing (wing 12) with large differences in shape in fresh and aged conditions and quantitatively compare the differences in camber and AoA to the development of circulation and isolate the effects of rigid shape.

When wing 12 was fresh, AoA varied along the span similar to how AoA is designed on engineered wings, with an increase in AoA beginning at 30% span and growing until a maximum AoA under $50°$ is reached at 60% span. After midspan, AoA rolls off back to $40°$. After aging, the variation in AoA is flattened, especially between 30%-60% span where AoA is maintained below $45°$ (Figure 3.4, bottom left).

Camber across the wing supports the spanwise AoA results and also shows differences in chordwise shape between wing 12 fresh and aged. Fresh wing 12 has a large positive camber between 30%-70% span followed by a small region of negative camber along the wingtip. After aging, wing 12 shows less deformation over the entire wing surface and the maximum positive camber at midspan is around 0.04 cm, half of the fresh wing value (Figure 3.4, bottom right). Additionally, the angle of the leading edge of the wing with the horizontal span axis is reduced (which may be described by changes in dihedral angle).

The coefficient of lift was calculated for wing 12 throughout a full 180° sweep. Averaging over the constant velocity portion of the wingstroke, the aged wing produces 13% less lift than the fresh wing (Figure 3.5, left and middle). We also calculated the LEV circulation across span and find that the fresh wing generates higher circulation (Figure 3.5, right). The increase in circulation occurs between 50%-80% span, the same spanwise position where LEV diameter increased in smoke visualization, with little difference between fresh and aged wing states elsewhere on the wing.

Discussion

LEV bursting is a relevant phenomena for flapping insects

Despite extensive investigation of LEV development across insect species, it was not clear whether LEV bursting occurred on real insect wings, especially for hawkmoths that fly in the range of Reynolds numbers where bursting is observed on rigid wings. Previous investigations into LEV structure on hawkmoth wings showed a coherent vortex extending from the wing root toward the tip, eventually merging with the tip vortex [172, 41, 138]. For *M. sexta*, the LEV was further classified as extending continuously across the wingspan, joining the wingtip vortices [6]. The observations for this conclusion came from smoke visualization of tethered hawkmoths only at midspan and over the thorax. Restricting the spanwise extent of LEV visualization may have hidden bursting effects.

Only the forewing was used in our current experiments, but freely flying hawkmoths use both fore- and hindwings during flight. Unlike the independently actuated wing pairs of dragonflies [65], hawkmoth hindwings are attached to the forewings such that the leading edge of the hindwing does not experience flow separation. Instead the hindwing essentially acts to extend the chord length of the forewing. All previous classification of the LEV on real hawkmoth wings was performed with the hindwing present. The smoke visualization

54

at midspan suggesting hawkmoth LEVs were not burst [6] was supported by Schlieran photography of the LEV. The LEV appeared to grow smoothly in diameter across the wingspan, without obvious signs of decoherence or bursting [138], but flow within the core was not resolved. Since the hindwing increases the effective chord length, LEVs on fore- and hindwing pairs could potentially grow to larger diameters without bursting.

We observed burst LEVs on fresh and aged hawkmoth wings in both flow conditions. The first flow condition was matched to previous work where burst LEVs were reliably produced at Re 2500 [28] and the second is tuned to hawkmoth flight at Re 5000. LEVs on *M. sexta* wings may not have been classified as burst previously because most studies define LEV structure only at mid-span and our results emphasize the importance of defining the LEV across span. However, it is still not known what impact a burst LEV would have on a freely behaving insect. In hover, a 10% reduction in force could have a negligible effect on aerodynamic performance, but the same loss during a maneuver could result in failure. While we only calculated lift force in our current experiments, aerodynamic efficiency and power requirements for flight are also impacted by LEV bursting, with more efficient wings often operating at lower angles of attack [168].

The current study uses simplified wing kinematics of a single 180° wing stroke, that is repeated to visualize multiple spanwise locations along the wings. Hawkmoths and other flapping insects using reciprocating wing motions where the wings will pass through wakes of previous wingstrokes. There is experimental evidence that flexible wings either increase [199, 103] or decrease [245] the induced downwash in the flow. Resolving the effects of wing flexibility on the induced downwash is important for understanding how flying insects maintain LEVs while interacting with disrupted air from previous wingstrokes. During stroke reversal, the previous LEV is shed and new LEV is formed, but we do not know how the build-up of LEV ciruclation is affected by interaction with a steady downwash. If flexible wings enhance the induced downwash, then the initial LEV circulation generated at stroke reversal may be reduced, leading to lower total lift generation during the wingstroke.

Our spanwise flexural stiffness results are consistent with from previous work [199] for *Manduca sexta*, but spanwise flexural stiffness ranges from $10^{-7} - 10^{-3}$ across insect species [187]. Flexural stiffness is not the only determinant of wing shape, but all our aged wings showed shape changes and were stiffer than in the fresh state, implying that stiffness influences wing deformation during flight. The exponentially decreasing spanwise stiffness distribution in insect wings can enhance lift and thrust compared to uniformly flexible wings [181, 244]. Given the connection between wing shape and aerodynamic performance, the broad range of spanwise flexural stiffness employed by biological fliers suggests diversity in LEV structure and dynamics across insect species. The use of LEVs by different insect species across diverse wing shapes emphasizes its robustness as an aerodynamic mechanism.

Changes in LEV structure not impacted by micro-texturing of scales

Surface roughness and micro-texture can influence flow around objects locally and globally [25]. Dimples on golf balls form local separation bubbles that result in a global reduction in drag, compared to smooth spheres, that persists across Reynolds number [275]. Scales in shark skin have also been shown to reduce drag through the formation of embedded vortices [58]. The scales on insect wings may operate in a similar way by increasing skin friction and dissipating energy within the LEV, causing induced drag to decrease.

The aerodynamic importance of wing scales has precedence, but the causes are unclear. Removal of scales on butterfly wings reduced climbing flight efficiency and strengthened secondary vorticity but had little effect on total LEV circulation [323, 69]. Scales on butterfly wings increase vorticity in the LEV, but since total circulation is not changed, LEV size may not be impacted by changes in surface roughness. Our smoke visualization results show very little change in relative LEV diameter across span with and without scales. This suggests that scales on moth wings behave similarly to scales on butterfly wings. Further experiments would be needed to confirm if moth scales also increase secondary vorticity

near the wing surface, leading to increased LEV strength.

Static wing deformation highlights importance of geometric angle of attack and camber for aerodynamic performance

While smoke visualization showed consistent qualitative differences in LEV structure across fresh and aged wings, forces measured on 3D-printed wing shapes revealed significant variation across individual wing pairs. Static snapshots of wing deformation extracted for each wing pair confirmed that aging the wings induces a strong shape change, but the high variability across wing pairs likely arises due to different initial stiffness in the fresh wing state and differential rates of desiccation. Previous measurements of spanwise flexural stiffness change between fresh and aged wings allowed the wings to dry for 12-24 hours [199] and the shorter drying times in our current study may have resulted in more variable shape changes. [199] also observed higher spanwise bending in fresh wings, while our results were dependent on each wing pair.

Deformation in insect wings was shown to be driven by inertial-elastic forces more than fluid-dynamic forces [238, 104] and we found that the effects of dynamic wing shape on aerodynamic force is not well described using static snapshots of wing deformation. We also saw that LEVs at higher Reynolds number are stabilized along more of the wingspan by enhanced Coriolis forces, but bursting still occurs past 50% span. Although inertial-elastic forces dominate wing bending, changes in wing shape influence LEV structure. Since the LEV also interacts with the freestream airflow, there could be a potential interaction in the LEV between shape-driven and aero-elastic effects.

In both flow conditions, more flexible fresh wings generated smaller LEVs than aged wings. Experimental and numerical models of fluid-structure interaction with compliant wings suggest that flexible wings produce stronger LEVs and delay the onset of vortex breakdown (or bursting) [65, 103]. Smaller vortices can be stronger, since vorticity is contained within a smaller area.

Taking wing 12 as an example, the fresh wing forms an LEV smaller than the local chord length out to 50% span with lift and circulation maxima located around 50%-60% span. After aging, the LEV increases in size and lift and circulation are reduced. Combining these results suggests that more flexible wings generate stronger LEVs, since increases in vortex size often accompany losses in strength. Additionally, computational models provide evidence that flexible wings achieve higher peak lift [215, 103, 171] which agrees with our result that C_L decreases for wing 12 after aging when the wing is stiffer. Future flow visualization experiments are necessary to determine if the smaller vortices on fresh hawkmoth wings are also stronger and capable of longer growth timescales.

Lift on complaint wings is shown to analytically depend on angle of attack, spanwise bending, and the rate of wing deformation [171, 247] with a butterfly-based model. Therefore, wing twist might be more influential than camber on aerodynamic performance [215]. Our experiments simplify the fluid-structure interaction with flexible wings by neglecting dynamic wing deformation. We still capture a link between C_L and shape change, defined as the geometric angle of attack, for each wing pair. Camber and geometric angle of attack are both important for understanding shape change and our experiments did not separate their effects on aerodynamic force. Explicit numerical investigation of how positive and negative camber impact LEV structure on fruit fly wing models found that 5%-15% negative camber shifted the spanwise location of vortex breakdown towards the root [311]. Fresh and aged wings are both capable of camber and our results confirm that shifts in camber cause the location of LEV bursting to shift along the span, however we did not extract a consistent trend for all wings with positive or negative camber, regardless of fresh or aged state. More work is needed to mechanistically describe how spanwise bending, camber, and geometric angle of attack influence the formation and stability of leading edge vortices on insect wings.

Investigating the effect of wing flexibility on LEV structure and dynamics we showed that flexibility does not prevent LEV bursting, but the degree of shape change influences

both LEV size and location of bursting along the wingspan. Our current understand of LEV dynamics assumes that for given wing kinematics the temporal evolution of the LEV is the same, but our results show that aeroelasticity introduces variation the LEV development. Understanding the pathway between shape change and aerodynamic performance is beneficial not only to resolve biomechanical questions in insect flight, but also for applications to engineered wing systems.
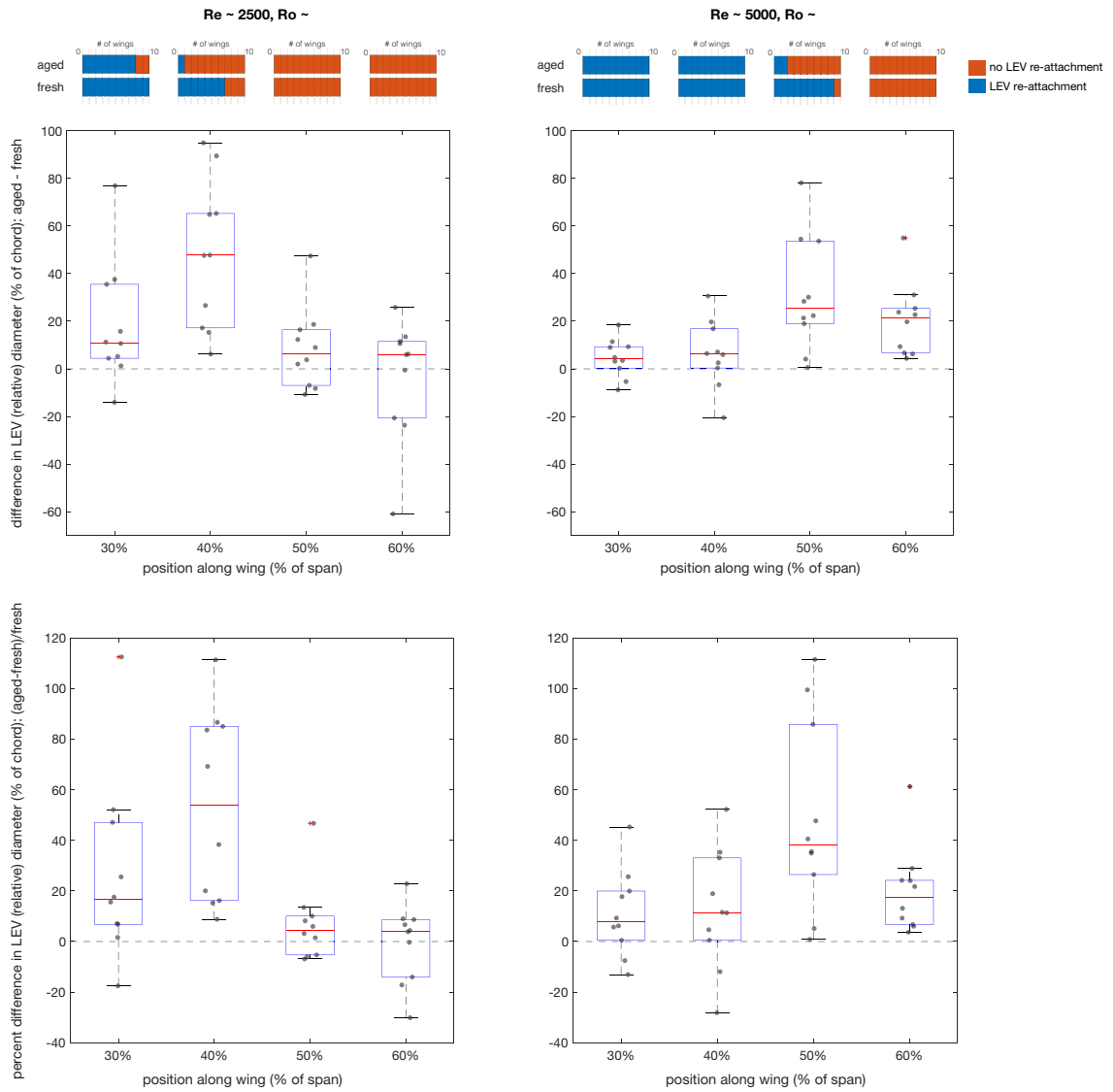
Figure 3.3: Difference in relative LEV size and re-attachment for fresh and aged wings. Bar plots along top row indicate whether the number of wings with and without re-attachment. Top row: absolute difference in LEV size (as percent of local chord length) between fresh and aged wings. Bottom row: percent difference in LEV size between fresh and aged wings.
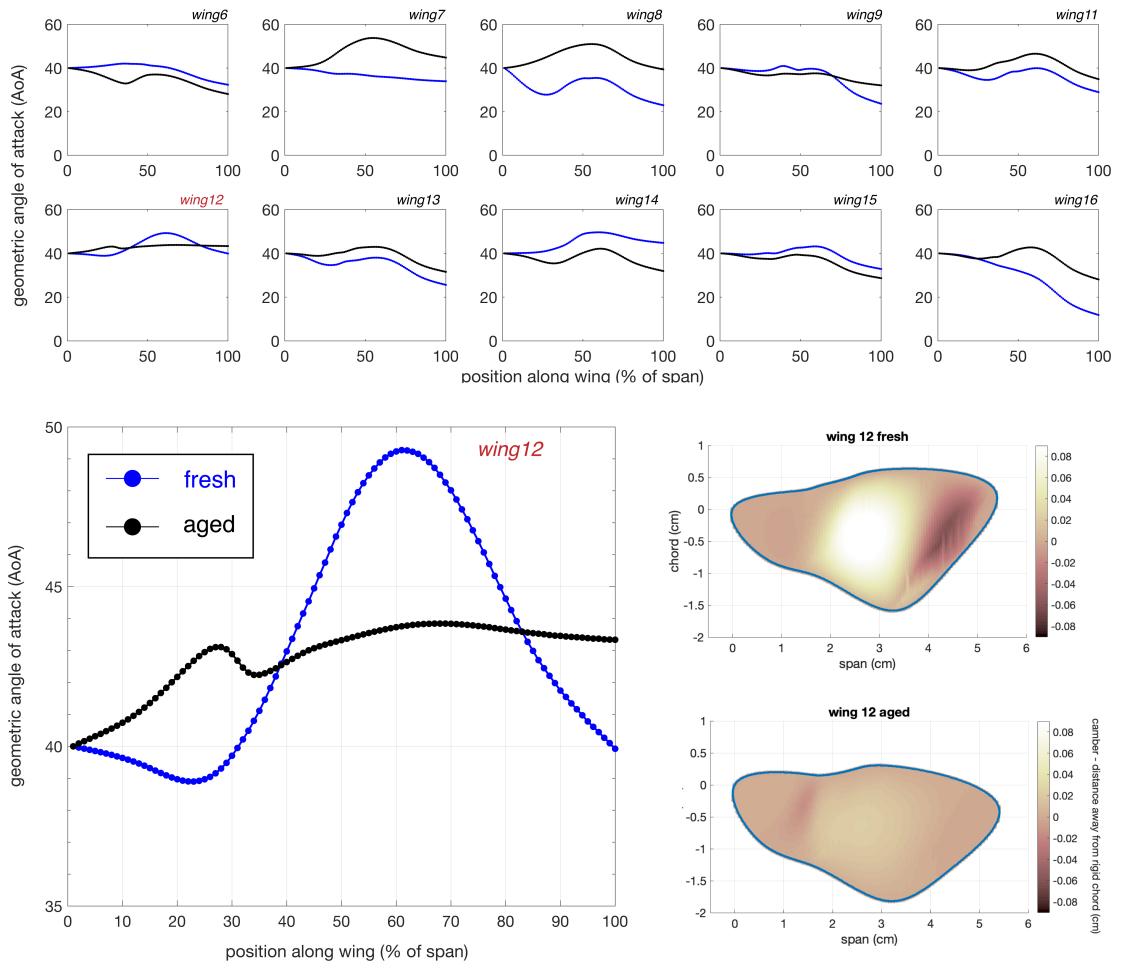
Figure 3.4: Change in geometric angle of attack (AoA) and camber (wing deformation) for wing 12 fresh vs. aged. The top two rows show the variation in geometric AoA across all wing pairs. The bottom row shows geometric AoA and camber for only wing 12.
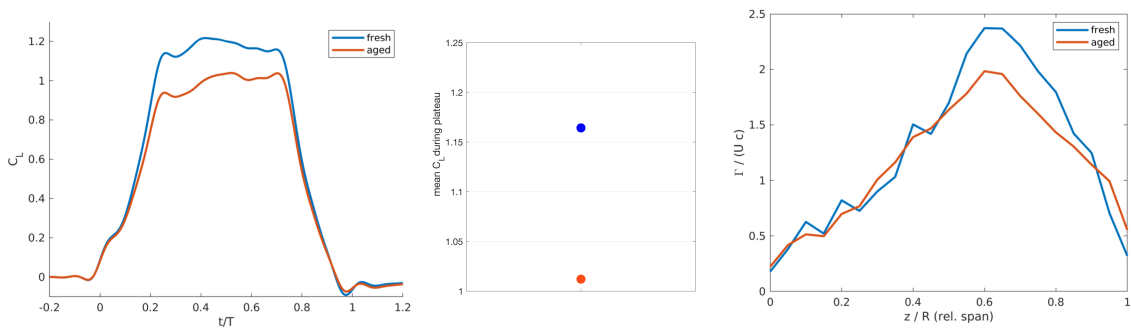
Figure 3.5: Lift and circulation for wing 12, fresh vs. aged.

61

CHAPTER 4

NATURAL FLOWER WAKES AND THEIR IMPACTS ON POLLINATORS

This chapter is formatted for future publication in an interdisciplinary or biology journal (e.g. Royal Society Interface, PLoS One). The authors contributing to this work are myself, Chris Crowley, Usama Bin Sikandar, Brett Aiello, and Simon Sponberg.

Introduction

Interactions between plants and pollinators occur in unsteady fluid environments. Flying pollinators, including bees, moths, and birds, encounter gusts while navigating cluttered visual environments as they forage for host plants [102]. The effects of wind gusts on the aerodynamics of pollinators has recently been explored for animals and microair vehicles (MAVs) [113, 135]. In addition to wind gusts, many studies are now investigating how other types of unsteady airflow impact the aerodynamic performance of flapping fliers. Although these experiments record freely behaving animals during flight, the unsteady environment is generated artificially so the flow characteristics are known. The natural environments for flying pollinators are diverse, but many are crowded by flowering plants, shrubs, and small trees. The fluid environment the flowers create locally through their interaction with air as well as the implications of this fluid flow for both plants and their pollinators remain largely unexplored.

Natural wind in a crowded environment may be turbulent, since energy in the flow is dissipated with each fluid-structure interaction. Birds, bees, and MAVs display reduced flight performance in turbulent flow environments [141, 282, 114, 40, 230]. In more structured unsteady flow, such as a tornado vortex [14] or von Karman street [264, 179], hawkmoths and bees have shown frequency-matching behavior reminiscent of the Karman gait in trout [33]. Hawkmoths, particularly *M. sexta*, are known as highly maneuverable fliers

capable of tracking flower motions up to 14 Hz, but tracking error increases in the wake of an artificial flower [137, 293]. While we are beginning to understand the effects of unsteady flow on aerodynamics, little is known about the characteristics of flow in natural environments for centimeter-scale pollinators [126, 91]. The flow regime for flower-foraging pollinators is created by fluid-structure interaction between the wind and host plants.

Plants must be robust enough to wind gusts to remain rooted, but flexible enough to adapt to changes in the surroundings [287, 20, 205]. Many plants rely on wind dispersal for pollination, but others require physical transfer of pollen to another animal that will visit another plant of the same species to pollinate [132, 84]. While the hawkmoth *Manduca sexta* hover-feeds from various trumpet-shaped flower species, pollen is deposited on the proboscis so the hawkmoth can carry it to the next patch of flowers. Hover-feeding and tracking behaviors in hawkmoths are well-studied, but often assume the surrounding air is quiescent or uniform [17, 154]. However, smoke visualization of the wake downstream of a robotic flower revealed unsteady vortex structures were shed from the rigid petals [293]. Although natural petals are more flexible, plants withstand wind through stem bending and hawkmoth-pollinated flowers maintain their trumpet-shaped morphology during flower movement. Even considering steady freestream air, we do not know whether the near wake of natural flowers has unsteady but regular features or if the local air is turbulent.

We characterized the flow downstream of different hawkmoth-pollinated flowers using 2D planar particle image velocimetry (PIV) in a low-speed wind tunnel to determine whether flower wakes are turbulent. The mean flow is subtracted out and analyzed separately from fluctuations. We expect the mean flow to be dominated by a re-circulation zone, which is common for bluff-body interactions with steady airflow. If flower size is the main determinant of wake structure, then the size of the re-circulation bubble should increase with flower diameter. The dominant fluctuations in the flower wakes are analyzed by performing partial orthogonal decomposition (POD) on the velocity. For turbulent wakes, model decomposition may not be successful because kinetic energy is distributed across

many modes. If flower wakes contain periodic or similarly time-dependent features, POD should capture dominant fluctuations within 3-5 modes. To assess how the airflow in flower wakes impacts pollinators, we extracted wake velocities along an estimated wingstroke plane and applied the values to a blade-element model (BEM) to calculate aerodynamic forces for a hovering hawkmoth, *Manduca sexta*. Although a freely-behaving hawkmoth can actively respond to changes in airflow, the BEM hawkmoth uses the same kinematics in all flower wakes. If aerodynamic forces in the flower wake are reduced, compared to flight in the freestream, this suggests that hawkmoths would need to modify their wing motion to enhance force production. However, if aerodynamic forces are the same in the flower wake and in the freestream, then flower wakes may not pose flight challenges to large pollinators like *Manduca sexta*.

Methods and Materials
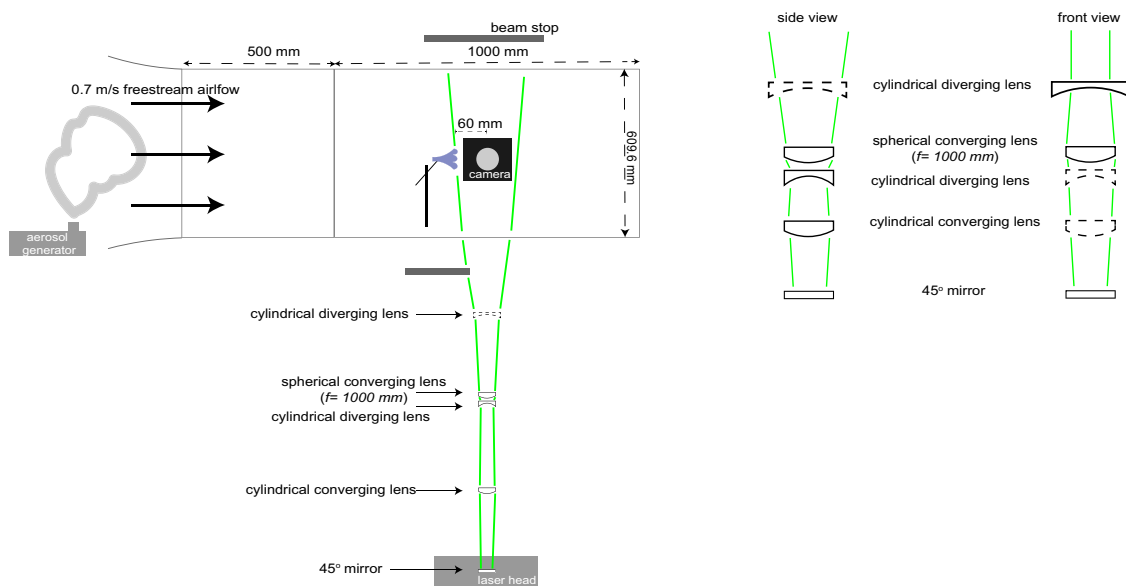
Figure 4.1: Methods figure.

Flower collection and species

Three species of hawkmoth-pollinated flowers (Figure 4.2) were considered in this study and flower sources varied depending on species. We obtained 15 *Datura metel* and 15 *Nicotiana alata* plants from White Flower Farm (Litchfield, CT, USA). *Petunia* plants were sourced from multiple local commercial nurseries around Atlanta, GA. Multiple *Petunia* species and hybrids were used including Ruellia Mayan Mexican Petunia, Supertunia Bordeaux Petunia hybrid, Supertunia Lovie Dovie Petunia hybrid, and Supertunia Mini Vista Hot Pink. All flowers were maintained in a temperature-controlled greenhouse located on Georgia Tech campus in Atlanta, GA. Flowering occurred between February-June 2020 and blooms were only removed from the plant 5-10 minutes before an experiment to limit material changes to the petals.

Flower size determination

Prior to data collection a reference image with the mounted flower and a ruler is saved to calibrate flower size and particle displacements. For each individual flower, the diameter is measured in ImageJ as the major axis of an ellipse drawn to bound the flower petals. Reynolds numbers based on flower diameters are $\mathcal{O} \sim 10^3$ with specific values listed in Figure 4.

Flower species	Diameter range	Reynolds number range
Petunia	27-58 mm	1218-2616
Datura	79-109 mm	3563-4916
Nicotiana	42-66 mm	1894-2977

65
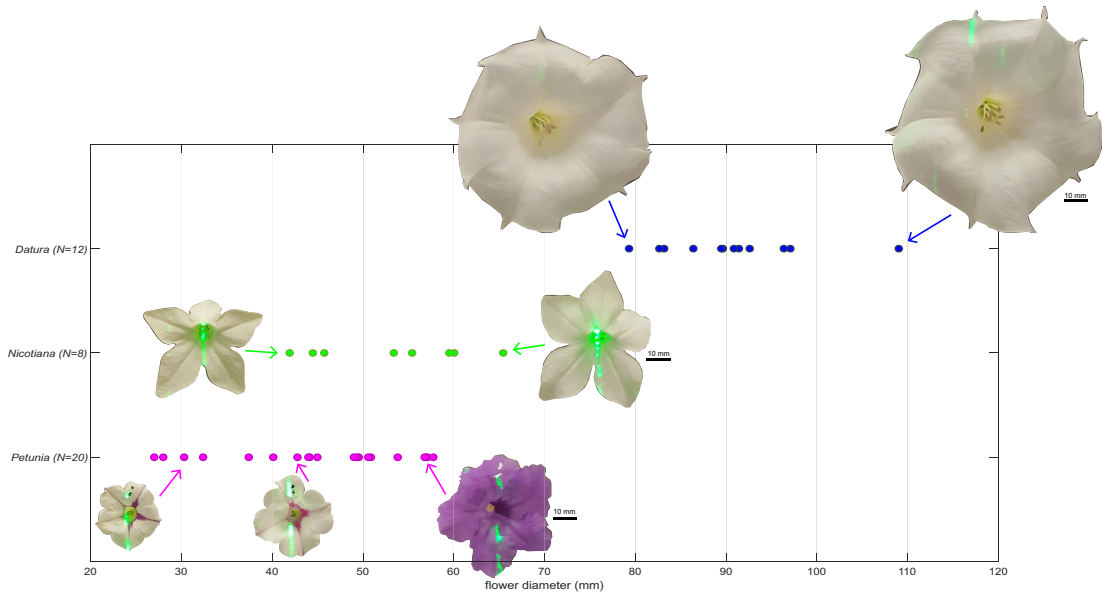
Figure 4.2: Flower size, N=40 total.

Data collection

Experiments were performed in an open-circuit wind tunnel (see Figure 4.1 and for technical details see [293]) at 0.7 m/s. Flowers were rigidly mounted in the test section of the tunnel with the front of the flower facing downstream and oriented at approximately 90° to the freestream airflow. The laser sheet was aligned with the center of the nectary and flowers were placed slightly upstream of the beam to limit flower reflectivity. The 2D light sheet was generated using a Photonics dual-head pulse Nd:YLF laser (DM30-527-DH, Photonics Industries International, Inc., Ronkonkoma, NY, USA) with beam shaping optics designed to first correct the divergence of the incident beam and then to expand the beam to a 2 mm thick light sheet. We centered the light sheet in the wind tunnel to capture streamwise (u) and vertical (v) velocity components. Since the tunnel is open-circuit, both the test section and surrounding room were seeded with DEHS (Di-Ethyl-Hexyl-Sebacat 5.0, LaVision, $< 1\mu$m mean particle diameter) particles using a LaVision Aerosol Generator placed at the inlet of the wind tunnel.

Videos of the illuminated flow field were recorded using a single Photron UX100 with a

66

50 mm lens. The frame rate of the camera and the laser pulse were synchronized at 1 kHz. We also aligned the exposure time with the duty cycle of the laser to capture maximum light per image (laser output 60 mJ per pulse at 1 kHz).

<u>Image pre-processing (MATLAB) and velocimetry (PIVLab) – MATLAB</u>

Raw particle images are saved as uncompressed tiffs (resolution: 1280 x 1024 px). Signal-to-noise ratios (SNRs) in raw images are low due to high ambient lighting during recording, so the MATLAB Image Processing Toolbox is used to reduce background noise and enhance intensity of the particles. Higher SNRs improve the accuracy of the correlations in PIVLab.

First, we perform 2D adaptive noise-removal Wiener filtering with the built-in MAT-LAB function, `wiener2`. The Wiener filter estimates the local image mean and variance over a 3 px by 3 px neighborhood and applies a low-pass filter to the image, assuming Gaussian white noise. Next, we subtract a sliding minimum value, again looking over a 3 px by 3 px window in each frame. Finally, the entire image intensity is scaled by a constant to enhance the signal of the particles. Since the background noise has been removed, scaling the intensity of the whole image now results in higher SNR. The processed images are then exported and saved as tiffs.

We post-processed our particle images using the most recent version of the MATLAB toolbox PIVLab [315, 127, 111]. Since data processing occurred over many months, there were minor updates to PIVLab during this time, so all data was processed using versions $2.36.4 - 2.46$. All image processing was done prior to loading in PIVLab, but the flower and non-beam areas of the FOV were masked for all frames using the built-in GUI. We used multi-pass FFT window deformation technique with a Gaussian sub-pixel estimator. During the experiments, the particle density and intensity fluctuated due to the open-circuit tunnel design and variable flower reflectivity. As a result, the number of passes and correlation window size was slightly tuned for each set of images, but window overlap was maintained

at 50% for all passes. Higher quality images required fewer passes with smaller interrogation windows: the first pass used a 64 x 64-pixel interrogation window and the third pass used a 16 x 16-pixel window. The lowest quality images required four passes: the first pass used a 128 x 128-pixel interrogation window and the fourth used a 32 x 32-pixel window. Following the PIV analysis, data was individually calibrated and outlier vectors were removed based on velocity limits, standard deviation, and local median thresholding.

Flower wake flow field analysis

Velocity components and vorticity for each flower flow field were calculated in the MATLAB PIVLab toolbox before exporting data as *.mat* file. Since the final size of the correlation windows changed, the number of vectors describing the FOV varied based on the flower. The finest vector resolution considered was 127 x 159 vectors (corresponding to a final pass with a 16 x 16-pixel correlation window with 50% overlap) and the coarsest resolution was 63 x 79 vectors. The vector fields are spatially smoothed using the MATLAB function `movmean` with a sliding window of 10 vectors before the mean flow over time is calculated using `mean` to average over all frames, (2910 frames for all data). Mean flow fields are visualized as vector fields and heat maps for individual velocity components and vorticity.

Power spectral density (PSD) and proper orthogonal decomposition (POD)

We calculated the power spectral density (PSD) for all flowers to identify characteristic timescales of fluctuations in the flow. For each flower, the temporal FFT and PSD calculations are performed on each individual vector in the arrays for velocity components ($v_x = u$ and $v_y = v$) using a Hamming window and $dt = 1$ kHz. Vectors were (spatially) ensemble averaged to generate a single spectra for each flower which was then normalized to the total energy. To spatially describe flow structures and understand the temporal variation in the flower wakes, we performed proper orthogonal decomposition (POD) on the combined u-

and v- velocity components [271, 276]. The first three to five modes are combined and compared to the actual fluctuations in the flow. A linear combination of the first two POD modes is visualized and described for a subset of all flowers: for 2 *Datura*, 2 *Nicotiana*, and 6 *Petunia*.

Stroke plane velocities and blade-element modeling (BEM) of aerodynamic forces

We extracted velocity vectors from the mean flow fields along a hawkmoth stroke plane and used the values as input wind velocites to an aerodynamic blade-element model [74]. Hover-feeding distances for *Manduca sexta* range from 2-10 cm downstream of flowers [241, 139, 293]. In this study, we chose a constant feeding distance of 5 cm downstream of the flower which is within the biological range and ensures that points along the stroke plane do not cross into the masked region of the flow. The center of the stroke plane is placed 5 cm downstream of the flower mask and aligned with the vertical midline of the flower. The same feeding distance and stroke plane were used for all flowers.

M. sexta flight kinematics were previously measured at multiple freestream wind speeds and the stroke plane angle increases from approx. 15°-20° at 0 m/s to approx. 20°-30° at 0.9-1 m/s [193]. Since our freestream wind speed is 0.7 m/s, we chose a constant stroke plane angle of 20°. Assuming a wing length of 5 cm, the stroke plane extrema (points of dorsal and ventral stroke reversals) are defined using sine and cosine of the stroke plane angle.

After the stroke plane is defined, velocity vectors are extracted as a 1D array, starting with velocity at dorsal stroke reversal and ending with velocity at ventral stroke reversal. We assume that the wing encounters the same mean flow during the downstroke and upstroke and convert the spatial array of velocities into a temporal array of velocities throughout a symmetric wingstroke. These velocities are used to update the incoming wind speed in the BEM during a wingstroke. The BEM applies the wind speeds to measured *M. sexta* kinematics [193] to calculate within-wingstroke and stroke-averaged aerodynamic forces.

69

To examine the impact of the flower wake on flight forces, we compare outputs of the BEM for each flower wake to two steady flow conditions: (1) 0 m/s freestream for ideal hovering and (2) 0.7 m/s freestream. The comparison to 0.7 m/s shows how flight forces change when an pollinator transitions from the freestream into the flower wake.

Results

<u>Mean flow is dominated by a re-circulation zone in the near wake</u>
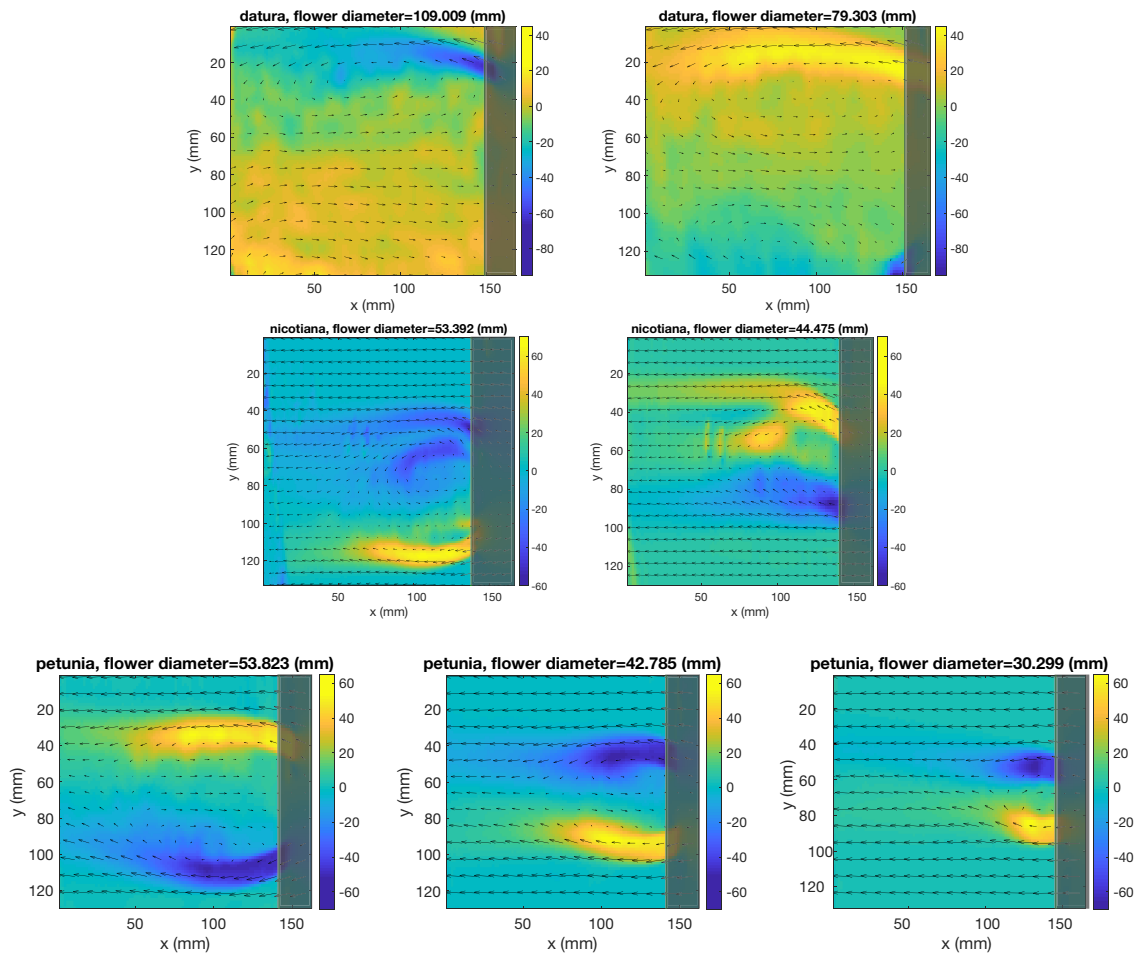
Figure 4.3: Mean flow vector fields and vorticity heat maps. The mean flow for all flower species is dominated by a downstream re-circulation zone. Flow around the petals generates vorticity shear layers at the boundary of the re-circulation bubble.

We characterized the features in the flower wake that persist for multiple pollinator

wingstrokes by analyzing the mean flow. For all three flower species, the mean flow in the near wake region (0.5-2 flower diameters downstream) forms a re-circulation zone. As shown in the mean vector field for each flower, incoming airflow (from the right) is accelerated around the the petals and that momentum is balanced by curving the flow back toward the flower face (Figure 4.3). The size of the re-circulation zone increases with flower diameter (Figure 4.3, $R^2 = 0.732$) and wake width scales with 1-2D, where D is flower diameter, across and within species (Figure 4.4). Vorticity in the freestream and inside the re-circulation zone is approximately zero, while the nonzero vorticity shear layers align with the petal tips (Figure 4.3). The range of mean vorticity is the same across size within each flower species, but generally increases for larger flower species. Vorticity in *Petunia* wakes ranges from -70 to +65 (/s), from -70 to + 80 (/s) in *Nicotiana* wakes, and from -90 to +65 (/s) in *Datura* wakes. Across flower species, vorticity is asymmetric with more negative vorticity than positive. Since we did not know the characteristic timescales in the flow, we were unable to phase-average the data and including half-periods of oscillating flow structures may lead to an asymmetric-looking wake. The enhanced asymmetry in vorticity for the much larger *Datura* is due to not capturing the entire wake in the FOV (Figure 4.3, top row). The FOV was set to capture the near wake flow relevant to a hawkmoth pollinator and kept constant across all flower species. Since we are only comparing local flow environments, we did not characterize the full wake of *Datura*, which would require different flow visualization. The size of the vorticity shear layers increases with flower diameter in *Petunia*, but appears more constant in *Datura* and *Nicotiana* (compare heat maps in Figure 4.3, top two rows vs. bottom row).

Width of re-circulation zone grows nonlinearly with flower size

In *Nicotiana* and *Petunia* wakes, the width of the re-circulation zone increases with flower diameter (Figure 4.4, linear regression $R^2 = 0.481$ and $R^2 = 0.732$, respectively). Unlike the smaller flowers, in the region of the wake where pollinators would hover, the width
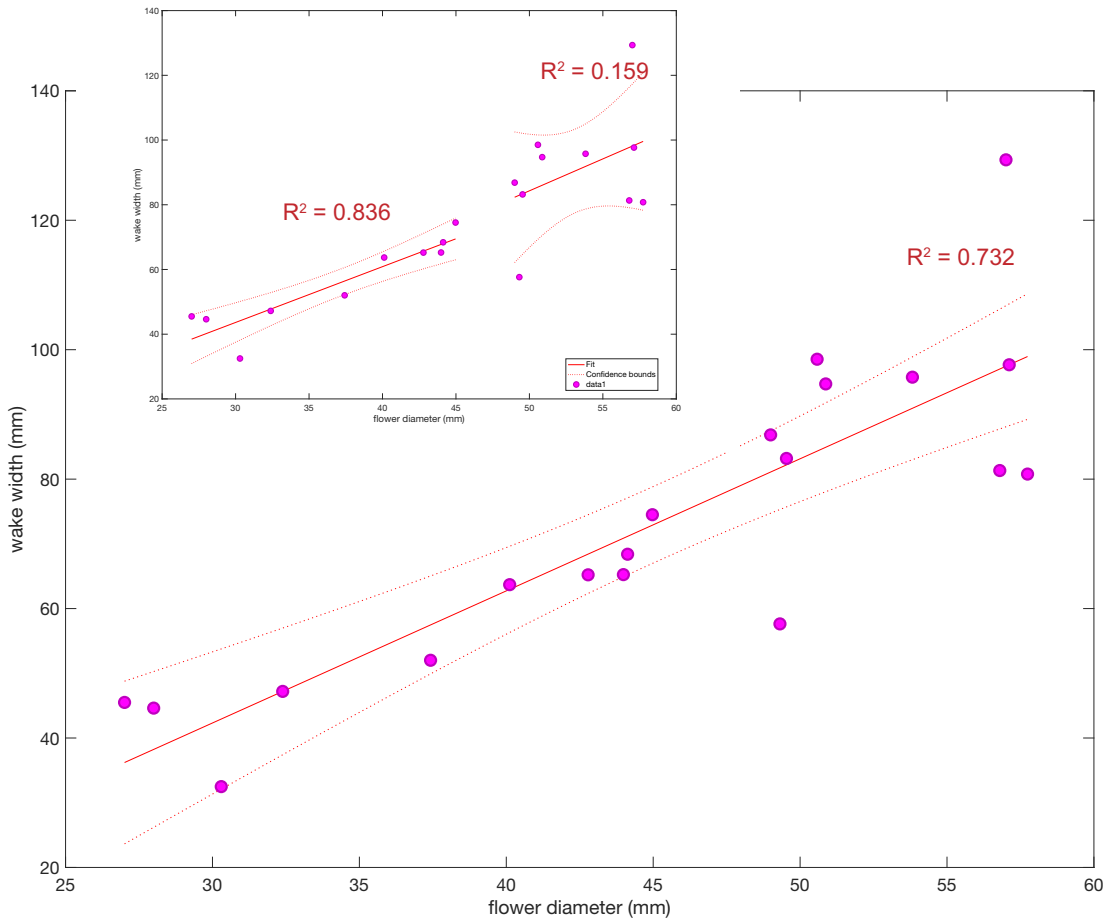
Figure 4.4: Wake (streamwise) width vs. flower diameter for all *Petunia*. The width of the re-circulation bubble increases with flower diameter (linear regression, $R^2 = 0.732$). Separating the data in half slightly improves the linear fit for flowers below 45 mm in diameter (linear regression, $R^2 = 0.836$).

of the re-circulation zone for *Datura* flowers is independent of flower size (Figure 4.5, $R^2 = 0.077$). We restricted our visualization of flower wakes to the near wake region most relevant for pollinators, so the full extent of *Datura* wakes was not considered. Including the far wake in future visualizations would resolve whether the width of the *Datura* re-circulation bubble increases in size like *Nicotiana* and *Petunia*.

Magnitude of flow reversal does not linearly depend on flower size

Inside the re-circulation zone, the maximum u-component magnitude was 30%-50% of the freestream and of opposite sign indicate a pocket of significant mean flow towards
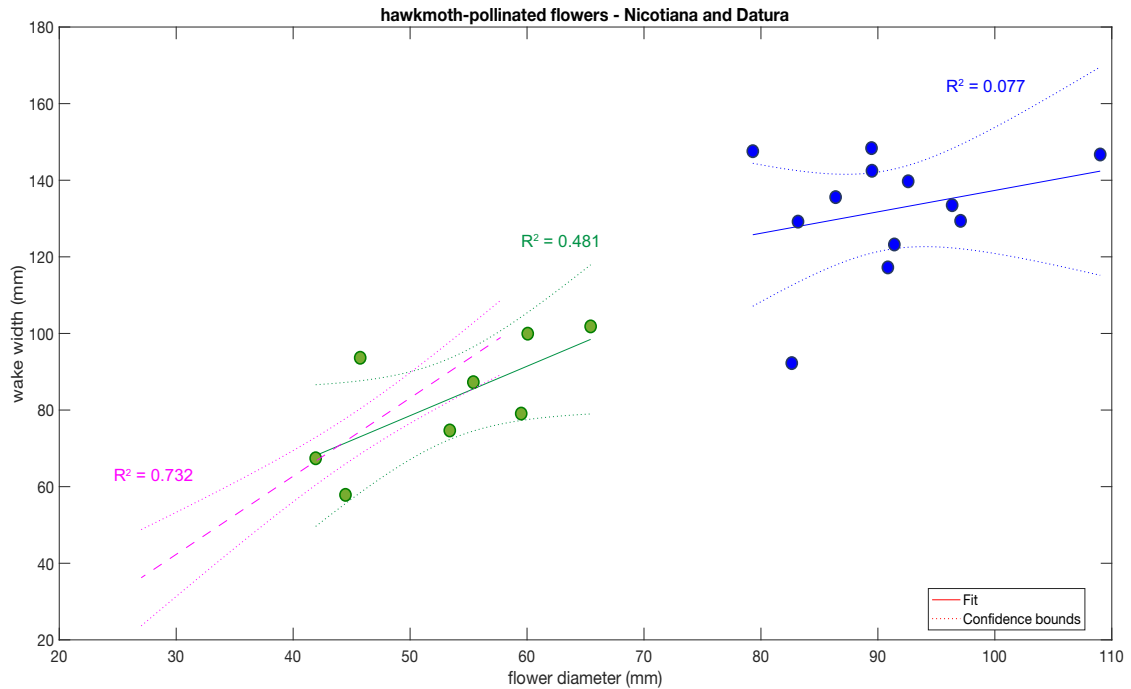
Figure 4.5: Wake (streamwise) width vs. flower diameter for *Nicotiana* and *Datura*. Like for *Petunia*, wake width increases with flower diameter for *Nicotiana*, but the correlation is weaker ($R^2 = 0.481$). The wake width for *Datura* is constant across flower size ($R^2 = 0.077$).

the flower within this bubble. *Nicotiana* and *Petunia* flowers achieved similar flow reversal maximums between 30%-45% of the freestream regardless of flower size, while larger *Datura* flowers showed flow reversal maxima between 40%-50% of the freestream (Figure 4.6, *Datura*: $R^2 = 0.272$, *Nicotiana*: $R^2 = 0.537$, and *Petunia*: $R^2 = 0.337$). Since the magnitude of flow reversal doesn't increase with size, it could also be driven by flower (petal) curvature.

Dominant unsteady wake features oscillate at characteristic timescales

After describing the mean flow, we next characterized the unsteady flow components. Given that the biological structure of flowers is more complex than idealized shapes, we tested for characteristic frequencies in the flow, the degree of turbulence, and the presence of modal structure in the flowers' wakes. Across all hawkmoth-pollinated flowers,
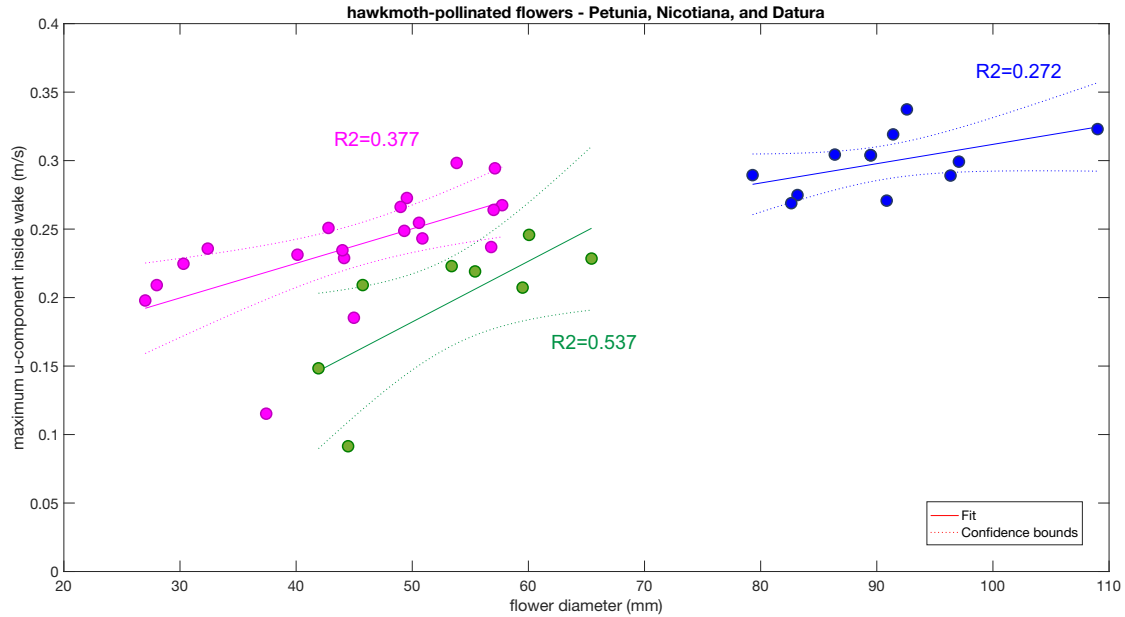
Figure 4.6: Maximum u-component inside re-circulation zone for all flowers. Flow reversal in *Nicotiana* and *Petunia* wakes is approximately 30%-45% of the freestream with little change across flower size, within and across species ($R^2 = 0.537$ and $R^2 = 0.337$, respectively). *Datura* wakes have higher magnitude flow reversal, up to 50% of the freestream across size ($R^2 = 0.272$).

the velocity power spectral density (PSD) has two main features, (1) dominant peaks occur between 0-10 Hz and (2) between 10-100 Hz power is distributed smoothly across many frequencies (Figure 4.7). Since wingbeat frequencies for hawkmoths are around 10-30 Hz [74], we do not describe frequencies above 100 Hz in this work. The smooth roll-off in power from 10-100 Hz is characteristic of a turbulent wake (Figure 4.7).

However, below 10 Hz the frequency of the dominant peak in the power spectra decreases from 6 Hz for *Petunia* around 30 mm in diameter to 1 Hz for *Petunia* and *Nicotiana* around 55 mm in diameter (Figure 4.8). Dominant peaks for *Datura* occurred below 2 Hz and multiple peaks were at the lowest possible frequencies (square data points, Figure 4.8). Longer recording times in future experiments can resolve the frequency dependence in the wakes below 1 Hz across flower species to determine if the trend of decreasing dominant frequency for increasing flower diameter continues. Strouhal numbers were calculated for flower wakes from the peak frequencies and diameters for individual flowers. For our

74
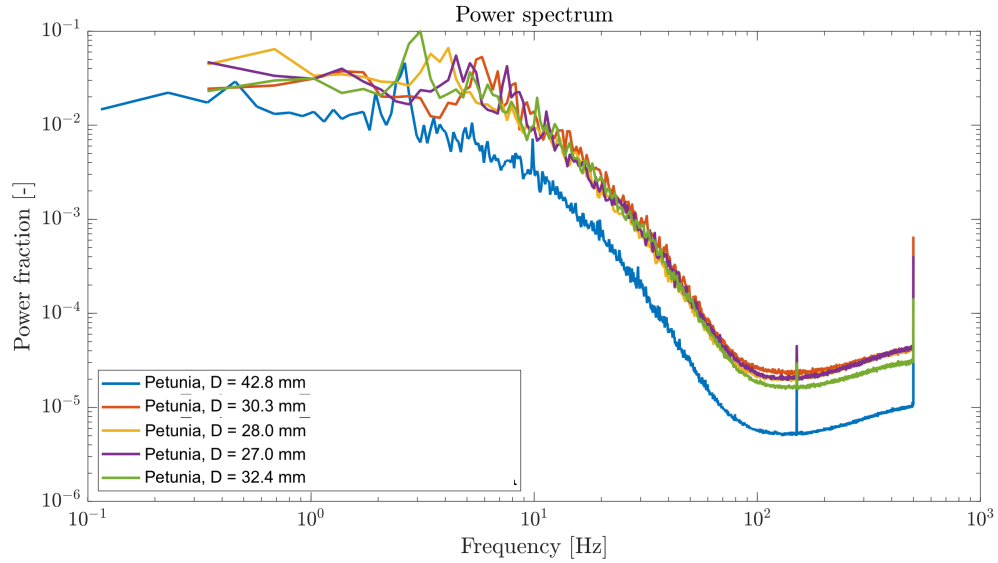
Figure 4.7: Example power spectra for *Petunia* with diameter below 45 mm. Power spectra for *Datura* and *Nicotiana* have the same shape with a smooth roll-off in frequency between 10-100 Hz and dominant peaks below 10 Hz.

range of Re, Strouhal number varies between 0 and 0.3 for all flowers (Figure 4.9), which is within the expected range for bluff body wakes.

At low frequencies, we used proper orthogonal decomposition (POD) to describe unsteady spatial structures. When POD is used to describe wakes of classic bluff bodies, such as cylinder wakes, the first two modes typically contribute up to 30% of the fluctuating energy [276]. In our flower wake modal analysis, the first 3-5 modes account for approximately 15% of fluctuations in the flow. The dominant POD modes show spatially oscillating flow structures reminiscent of classical bluff body wakes, such as disks and cylinders (alternating blobs of opposite-signed vorticity in near wake Figure 4.10).

For the six representative *Petunia*, the first two POD modes combined capture between 20%-30% of the total kinetic energy (Figure 4.11, right). Similar to the PSD, long tails in the plot of % TKE per mode indicate that energy in distributed across a larger number of modes, but beyond the fifth mode, each contributes less than 5% TKE. All POD results are based on the linear combination of the first two modes. In *Petunia* flower wakes, strong up- and downdrafts of flow occur between 1-1.5 flower diameters downstream and velocity

75
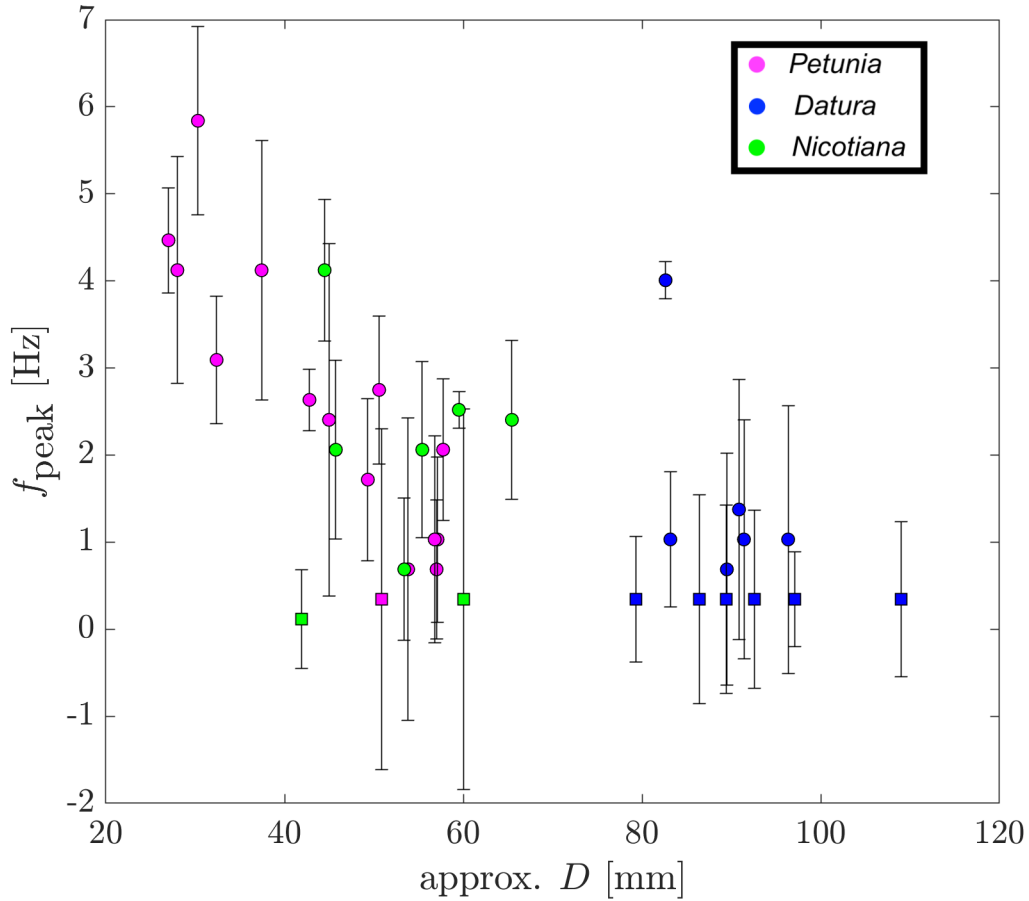
Figure 4.8: Dominant frequency of PSD peak for hawkmoth-pollinated flowers. Error bars show the half-width of the peak (at half-height). Peak frequency decreases for increasing flower diameters down to the resolution limit of 1 Hz.

magnitude in the mode reconstruction fluctuates around 0.1 m/s within one flower diameter downstream. Fluctuations in the wake show alternating upward and downward flows with an obvious spatial wavelength separating the structures (Figure 4.10). The flow reflected in the reconstructed POD modes for *Petunia* suggests that 15%-30% of the energy in flower wakes at this scale can be approximated by periodic shedding of regular flow structures.

The first two POD modes for *Datura* flowers contain approximately 30% of the total kinetic energy and each mode beyond mode 6 contributes less than 5% (Figure 4.11, left). Although there is a sharp roll-off in % TKE after the first mode for the largest *Datura*
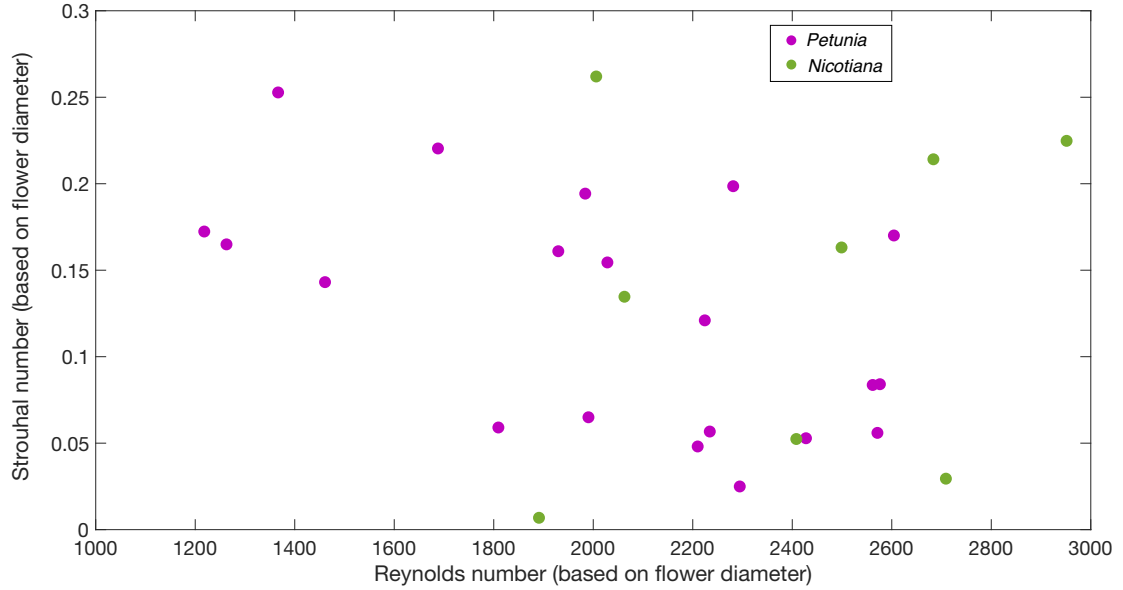
Figure 4.9: Relationship between Strouhal number (St) and Reynolds number (Re) based on individual flower diameters and peak PSD frequencies.

flower, the following modes contribute enough energy to cause long tails (**??**). The alternating down- and updrafts of flow seen for *Petunia* are not visible in the POD reconstruction of the first two modes in *Datura* wakes. In the near wake, within 1 flower diameter downstream, the flow remains near zero, but at the downstream limit of the FOV, symmetric areas of opposing flow grow in magnitude. Fluctuations in this region approach velocity magnitudes of 0.5 m/s.

The % TKE across modes for *Nicotiana* is lower than for *Datura*, with the first two modes capturing only 20%-25% TKE (Figure 4.11, left). Reconstructing the first two modes reveals regular structures in *Nicotiana* wakes, which appear periodic but not symmetric about the centerline of flower. The structures generate alternating angled jets that occur between 0.5-2 flower diameters downstream. While the spatial and temporal features of the modes are similar for large and small *Nicotiana*, the smaller flower has reduced magnitude of fluctuation. The consistency in flow features for different sizes of *Datura* and *Nicotiana* indicates that the wake structure does not change with flower diameter.

77

Wake effects on the flow environment around a hovering pollinator

Given that the flower species we investigate are all pollinated (not necessarily exlusively) by hover-feeding pollinators like hawkmoths, we next use the foraging kinematics of the model hawkmoth species, Manduca sexta, to ask what scale of aerodynamic consequences are produced by floral wakes on these pollinators. Assuming a constant feeding distance of 5 cm [139, 293] and a 20° stroke plane angle [41], we extracted the mean velocity in the flower wake along the stroke plane. At this feeding distance, the moth is surrounded by flower-directed flow for all three flower species. The re-circulation bubble in *Datura* wakes is large enough that the moth and the entire wingstroke are inside and there is no interaction with vortices shed from the petals. For both sizes of *Datura* the effective incoming air velocity is mostly constant along the stroke plane, but is very different from the freestream environment. Instead of a 0.7 m s^{-1} horizontal flow , the moth would encounter a flow pointing back toward the flower at 30%-50% freestream, with a less than 10° upward inflection.

For smaller *Nicotiana* and *Petunia* the amount of the wingstroke inside the re-circulation bubble increases with flower size, which reflects the growth of the bubble with flower diameter (Figure 4.13 and (Figure 4.14). The wakes of *Nicotiana* flowers are have an asymmetric re-circulation zone, so wind velocity increases and decreases along the stroke plane. At dorsal stroke reversal, the wingtips pass through the boundary of the re-circulation bubble and at ventral stroke reversal the wingtips may interact with shedding vorticity from the petals, especially for the smaller flower (Figure 4.13). In the wake of the smallest *Petunia*, the hawkmoth is on the boundary of the re-circulation bubble, so the first half of the wingstroke is in the freestream and the wings cross into the bubble during the second half. Ventral stroke reversal occurs within the region of negative vorticity shed from the petals in the two smaller *Petunia* (Figure 4.14). As flower diameter increases, less of the wingstroke

interacts with the freestream airflow. For the largest *Petunia*, none of the wake is in the freestream and wingtips may pass through vorticity shed from the petals at dorsal stroke reversal.

Flight forces are reduced in flower wakes

To assess changes to aerodynamic forces for hovering in the freestream versus the flower wake, velocities along the stroke plane were used as inputs to a blade element model (BEM) for *M. sexta* hovering [74]. The BEM shows how the steady mean flow inside the re-circulation bubble influences forces, but does not capture the unsteady interactions between the wings and turbulent portions of the wake. Since the wingtip moves along the stroke plane during a full wingstroke, the spatially distributed velocity vectors are converted into a time-series of incoming air flow velocities. The BEM is used to assess the impact of the flower wake on total aerodynamic force. Although the BEM calculates all force components in three dimensions, we only discuss horizontal (F_x) and vertical (F_z) forces, since we did not have velocity information in the spanwise direction.

Wingstroke-averaged horizontal forces (F_x) are have reduced magnitude and change sign in the flower wake, compared to the 0.7 m/s freestream, for all flower species (single wing force: -1.277 mN in freestream and 0.198 mN averaging across all flowers Figure 4.15). Changes in horizontal force during the up- and downstrokes comes from increased translational forces in the flower wake. The change in F_x at ventral stroke reversal is due to higher rotational forces (Figure 4.12-Figure 4.14, second column, right). Since the velocity magnitude is decreased inside the re-circulation bubble, we also calculated forces for a hawkmoth hovering in a 0 m/s freestream. Translational and rotational forces in the flower wake are similar more similar to still air hovering than to forces in the steady 0.7 m/s freestream.

Across all hawkmoth-pollinated flowers, vertical forces (F_z) decreased during the downstroke and increased during the upstroke. The wingstroke-averaged total vertical force in all

flower wakes is decreased compared to the freestream, but maintains enough wingstroke-averaged vertical force to greatly exceed body weight (approx. 4.9 mN, Figure 4.15). In the freestream, vertical force from both wings is 10.37 mN and averaging across all flowers vertical force in the wake reduces to 9.82 mN. There were minimal differences in force production between flower sizes *Datura* and *Nicotiana* but for *Petunia*, the change in vertical force scales with flower diameter (Figure 4.14 and Figure 4.15). Larger flowers had the largest drop in force during the downstroke and largest increase during the upstroke (Figure 4.14, bottom row, left). As with horizontal forces, changes in F_z from the freestream to the flower wake arise from variation in both translational and rotational forces (Figure 4.14, bottom row, left). In both F_x and F_z added mass forces in the flower wake and in both steady freestream conditions were similar for all flowers.

Discussion

Interactions between plants and wind create local environments for flying pollinators. Dynamics of plant motion in response to wind loading have been studied using simple beam bending models and finite-element models to describe stem bending and leaf flutter [287], but we do not know how inflorescences (flower heads) on flowering plants change the local airflow. In steady freestream air, trumpet-shaped flowers generate a re-circulation bubble in the near wake, within 1-2 flower diameters downstream. Although flowers in nature will not always be oriented horizontally, many plants reconfigure their shape in wind [94, 125, 218] and daffodils re-orient to face downstream by stem twisting [205]. Re-orientation in daffodils occurred in 8-10 m/s freestream wind, but hawkmoth-pollinated flowers could rely on stem mechanics to re-orient the flower face at lower wind speeds to maintain formation of the re-circulation bubble. Frequencies that flowers wiggle in the wind likely depend on the dynamics of the wind itself. For example, flowers blowing in natural, variable wind produce frequencies of oscillations lower than 1.7 Hz [137], but the dominant frequencies in the wake we observe under steady wind are typically higher Figure 4.8. However, it is

difficult given the length of our observations to resolve peaks below 1 Hz.

The conclusions about fluctuating structures in the flow are based on POD modes calculated for representative flowers within each species, 2 each for *Datura* and *Nicotiana* and 6 *Petunia*. The wakes of natural hawkmoth-pollinated flowers are characterized by turbulence at frequencies above 10 Hz and bluff body-like flow structures that oscillate at frequencies below 10 Hz. Most investigations of flow at pollinator scales assume broadband turbulence [126] or well-structured cylinder wakes [179], but our results show that flower wakes are best described by the combination of both flow regimes. In addition to the turbulent regime, the first few modes of the wake do show regular oscillations, but these do not include clearly defined alternating vortices as would be expected cylinder. The first and second POD modes explain between 8-25% and 5-15% of the total kinetic energy in the wake, respectively. Higher modes fall off slowly the incremental kinetic energy each explains. However, this component of the flow that is structured depends on size in the data that we have so far analyzed with larger flower diameters producing more structure energy in the first two modes (Figure 4.11). Further analysis of POD structures will be needed to determine if there are species-specific differences in the floral wakes.

The other key feature of the floral wake is the presence of a re-circulation bubble that includes flow reversal from freestream. The width of the re-circulation bubble extends 1-2 flower diameters downstream Figure 4.5. Inside the near wake, the flow velocity is reduced to 20-50% of the freestream. A re-circulation zone is expected to form downstream of bluff body in horizontal airflow due to fluid-structure interactions at the boundary [309]. Unlike a flat plate or disk, hawkmoth-pollinated flowers are trumpet-shaped. Incoming flow is accelerated around the curved nectary before interacting with the flower petals to form shear layers and a re-circulation zone. Flow inside the re-circulation bubble first increases to a maximum between 20-50% of the freestream before decreasing toward the face of the flower (Figure 4.6). For a flat bluff body, horizontal flow would be forced to zero at the surface, but this is not necessary for flow into the nectary (a cavity in the

flower). Previous studies on the foraging behavior of moths have explored how flower shape influence foraging success and preference [207, 139]. While these studies were done in still air and often with horizontally oriented flower faces, it is important to consider how curvature in flower morphology may affect the wake structure especially in the re-circulation zone.

Consequences of floral wakes on pollinator aerodynamics

The combination of the re-circulation zone, mean flow changes in the wake and unsteadiness can produce a profoundly different flow environment for a pollinator as it moves from freestream into the floral wake. Depending on the direction a pollinator approaches the flower they would traverse different flow challenges. If approaching from above or below, the pollinator would need to pass through the highly rotational shear layers near the petal tips while pollinators approaching from downstream would only encounter the freestream and the stagnation point of the re-circulation bubble (Figure 4.12-Figure 4.14).

Inside the re-circulation bubble, smaller pollinators would experience a different environment than larger pollinators. Small pollinators, such as bees [209, 112], hoverflies [88], and mosquitoes [201], would only interact with the steady airflow directed at the flower since their wingstrokes are small enough not to extend into the petal shear layers. Additionally, smaller insects generally use higher wingbeat frequencies suggesting their wing motion may dominate over the low-magnitude (approx. 0.2-0.3 m/s) motion of the airflow. For larger pollinators like hawkmoths [285] and hummingbirds [223], the majority of the wingstroke would be within the re-circulation zone, but wings would pass through the shear layers at the boundary during stroke reversals. While the body of the animal experiences steady flow, on average, the wings interact with unsteady rotational flow at the end of each half-wingstroke.

Based on a BEM model for a hovering hawkmoth, flight in the flower wake reduces wingstroke-averaged vertical forces by 2-8% but the force is approximately double body

82

weight in both flow regimes (Figure 4.15). Wingstroke-averaged horizontal forces are reduced by about 80% in two smaller flower wakes, with diameters between 30-40 mm, but reverse direction and increase by 120-140% in larger flower wakes. In wakes of larger flowers, the average horizontal force points toward the flower face. The reversal in the average horizontal force direction may help the moth stay in the wake or push them toward the nectary. The BEM only describes forces for a hawkmoth that maintains the same wing kinematics in the freestream and the flower wake. Although the freestream kinematics produce sufficient force for hovering in the flower wake, when foraging in nature hawkmoths could adjust kinematics to alter force production.

Although 2D PIV only measures two components of velocity, the BEM generates forces in three dimensions. Assuming lateral flow (along the wingspan of the moth) is zero, flight in the flower wake results in a lateral force on the hawkmoth directed into the flower wake which may also help reduce positional error during flower tracking and foraging. Energetic costs of flower tracking in still air depend on the direction of motion [17] with best performance in the lateral direction achieved with side-slips [214]. Lateral and horizontal forces in the flower wakes act to keep the moth inside the re-circulation bubble, potentially aiding in flower tracking maneuvers.

A symmetric wingstroke leads to differential force effects during the up- and down-strokes. At each half-wingstroke, the wings pass through opposite-signed vorticity shear layers (Figure 4.12-Figure 4.14). In flapping wing flight, modification of flight forces is thought to occur during transitions, such as stroke reversal [107]. Rotational forces in the flower wake show a larger reduction in magnitude at the downstroke to upstroke transition suggesting that hawkmoths could use the asymmetry in the wake for flight control.

Finally, changes in the flow environment of the flower may also influence passive particles undergoing transport in the wake, most notably pollen. The presence of a re-circulation bubble on the same scale as a hovering pollinator suggests that pollen disturbed and released from the flower may re-circulate in the appropriate region to interact with the pol-

linator. In addition pollen carried by the pollinator to other flowers may be effectively trapped within this bubble facilitating pollination even without direct contact between plant and pollinator. It has been suggested that the evolution of long tongues in hawkmoths and deep nectaries leading to specialization also seen in hummingbirds and some bees [243]. However, it could also be that moths are evolving long proboscises to keep their distance from flowers and allow themselves to bob back and forth so as to avoid huntsman spiders lying in ambush in the foliage. The flower evolves deeper and deeper nectaries to try to "reel in" then moth. However, these hypotheses seem to presume contact between plant and pollinator. The presence of favorable flow environments for pollination-at-a-distance may support these ideas by providing a mechanism for pollen transport without contact.

Conclusion

Steady airflow interacts with flowers to generate unsteady flow downstream with features of both turbulence and bluff-body wakes. In addition to affecting force production, hovering in flower wakes may have functional consequences for foraging and pollen transport, similar to how oceanic organisms use turbulent plumes to navigate coral environments [327]. The diversity of unsteady aerial environments for pollinators beyond hawkmoths provide a rich space to explore how flow affects forces for locomotion.
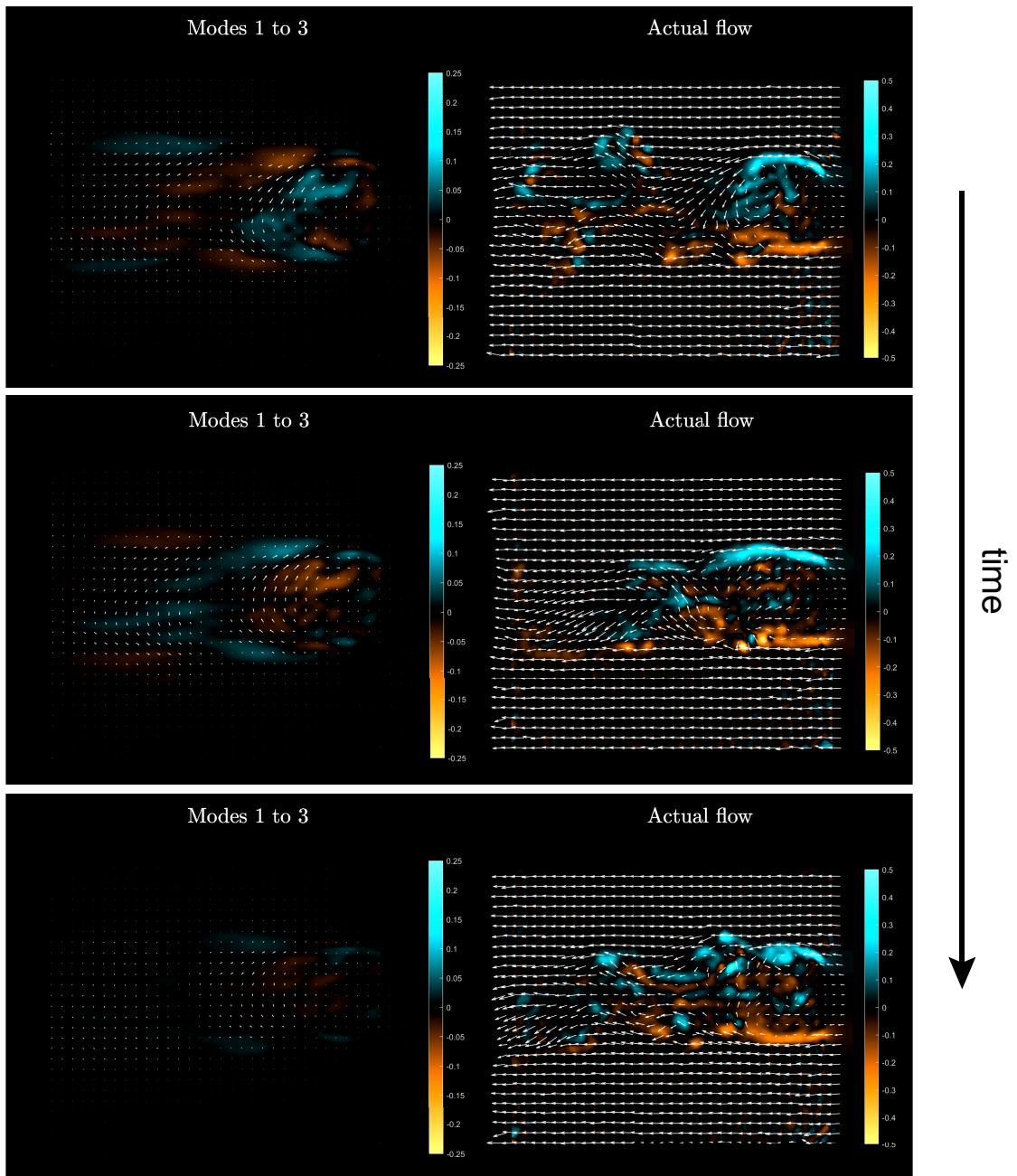
Figure 4.10: Example snapshots of POD modes for *Petunia*, D = 32.4 mm. Colorbar is vorticity ($/s$). The snapshots over time show alternating regions of opposite-signed vorticity in the near wake of the flower.
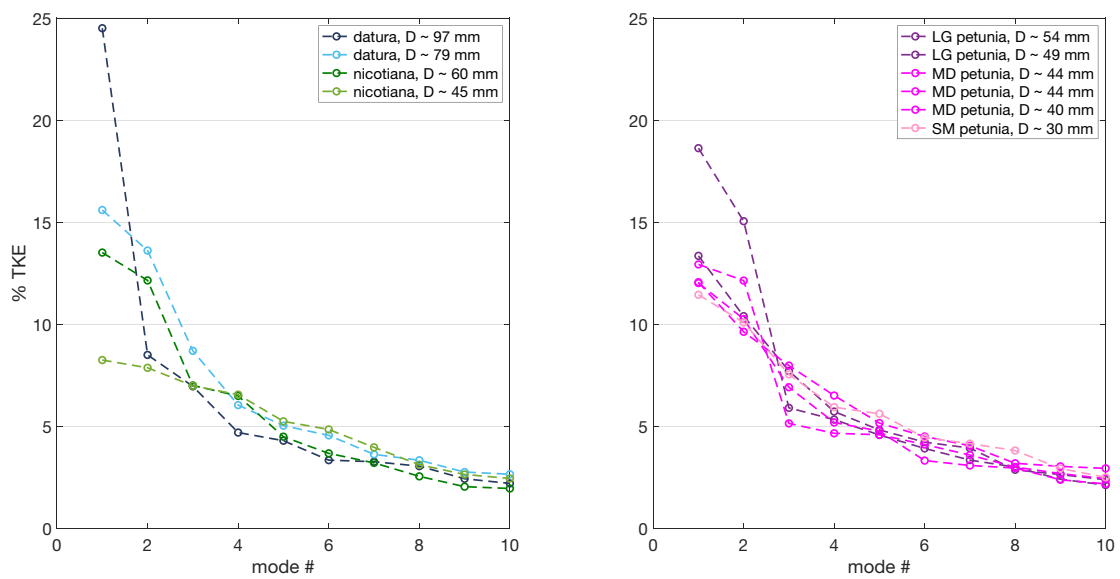
Figure 4.11: Percent total kinetic energy in the first 10 POD modes for representative flowers. The combination of the first two modes contributes 15%-26% TKE for *Nicotiana*, 29%-33% TKE for *Datura*, and 22%-33% for *Petunia*.
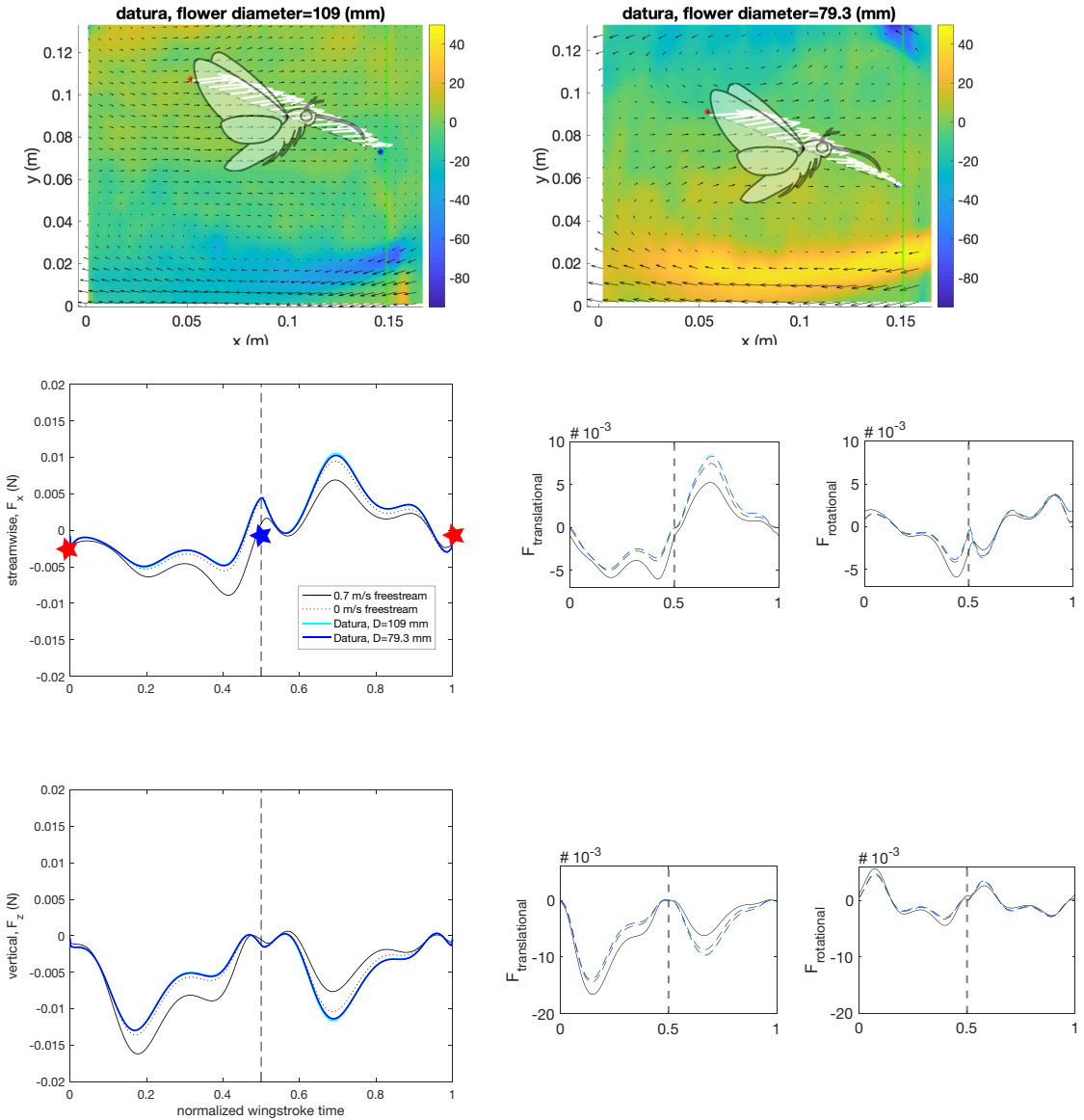
Figure 4.12: Mean flow vector fields with model stroke plane for *Datura*. Both horizontal (middle row) and vertical (bottom row) forces are lower in the flower wake and changes are due to differences in translational (second column, left) and rotational force components (second column, right).
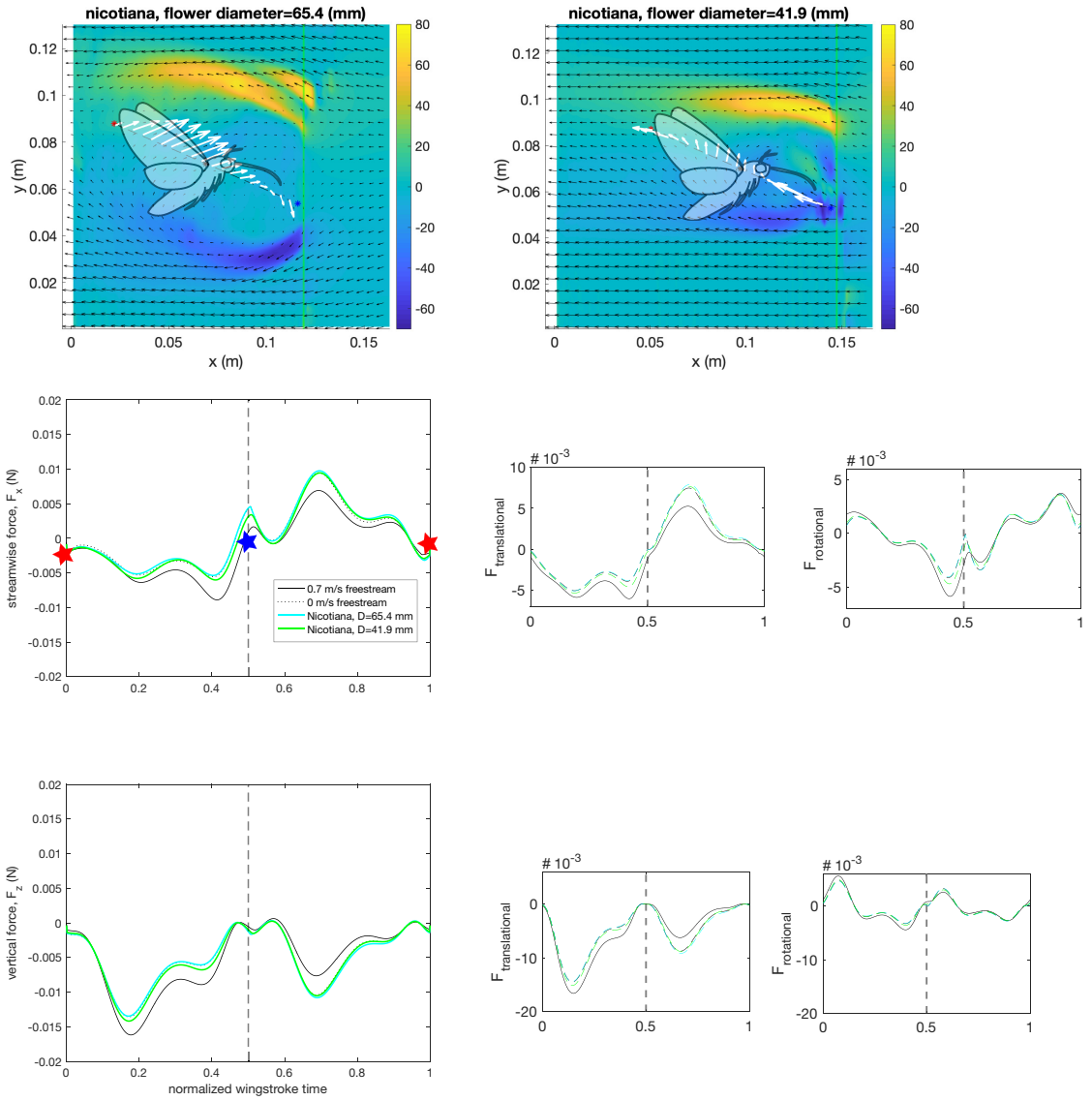
Figure 4.13: Mean flow vector fields with model stroke plane for *Nicotiana*. Both horizontal (middle row) and vertical (bottom row) forces are lower in the flower wake and changes are due to differences in translational (second column, left) and rotational force components (second column, right).
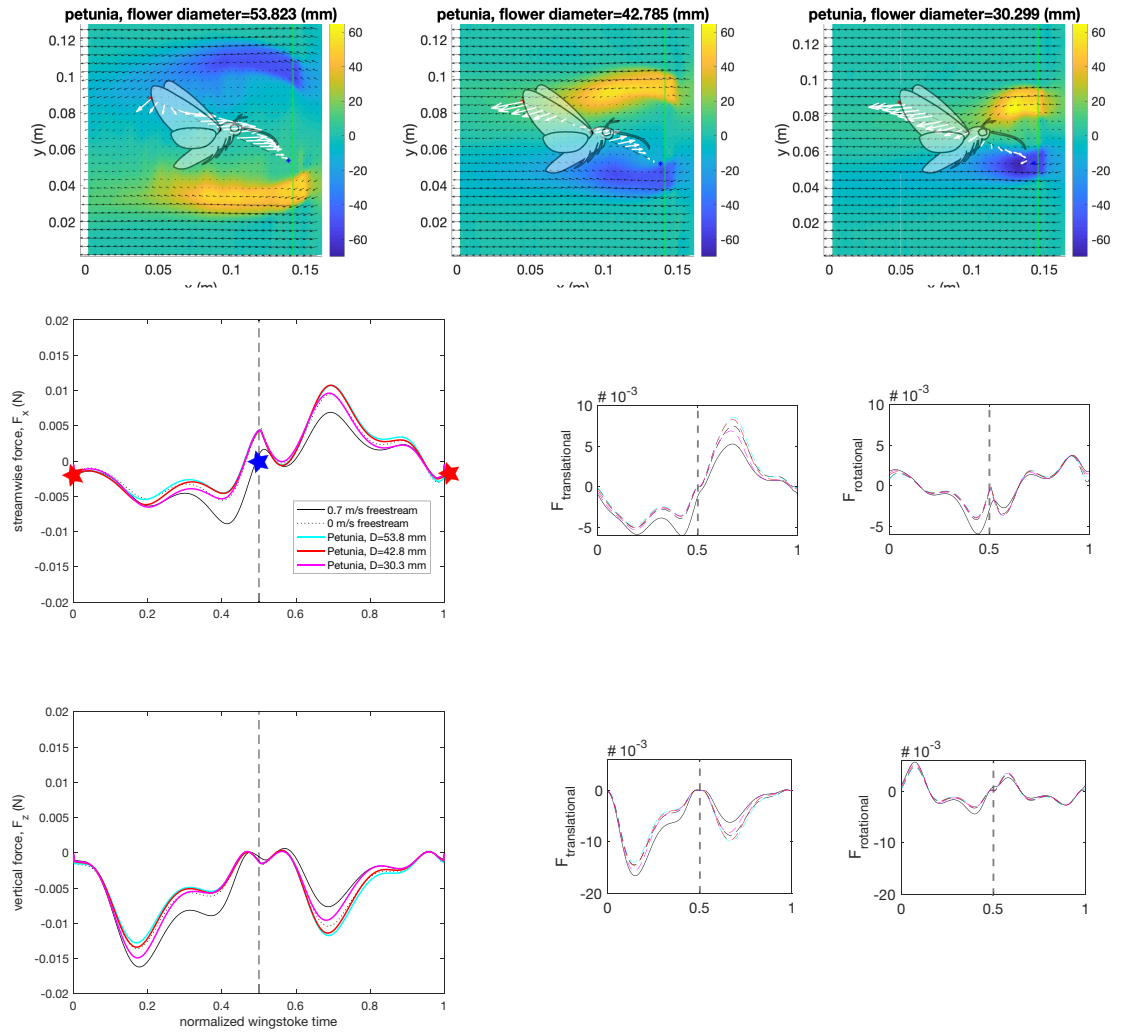
Figure 4.14: Mean flow vector fields with model stroke plane for *Petunia*. Both horizontal (middle row) and vertical (bottom row) forces are lower in the flower wake and changes are due to differences in translational (second column, left) and rotational force components (second column, right).
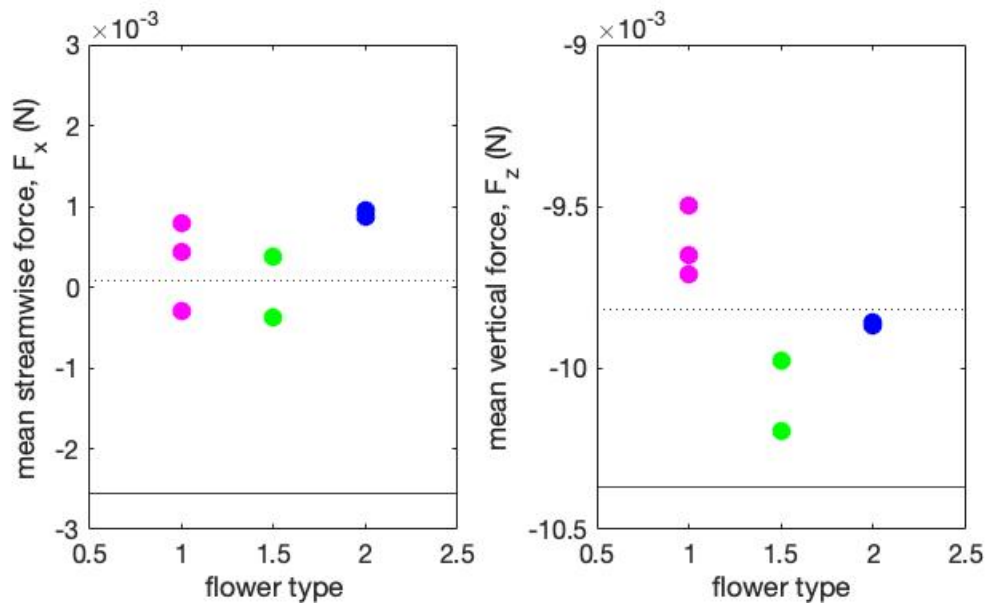
Figure 4.15: Total stroke-averaged forces.

CHAPTER 5

CONCLUSION

The interdisciplinary study of plant-pollinator aerodynamics requires integration of physics, biology, and ecology. This thesis explored the impact of unsteady environments on pollinator behavior and aerodynamics. Flow visualization also quantified the features in natural flower wakes, establishing an ecologically-informed aerodynamic context for insect flight during foraging and pollination. My work resulted in three new insights.

First, studying the impact of an artificial flower wake on maneuverability revealed emergent simplicity in hawkmoth flower tracking dynamics with increased tracking error at the vortex shedding frequencies of the 3D-printed flower. These results establish that unsteady flow affects controlled maneuvers as well as steady flight performance. However, these effects are not necessarily detrimental. The lower-order dynamics in the flower wake suggest that unsteady environments could be advantageous for flight performance.Moving forward, the natural environment of an organism should be considered when investigating behavior.

Next, the interplay between steady airflow and wing flexibility was explored in two flow regimes: (1) matching airflow conditions for *Manduca sexta* flight and (2) matching flow conditions known to produce decoherent leading-edge vortices (LEVs) on rigid wings. Although LEVs still burst on flexible hawkmoth wings, the LEV is decoherent over more of the wingspan as flexibility decreases with aging. Enhanced LEV stability in the hawkmoth flight regime revealed that trade-offs between Coriolis forces (from wing rotation) and inertial forces (from both wing translation and the incoming airflow) influence LEV structure and lift force. Aging changes the dynamic deformation of the wing and quasi-static snapshots of fresh and aged wing shapes at $90°$ through a wingstroke capture how differences in deformation relate to wing twist and camber along span. Future experiments are needed to understand how dynamic wing deformation impacts the LEV and to separate how wing

shape and interaction with incoming flow disrupt LEV stability.

Last, the wakes of hawkmoth-pollinated flowers were found to be turbulent but some irregular periodic structures and distinct spatial modes were present downstream of small flowers (diameter less than 40 mm). Like many bluff body flow interactions, flower wakes are dominated by a re-circulation zone downstream and hawkmoths hover-feed within the re-circulation bubble. In addition to characterizing the local flow environment for a hovering hawkmoth, this work showed how flow in the flower wake impacts aerodynamic force (with a blade-element model). Despite the broad diversity in floral environments for pollinators, flapping flight (and the LEV in particular) remains a highly effective strategy. Future work can investigate how insects achieve consistent performance across variable environments from behavioral, neurological, and aerodynamic perspectives. Overall, this thesis has two main contributions: (1) natural environments for pollinators have steady, unsteady, and turbulent features and (2) external flow environments directly influence aerodynamic force through fluid-structure interactions. Additionally, it is obvious that much more work needs to be done considering the natural environment where an animal behaves. Future studies with hawkmoths can use the flow features described in this work to design experiments or as inputs for computational fluid dynamics (CFD) and other numerical models. Hawkmoths are only a narrow subset of flying pollinators, so there are also many other local flow environments to investigate depending on the target plant-pollinator system. Since animals actively respond to their environments, future behavioral experiments can reveal how animals adapt to ecologically-relevant flow changes, building up our biological understand and also providing foundation for robustness in engineered systems. The interplay between compliant wings and the surrounding air is only just begin explored, but shows potential for expanding flow control on small flapping robots beyond sensing and feedback.

Future directions for LEV aerodynamics

Despite decades of research, we still do not fully understand the dynamics of leading-edge vortex evolution on flapping wings, especially on the flexible wings of insects. Features of LEV bursting were characterized on rigid flappers [28, 140], but the mechanism that leads to flow stagnation within the vortex core remains unknown. Further complicating LEV interactions, our current knowledge is based on vortices interacting with irrotational or still airflow and little is known about how wing-wake interactions directly affect LEV structure. The smoke visualization of the hawkmoth hovering in a robotic flower wake in Chapter 2 was one of the first observations of LEVs in unsteady flow, confirming the persistence of the mechanism, but more work is needed to understand how circulation, lift, and coherence are affected. These are the key areas to explore to deepen our understanding of leading-edge vortex dynamics on flapping wings.

What mechanism leads to bursting?

Although LEV bursting is well-defined there are many open questions about the source of instability in the flow. The rapid expansion of LEV diameter at midspan is induced by axial flow reversal and the entrainment of opposite-signed vorticity into the LEV core [140]. The attached LEV is fed by the vorticity shear layer at the leading edge and growth is balanced by secondary vorticity close to the surface of the wing. As wing sweep reaches a critical angle, between $90° - 120°$ for rigid wings at $Re \sim 10^3$, the balance of vorticity maintaining LEV structure is disrupted leading to decoherence [82, 311, 28]. Since the characteristics of burst LEVs are known, future experiments can focus on determining how secondary vorticity near the wing surface develops prior to bursting with time-resolved stereo particle image velocimetry (TR-sPIV). Assuming growth of boundary layer (secondary) vorticity precedes LEV bursting, understanding the time evolution of flow close to the surface may reveal predictors in the flow. Then, future work can explore why bursting occurs at a critical

sweep angle and only for fluid-structure interactions at $Re \sim 10^3$.

How do dynamic and quasi-static wing flexibility contribute to force production and influence flow structure?

The roles of wing morphology and kinematics in LEV stability are only recently being studied on flexible wings. Given the complex combination of unsteady fluid-structure interactions and aeroelastic deformation, recent work is done with numerical and computational models of flapping wings [103, 57, 244], but many assumptions are made to simplify interactions. While challenging, there is a need for experimental data to go hand and hand with these computational studies. Our results on flexible hawkmoth wings suggest that changing the structural dynamics of the wing (e.g. changing flexural stiffness) impacts aeroelastic effects which disrupts fluid-structure interaction and leads to LEV burst across more of the wingspan. Experimental investigations of wing compliance often use rigid plates with a hinge to approximate chordwise flexibility [213, 245]. From our analysis of shape change on hawkmoth wings, both chordwise and spanwise wing deformations influence LEV structure, especially past midspan. Moving forward, the influence of wing flexibility can be separated into quasi-static shape effects, as explored in this thesis, and dynamic aeroelastic effects due to the temporal evolution of wing deformation. Resolving the interplay between dynamic wing deformation and LEV structure will require simultaneous measurement of wing shape and quantitative flow visualization close to the wing surface. Quasi-static shape effects on LEV stability can be more easily quantified since geometric and kinematic parameters can be isolated. We encountered significant biological variation in wing shape change due to differential drying and flexural stiffness on hawkmoth wings, but engineered wings can be tuned to a particular camber or wing twist. By systematically varying geometric wing parameters and measuring LEV stability and circulation we can understand how wing shape parameters influence vortex structure and force production.

Advantages and disadvantages of flight in wakes

In the three-way interaction between pollinators, plants, and wind both plants and pollinators rely on local airflow for force generation. Plants reduce drag in response to wind with stem torsion and bending causing daffodils to face downstream and leaves to streamline [205, 287, 218]. In the absence of pollinators, wind-pollinated plants may require steady airflow to dislodge pollen particles with turbulence assisting transport by inducing stamen oscillations [98]. Pollinators that use flapping wing aerodynamics produce and shed vortical structures that wings interact with on subsequent wingstrokes [235, 301]. Successful foraging and pollination benefits both organisms in the environment, but depending on the specific dynamics used by a plant and pollinator in unsteady flow, the impact of flower wakes could be advantageous or disruptive.

Aerodynamic advantages for plants and pollinators

Since both steady and turbulent airflow contribute to pollen transport in wind-pollinated plants [98], the mean flow and turbulent features we measured in flower wakes may also assist in pollen transport between plants and pollinators. The steady mean flow in the recirculation bubble could be sufficient to dislodge pollen from the pollinator and transport it toward the stamens of the flower. Additionally, turbulence in the flower wakes could excite motion of the stamens and release pollen onto the proboscis or body of a hovering pollinator. Measuring the pollen transport capabilities of flower wakes may be crucial for success of plant-pollinator networks in many different environments. Flower wakes in our study were based on flowers removed from their stems, but wind would also induce stem bending and twisting [205, 218]. Purely wind-pollinated plants may have more flexible stems compared to insect-pollinated plants [98], but future flow visualization would need to quantify how stem motion affects the features of the flower wake measured here. If flower wakes are beneficial for pollination, then insect-pollinated plant stems could be op-

timally stiff: flexible enough to re-orient flowers downstream for wake formation, but stiff enough not to induce petal flutter. In hydrodynamic flows, trout adopt a slaloming Karman gait while station-holding in cylinder wakes [33]. Fish benefit from swimming in the cylinder wake in two distinct, but non-mutually exclusive ways: (1) drafting or swimming more slowly (on average) in the reduced flow region in the near wake and (2) reducing muscle costs by adopting the Karman gait [202]. These mechanisms may also apply to insects in hawkmoth-pollinated flower wakes. All hawkmoth-pollinated flowers generated wakes with a mean flow re-circulation bubble, similar to the near wake region downstream of cylinders. Airflow inside the bubble is directed back toward the flower at 30%-50% of the freestream speed. Pollinators hovering fully inside the re-circulation bubble may be able to reduce flight costs relative to the freestream by drafting. We also saw moth motion above 10 Hz effectively removed from tracking dynamics by the "environmental filter," suggesting moths may slalom like fish using the Karman gait. Recordings of flight muscle activity and metabolic rates during hovering in flower wakes are necessary to determine if muscle power requirements are reduced in flight, but insects may not need to save muscle power if flower wakes reduce aerodynamic or mechanical power costs through slaloming, drafting, and wing-wake interactions. Additionally, the true costs of hover-foraging are unknown and optimization of power and energy costs may not be relevant to insects, if they need to maximize forces for behavior. Using Strouhal number to describe flapping and swimming in flow, propulsive efficiency is greater than 60% in the range of $0.2 < St < 0.4$ which matches the St range for cruising kinematics [160], but St for hovering or maneuvering animals is likely higher. During robotic flower tracking in wind, we observed the wing-driven flow structures qualitatively dominated over shed flower wake structures, but we did not determine St for the moth based on flapping kinematics. Measuring hawkmoth kinematics could reveal whether they maintain a high St during complex maneuvers (potentially maximizing force coefficients) or if interaction with the flower wake lowers St into the range of maximum efficiency. Based on flower diameter, the St in flower wakes is

between 0-0.3, which is within the range where vortex shedding occurs on bluff bodies and overlaps the range of peak propulsive efficiency for cruising. In turbulent flow, increasing flapping frequency decreases the dominance of turbulence on the instantaneous flow field around rigid plates, however turbulence still modulates LEV growth timing and stability [113]. By using high wingbeat frequencies, hawkmoths and other insects are able to attenuate the influence of external turbulence on local airflow. Vortex wakes from flapping wings also become more chaotic as flapping frequency and St increase [318], but interaction with the flower wake could help dissipate wake energy from previous wingstrokes. In addition to turbulence, our flower wakes shed rotational flow structures at 1-10 Hz depending on flower diameter. When a wing passes through rotating flow the timing between flow shedding and wing motion becomes a predictor of whether the wing-wake interaction is beneficial or deleterious [301]. Periodic rotational components of flower wakes could enhance or reduce circulation build-up during stroke reversals based on whether flow rotates with or against wing motion, respectively. However, most existing literature on pollinators flying in unsteady wakes suggests that wake structures have negative impacts on flight performance.

Biomechanical disadvantages for pollinators

Unsteady aerodynamic mechanisms in flapping flight are based on the formation and shedding of vortex structures. Vortices formed during one wingstroke are shed and influence subsequent wingstrokes, leading to reductions in aerodynamic angle of attack and force attenuation [235]. Employing the same unsteady mechanisms in flower wakes could compound the effects of wing-wake interaction leading to further force attenuation in late downstroke. Studies on the dual-wing aerodynamics of dragonflies can inform predictions for wing-level fluid-structure interactions and suggest that the phase of the vortex wake relative to the wingstroke could impact LEV formation as seen on dragonfly hindwings [65]. The size of a pollinator relative to the wake is also a crucial indicator of how destabilizing the

airflow will be to a flapping flier. Hawkmoth and hummingbird wingspans and body sizes are approximately 10 cm, while bee sizes and wingspans are at most 5 cm. Pollinator size determines how much of the wingspan is inside the re-circulation bubble. In turbulence and cylinder wakes, both bees and hummingbirds reach reduced flight speeds, compared to steady airflow, suggesting flight costs are increased in the wake [264, 114, 40]. For hummingbirds in cylinder wakes, metabolic costs were confirmed to increase 25% and it was proposed that wakes pose flight challenges to pollinators when vortex diameters in the wake are equal to 0.75-1 wingspan [77]. Since hawkmoths are approximately the same size as hummingbirds, metabolic costs may also increase for them in flower wakes and we see similar kinematic responses for both pollinators in cylinder wakes, including synchronizing lateral oscillations with vortex shedding frequencies [77, 179]. Although our hawkmoth-pollinated flower wakes included periodic flow shedding between 1-10 Hz, pollinators in these wakes may not be able to synchronize body motion due to the additional influence of turbulence between 10-100 Hz. Combined perturbations from turbulence and shedding could cause energetic costs to be even higher in a flower wake compared to more uniform cylinder wakes or full turbulence. For smaller bee pollinators, costs in the same hawkmoth-pollinated flower wake could be reduced since the bee is able to draft in the re-circulation bubble and avoid interacting with shedding flow structures.

Differences in pollinator morphology lead to differences in maneuverability and rotational stability [162] that are emphasized during interactions with unsteady flow. Hummingbirds in turbulence and hawkmoths in tornadoes mitigate perturbations in the cylinder wake by inducing asymmetry in their kinematics between wingstrokes [40, 14]. In smaller flower wakes, asymmetry between up- and downstrokes could have significant impact on rotational force generation since wings pass through vorticity shear layers at the boundary of the re-circulation bubble. Using a blade-element model (BEM), we found that a hovering hawkmoth would experience a sign change in wingstroke-averaged horizontal forces when flying from the freestream into the flower wake, assuming no kinematic change. For a

freely hovering hawkmoth, flower tracking is most energetically costly in the fore-aft direction [17], so the animal may need to actively stabilize against horizontal wake perturbations to maintain tracking performance. Both hummingbirds and hawkmoths adjust wingstroke amplitude and stroke plane angle in unsteady flow, but wingbeat frequency is unchanged [14, 40]. By adjusting kinematics, pollinators can partially reject wake perturbations and station-hold downstream of flowers, albeit with higher energetic costs of flight. The flower wake introduces an inherent asymmetric effect on the wings at dorsal and ventral stroke reversals, but animals can adjust the extent of the asymmetry by changing body position or stroke plane angle. Behavioral assays of flower tracking and station-holding in wakes with both turbulence and periodic shedding could reveal whether the combined wake effects require more kinematic corrections and increased flight costs or if the complex flower wake can effectively "filter out" corrections, as was the case in robotic flower tracking.

Next steps in plant-pollinator aerodynamics

This thesis explores some of the physics and biology involved in plant-pollinator aerodynamics, but most of the work inspired new questions about the ecologically-vital interactions between plants, pollinators, and their environments. While specific questions about the physics of flows around wings and biomechanical consequences of unsteady wakes are discussed above, the integration of ecological diversity and evolutionary context is the next big challenge in understanding plant-pollinator aerodynamics.

Potential benefit of 3D flower wake characterization

We quantified features of hawkmoth-pollinated flower wakes using 2D planar particle image velocimetry (PIV), which is the simplest form of velocimetry since it requires a single camera and yields only two components of velocity in a plane. All flowers used here were roughly bilaterally symmetric (about the vertical axis) and *Petunia* and *Datura* were rotationally symmetric, so we assumed that flower wakes would be rotationally symmetric

but this can be verified with either simultaneous, orthogonal planes of stereographic PIV (sPIV) or 3D tomographic PIV (tomoPIV) or particle tracking velocimetry (PTV). The challenges associated with setting up and maintaining 3D flow visualization techniques outweigh the benefits for studying flow close to the surface of airfoils. Although some example cases are able to quantify structures in the wakes of flapping insects and micro-air vehicles (MAVs) [11, 130], flow visualization in air is harder than in liquid. To resolve dynamics of flow structures on centimeter-scale wings in low wind speeds, $\sim 1\mu m$ diameter particles are needed and getting sufficient illumination of those particles over a volume requires a powerful Class IV laser (60mJ per pulse at 1kHz, in our experiments). In our attempt to setup 3D-PTV in the wind tunnel, we consistently achieved poor signal-to-noise ratios and reconstructed approximately 10% of particle tracks using the Shake-the-Box algorithm [123]. The maximum volume size we measured was approximately 5 cm x 8 cm x 2 cm. While this volume is not large enough to capture the full wingstroke of a large pollinator like the hawkmoth *Manduca sexta*, it is sufficiently large to capture half of the 3D near wake of *Petunia* or *Nicotiana*, especially for smaller diameter flowers. Flowering plants represent a vast morphospace with a potentially broad diversity in wake features. To study this diversity systematically, we need adaptable flow visualization methods to quantify wake velocities, turbulence intensities, and flow structures in comparable ways. Ultimately a combined approach may be best: we can employ simple, planar PIV techniques to capture flow characteristics in real-world environments and use those results as context for tomoPIV or PTV experiments quantifying the three-dimensional flow structure for individual flowers and consequences for pollinators, especially when morphological features of the plants or behavioral features of the animals suggest that out of plane components may be especially important.

<u>What is the link between wing morphology, kinematics, and LEV structure across hawkmoth species? Across Lepidoptera?</u>

Ecological diversity and evolutionary context can be integrated into studying plant-pollinator aerodynamics by expanding the analysis in this thesis to hawkmoths beyond *Manduca sexta*. Wing morphology shows significant adaptive change across hawkmoth species [224] and these changes have functional and evolutionary consequences for flight forces [74]. Since forces in flapping wing flight are generated from unsteady vortex mechanisms, adaptive shifts in wing shapes could indicate that LEV structure also varies across species. The direct impact of quasi-static wing shape on LEV structure and circulation can be explored using a similar approach to our study of bursting on hawkmoth wings, but with systematic variation of inflow wind velocities, advance ratios, and wing shape parameters. If bursting and LEV dynamics are as essential to flapping wing flight as we think, then changes in vortex structure could be investigated as an evolutionary-driver of wing morphology and wing sensors. Going further, hawkmoths represent only one family within the insect order Lepidoptera and the link between wing morphology and LEV structure can be broadened to include wild silkmoths, which have very different kinematics compared to hawkmoths.

<u>How is the LEV used by other species, especially considering how circulation is initially built up on the wings?</u>

All flapping wing fliers are proposed to rely on the same suite of unsteady aerodynamic mechanisms including translational forces (and the LEV), rotational forces, added mass forces, and wake capture, but the interaction between these mechanism varies across insect species. Smaller insects like bees and mosquitoes tend rely mostly on rotational forces for body weight support [115, 1] while larger insects and hummingbirds can offset body weight with only translational forces [51]. In our limited studies of flight in unsteady wakes, pollinators alter kinematics but maintain wingbeat frequency [179, 40, 264], suggesting the timescale of the wingstroke is important for flight performance. Wingbeat frequency de-

termines the global timescale of vortex formation and shedding during a wingstroke, but different insect species will rely on each mechanism in different proportions. We can generalize the impact of realistic unsteady wakes on pollinators by studying the relative contributions of each unsteady force mechanism to total lift across species and in different flow environments. Understanding these relative contributions of rotational and translational forces will also inform how LEVs interact with unsteady flow. If LEVs are robust to turbulence and unsteadiness in flower wakes, then insects may rely on the same ratios of aerodynamic mechanisms for circulation build-up and force production across highly variable airflow. Alternatively, any observed shifts in unsteady aerodynamic interactions would reveal that not only are insects capable of adapting to dynamic environments, but that they must be able to actively sense and respond changes in flow. Shifts away from LEV and translational force dominance could indicate that the LEV is more susceptible to disruption in certain environments. Both possibilities create new areas of study around how the environment might be internally represented and how we could harness robustness of biology to improve the flexibility of our engineered systems in changing environments.

REFERENCES

[1] R. J. Bomphrey, T. Nakata, N. Phillips, and S. M. Walker, "Smart wing rotation and trailing-edge vortices enable high frequency mosquito flight," *Nature*, vol. 544, no. 7648, pp. 92–95, 2017.

[2] Z. R. Carr, C. Chen, and M. J. Ringuette, "Finite-span rotating wings: Three-dimensional vortex formation and variations with aspect ratio," *Experiments in Fluids*, vol. 54, no. 2, 2013.

[3] A. Späthe, A. Reinecke, S. B. Olsson, S. Kesavan, M. Knaden, and B. S. Hansson, "Plant species-and status-specific odorant blends guide oviposition choice in the moth Manduca sexta," *Chemical Senses*, vol. 38, no. 2, pp. 147–159, 2013.

[4] T. Biology, "Wing and Proboscis Dimensions in a Sphingid Fauna From Western Mexico Author (s): Stephen H . Bullock and Alfonso Pescador Published by : The Association for Tropical Biology and Conservation," vol. 15, no. 4, pp. 292–294, 2010.

[5] O. Speck, "Field measurements of wind speed and reconfiguration in Arundo donax (Poaceae) with estimates of drag forces," *American Journal of Botany*, vol. 90, no. 8, pp. 1253–1256, 2003.

[6] R. J. Bomphrey, N. J. Lawson, N. J. Harding, G. K. Taylor, and A. L. R. Thomas, "The aerodynamics of Manduca sexta: digital particle image velocimetry analysis of the leading-edge vortex," *Journal of Experimental Biology*, vol. 208, pp. 1079–1094, 2005.

[7] N. B. M. Brantjes, "Wind as a factor influencing flower-visiting by Hadena bicruris (Noctuidae) and Deilephila elpenor (Sphingidae)," *Ecological Entomolgy*, vol. 6, pp. 361–363, 1981.

[8] C. J. Wojcik and J. H. J. Buchholz, "Vorticity transport in the leading-edge vortex on a rotating blade," *Journal of Fluid Mechanics*, vol. 743, no. 2014, pp. 249–261, 2014.

[9] A. L. Stöckl, D. O'Carroll, and E. J. Warrant, "Higher-Order neural processing tunes motion neurons to visual ecology in three species of hawkmoths," *Proceedings of the Royal Society B: Biological Sciences*, vol. 284, no. 1857, 2017.

[10] M. H. Dickinson, C. T. Farley, R. J. Full, M. A. R. Koehl, R. Kram, and S. Lehman, "How Animals Move: An Integrative View," *Science*, vol. 288, pp. 100–106, 2000.

[11]   R. J. Bomphrey, P. Henningsson, D. Michaelis, and D. Hollis, "Tomographic particle image velocimetry of desert locust wakes: instantaneous volumes combine to reveal hidden vortex elements and rapid wake deformation.," *Journal of the Royal Society, Interface / the Royal Society*, vol. 9, no. 77, pp. 3378–86, 2012.

[12]   N. H. Werner, H. Chung, J. Wang, G. Liu, J. Cimbala, H. Dong, and B. Cheng, "Vorticity dynamics of revolving wings : The role of planetary vortex tilting on the stability of the leading-edge vortex," *arXiv preprint*, pp. 1–19, 2018. arXiv: 1806.10497.

[13]   T. L. Hedrick, B. Cheng, and X. Deng, "Wingbeat Time and the Scaling of Passive Rotational Damping in Flapping Flight," *Science*, vol. 324, no. 5924, pp. 252–255, 2009.

[14]   V. M. Ortega-Jimenez, R. Mittal, and T. L. Hedrick, "Hawkmoth flight performance in tornado-like whirlwind vortices," *Bioinspiration & Biomimetics*, vol. 9, 2014.

[15]   C. Martínez-Bazán, "About bubbles and vortex rings," *Journal of Fluid Mechanics*, vol. 780, pp. 1–4, 2015.

[16]   M. Shiono, K. Kitadera, and S. Sudo, "Dynamics of Flower Head Movement in Bio-System," *Advanced Materials Research*, vol. 123-125, pp. 311–314, 2010.

[17]   J. D. H. Sprayberry and T. L. Daniel, "Flower tracking in hawkmoths: behavior and energetics," *Journal of Experimental Biology*, vol. 210, pp. 37–45, 2007.

[18]   K. Mulleners, P. Mancini, and A. R. Jones, "Experimental investigation of a large aspect ratio flat plate encountering a steam-wise gust," *46th AIAA Fluid Dynamics Conference*, no. June, 2016.

[19]   E. Roth, R. W. Hall, T. L. Daniel, and S. Sponberg, "Integration of parallel mechanosensory and visual pathways resolved through sensory conflict," *Proceedings of the National Academy of Sciences*, vol. 113, no. 45, pp. 12 832–12 837, 2016.

[20]   J. Read and A. Stokes, "Plant biomechanics in an ecological context," *American Journal of Botany*, vol. 93, no. 10, pp. 1546–1565, 2006.

[21]   C. J. Majetic, S. D. Wiggam, C. J. Ferguson, and R. A. Raguso, "Timing is Everything: Temporal Variation in Floral Scent, and its Connections to Pollinator Behavior and Female Reproductive Success in Phlox divaricata," *The American Midland Naturalist*, vol. 173, no. 2, pp. 191–207, 2015.

[22]   J. Goyret and R. A. Raguso, "The role of mechanosensory input in flower handling efficiency and learning by ¡i¿Manduca sexta¡/i¿.," *The Journal of experimental biology*, vol. 209, no. Pt 9, pp. 1585–1593, 2006.

[23] P. J. Rudall and R. M. Bateman, "Evolutionary change in flowers and inflorescences: Evidence from naturally occurring terata," *Trends in Plant Science*, vol. 8, no. 2, pp. 76–82, 2003.

[24] C.-J. Ruan and J. A. Teixeira da Silva, "Adaptive Signficance of Floral Movement," *Critical Reviews in Plant Sciences*, vol. 30, no. 4, pp. 293–328, 2011.

[25] S. Kurth, C. Hamann, J. R. Seume, and K. Mulleners, "Experimental investigation of the influence of anisotropic surface structures on the boundary layer flow," *AIAA Aerospace Sciences Meeting, 2018*, no. 210059, pp. 1–13, 2018.

[26] A. P. Willmott and C. P. Ellington, "The mechanics of flight in the hawkmoth Manduca sexta. II. Aerodynamic consequences of kinematic and morpholocial variation," *Journal of Experimental Biology*, vol. 200, pp. 2723–2745, 1997.

[27] T. Rusin and P. Kojs, *Plant biomechanics*. 2011, vol. Part 4, pp. 602–604, ISBN: 9783319790985.

[28] A. Medina and A. R. Jones, "Leading-edge vortex burst on a low-aspect-ratio rotating flat plate," *Physical Review Fluids*, vol. 1, no. 4, p. 044 501, Aug. 2016.

[29] J. Nattero and A. A. Cocucci, "Geographical variation in floral traits of the tree tobacco in relation to its hummingbird pollinator fauna," *Biological Journal of the Linnean Society*, vol. 90, no. 4, pp. 657–667, 2007.

[30] A. Haverkamp, J. Bing, E. Badeke, B. Hansson, and M. Knaden, "Innate olfactory preferences for flowers matching proboscis length ensure optimal energy gain in a hawkmoth," *Nature Communications*, vol. 7, pp. 1–9, 2016.

[31] P. K. Maruyama, G. M. Oliveira, C. Ferreira, B. Dalsgaard, and P. E. Oliveira, "Pollination syndromes ignored: Importance of non-ornithophilous flowers to Neotropical savanna hummingbirds," *Naturwissenschaften*, vol. 100, no. 11, pp. 1061–1068, 2013.

[32] T. Weis-Fogh, "Quick Estimates of Flight Fitness in Hovering Animals, Including Novel Mechanisms for Lift Production," *Journal of Experimental Biology*, vol. 59, pp. 169–230, 1973.

[33] J. C. Liao, D. N. Beal, G. V. Lauder, and M. S. Triantafyllou, "The Kármán gait: Novel body kinematics of rainbow trout swimming in a vortex street," *Journal of Experimental Biology*, vol. 206, no. 6, pp. 1059–1073, 2003.

[34] T. L. Hedrick, J. Martinez-Blat, and M. J. Goodman, "Flight motor modulation with speed in the hawkmoth Manduca sexta," *Journal of Insect Physiology*, vol. 96, pp. 115–121, 2017.

[35] L. Tadrist, K. Julio, M. Saudreau, and E. de Langre, "Leaf flutter by torsional galloping: Experiments and model," *Journal of Fluids and Structures*, vol. 56, pp. 1–10, 2015.

[36] S. Pournazeri, P. S. Segre, M. Princevac, and D. L. Altshuler, "Hummingbirds generate bilateral vortex loops during hovering: Evidence from flow visualization," *Experiments in Fluids*, vol. 54, no. 1, 2013.

[37] T. H. Fleming, M. D. Tuttle, and M. A. Horner, "Pollination Biology and the Relative Importance of Nocturnal and Diurnal Pollinators in Three Species of Sonoran Desert Columnar Cacti," *The Southwestern Naturalist*, vol. 41, no. 3, pp. 257–269, 1996.

[38] R. Alarcón, "Congruence between visitation and pollen-transport networks in a California plant-pollinator community," *Oikos*, vol. 119, no. 1, pp. 35–44, 2010.

[39] G. V. Lauder, "Swimming hydrodynamics: Ten questions and the technical approaches needed to resolve them," *Experiments in Fluids*, vol. 51, no. 1, pp. 23–35, 2011.

[40] S. Ravi, J. D. Crall, L. McNeilly, S. F. Gagliardi, A. A. Biewener, and S. A. Combes, "Hummingbird flight stability and control in freestream turbulent winds," *Journal of Experimental Biology*, vol. 218, pp. 1444–1452, 2015.

[41] A. P. Willmott, C. P. Ellington, and A. L. R. Thomas, "Flow visualization and unsteady aerodynamics in the flight of the hawkmoth, Manduca sexta," *Philosophical Transactions of the Royal Society B: Biological Sciences*, vol. 352, pp. 303–316, 1997.

[42] A. Haverkamp, X. Li, B. S. Hansson, I. T. Baldwin, M. Knaden, and F. Yon, "Flower movement balances pollinator needs and pollen protection," *Ecology*, vol. 100, no. 1, pp. 1–11, 2019.

[43] E. Moyroud and B. J. Glover, "The Evolution of Diverse Floral Morphologies," *Current Biology*, vol. 27, no. 17, R941–R951, 2017.

[44] H. C. Astley, J. R. Mendelson, J. Dai, C. Gong, B. Chong, J. M. Rieser, P. E. Schiebel, S. S. Sharpe, R. L. Hatton, H. Choset, and D. I. Goldman, "Surprising simplicities and syntheses in limbless self-propulsion in sand," *Journal of Experimental Biology*, vol. 223, no. 5, pp. 1–12, 2020.

[45] F.-O. Lehmann, S. P. Sane, and M. H. Dickinson, "The aerodynamic effects of wing-wing interaction in flapping insect wings," *The Journal of experimental biology*, vol. 208, no. Pt 16, pp. 3075–92, 2005.

[46] B. Gardiner, P. Berry, and B. Moulia, "Review: Wind impacts on plant growth, mechanics and damage," *Plant Science*, vol. 245, pp. 94–118, 2016.

[47] J. Goyret, "Look and touch: multimodal sensory control of flower inspection movements in the nocturnal hawkmoth Manduca sexta.," *The Journal of experimental biology*, vol. 213, no. Pt 21, pp. 3676–3682, 2010.

[48] D. Lentink and M. H. Dickinson, "Biofluiddynamic scaling of flapping, spinning and translating fins and wings," *Journal of Experimental Biology*, vol. 212, no. 16, pp. 2691–2704, 2009. arXiv: arXiv:1011.1669v3.

[49] A. Placzek, J. F. Sigrist, and A. Hamdouni, "Numerical simulation of an oscillating cylinder in a cross-flow at low Reynolds number: Forced and free oscillations," *Computers and Fluids*, vol. 38, pp. 80–100, 2009.

[50] K. Suzuki, T. Aoki, and M. Yoshino, "Effect of chordwise wing flexibility on flapping flight of a butterfly model using immersed-boundary lattice Boltzmann simulations," *Physical Review E*, vol. 100, no. 1, pp. 1–16, 2019.

[51] C. P. Ellington, "The Aerodynamics of Hovering Insect Flight . IV . Aerodynamic Mechanisms," vol. 305, no. 1122, pp. 79–113, 1984.

[52] N. J. Cowan and E. S. Fortune, "The critical role of locomotion dynamics in decoding sensory systems," *J. Neurosci.*, vol. 27, no. 5, pp. 1123–1128, 2007.

[53] A. S. Dunlap, D. R. Papaj, and A. Dornhaus, "Sampling and tracking a changing environment: persistence and reward in the foraging decisions of bumblebees," *Interface Focus*, vol. 7, 2017.

[54] K. Bowman, "Hefty vs. wimpy: a biomechanical hypothesis for plant pollinator associations," Ph.D. dissertation, 2016.

[55] A. Ushimaru, I. Dohzono, Y. Takami, and F. Hyodo, "Flower orientation enhances pollen transfer in bilaterally symmetrical flowers," *Oecologia*, vol. 160, no. 4, pp. 667–674, 2009.

[56] S. Nadot and E. Dodinet, "Letters to the twenty-first century botanist: "what is a flower?"," *Botany Letters*, vol. 163, no. 1, pp. 9–10, 2016.

[57] a. L. Eberle, P. G. Reinhall, and T. L. Daniel, "Fluid-structure interaction in compliant insect wings.," *Bioinspiration & biomimetics*, vol. 9, no. 2, p. 025 005, 2014.

[58] A. W. Lang, P. Motta, P. Hidalgo, and M. Westcott, "Bristled shark skin: A microgeometry for boundary layer control?" *Bioinspiration and Biomimetics*, vol. 3, no. 4, 2008.

[59] P. Henningsson and R. J. Bomphrey, "Span efficiency in hawkmoths," *Journal of the Royal Society Interface*, vol. 10, p. 20 130 099, 2013.

[60] J. S. Miller and D. L. Venable, "Floral morphometrics and the evolution of sexual dimorphism in Lycium (Solanaceae)," *Evolution*, vol. 57, no. 1, pp. 74–86, 2003.

[61] M. R. A. Nabawy and W. J. Crowther, "The role of the leading edge vortex in lift augmentation of steadily revolving wings : a change in perspective," 2017.

[62] A. Haverkamp, F. Yon, I. W. Keesey, C. Mißbach, C. Koenig, B. S. Hansson, I. T. Baldwin, M. Knaden, and D. Kessler, "Hawkmoths evaluate scenting flowers with the tip of their proboscis," *eLife*, vol. 5, no. MAY2016, pp. 1–12, 2016.

[63] D. Kolomenskiy, S. Ravi, T. Takabayashi, T. Ikeda, K. Ueyama, T. Engels, A. Fisher, H. Tanaka, K. Schneider, J. Sesterhenn, and H. Liu, "Added costs of insect-scale flapping flight in unsteady airflows," *arXiv preprint*, pp. 1–15, 2016. arXiv: 1610.09101.

[64] G. H. Toebes, "The unsteady flow and wake near an oscillating cylinder," *Journal of Basic Engineering*, vol. 91, pp. 493–502, 1969.

[65] Y. Zheng, Y. Wu, and H. Tang, "A time-resolved PIV study on the force dynamics of flexible tandem wings in hovering flight," *Journal of Fluids and Structures*, vol. 62, pp. 65–85, 2016.

[66] K. Hermann and C. Kuhlemeier, "The genetic architecture of natural variation in flower morphology," *Current Opinion in Plant Biology*, vol. 14, no. 1, pp. 60–65, 2011.

[67] D. W. Murphy, D. Adhikari, D. R. Webster, and J. Yen, "Underwater flight by the planktonic sea butterfly," *Journal of Experimental Biology*, vol. 219, no. 4, pp. 535–543, 2016.

[68] W. L. Mechaber and J. G. Hildebrand, "Novel, Non-Solanaceous Hostplant Record for ¡I¿Manduca sexta¡/I¿ (Lepidoptera: Sphingidae) in the Southwestern United States," *Annals of the Entomological Society of America*, vol. 93, no. 3, pp. 447–451, 2006.

[69] J. Wilroy, R. A. Wahidi, and A. Lang, "Effect of butterfly-scale-inspired surface patterning on the leading edge vortex growth," *Fluid Dynamics Research*, vol. 50, no. 4, 2018.

[70] A. Mira and E. A. Bernays, "Trade-offs in host use by Manduca sexta: Plant characters vs natural enemies," *Oikos*, vol. 97, no. 3, pp. 387–397, 2002.

[71] M. Wakakuwa, D. G. Stavenga, and K. Arikawa, "Spectral Organization of Omma-tidia in Flower-visiting Insects†," *Photochemistry and Photobiology*, vol. 83, no. 1, pp. 27–34, 2007.

[72] K. J. Niklas and D. J. Paolillo, "The role of the epidermis as a stiffening agent in Tulipa (Liliaceae) stems," *American Journal of Botany*, vol. 84, no. 6, pp. 735–744, 1997.

[73] K. B. Lua, Y. J. Lee, T. T. Lim, and K. S. Yeo, "Wing-Wake Interaction of Three-Dimensional Flapping Wings," *AIAA Journal*, vol. 55, no. 3, pp. 729–739, 2017.

[74] B. R. Aiello, U. Bin, H. Minoguchi, B. Bhinderwala, and A. Chris, "The evolution of two distinct strategies of moth flight," pp. 1–13, 2021.

[75] Y. Savriama, *A Step-by-step guide for geometric morphometrics of floral symmetry*, 2018.

[76] M. Santosh, R. Carbonell, I. Artemieva, and J. Badal, "Advances in seismic imag-ing of crust and mantle: Preface," *Tectonophysics*, vol. 627, no. 1, pp. 1–3, 2014.

[77] V. M. Ortega-Jimenez, N. Sapir, M. Wolf, E. A. Variano, and R. Dudley, "Into turbulent air: size-dependent effects of von Karman vortex streets on hummingbird flight kinematics and energetics," *In Proceedings of the Royal Society B: Biological Sciences*, vol. 281, no. 1783, p. 20 140 180, 2014.

[78] R. R. Harbig, J. Sheridan, and M. C. Thompson, "The role of advance ratio and as-pect ratio in determining leading-edge vortex stability for flapping flight," *Journal of Fluid Mechanics*, vol. 751, pp. 71–105, 2014.

[79] J. D. Crall, S. Ravi, A. M. Mountcastle, and S. A. Combes, "Bumblebee flight performance in cluttered environments: effects of obstacle orientation, body size and acceleration," *Journal of Experimental Biology*, vol. 218, pp. 2728–2737, 2015.

[80] E. Roth, S. Sponberg, and N. J. Cowan, "A comparative approach to closed-loop computation," *Current Opinion in Neurobiology*, vol. 25, pp. 54–62, 2014.

[81] O. M. Griffin, "The Unsteady Wake of an Oscillating Cylinder at Low Reynolds Number," *Journal of Applied Mechanics*, vol. 38, p. 729, 1971.

[82] M. Bross, C. A. Ozen, and D. Rockwell, "Flow structure on a rotating wing: Effect of steady incident flow," *Physics of Fluids*, vol. 25, no. 8, 2013.

[83] B. Cheng, S. P. Sane, G. Barbera, D. R. Troolin, T. Strand, and X. Deng, "Three-dimensional flow visualization and vorticity dynamics in revolving wings," *Experi-ments in Fluids*, vol. 54, no. 1, 2013.

[84] J. D. Thomson, "Pollen Transport and Deposition by Bumble Bees in Erythronium : Influences of Floral Nectar and Bee Grooming Author (s): James D . Thomson Published by : British Ecological Society Stable URL : https://www.jstor.org/stable/2260258 REFERENCES Linked refe," *British Ecological Society*, vol. 74, no. 2, pp. 329–341, 1986.

[85] D. E. Rival, J. Kriegseis, P. Schaub, A. Widmann, and C. Tropea, "Characteristic length scales for vortex detachment on plunging profiles with varying leading-edge geometry," *Experiments in Fluids*, vol. 55, no. 1, pp. 1–8, 2014.

[86] M. H. Dickinson, F. O. Lehmann, and S. P. Sane, "Wing rotation and the aerodynamic basis of insect flight," *Science*, vol. 284, pp. 1954–1960, 1999.

[87] J. D. H. Sprayberry and M. Suver, "Hawkmoths' innate flower preferences: A potential selective force on floral biomechanics," *Arthropod-Plant Interactions*, vol. 5, pp. 263–268, 2011.

[88] T. Doyle, W. L. Hawkes, R. Massy, G. D. Powney, M. H. Menz, and K. R. Wotton, "Pollination by hoverflies in the Anthropocene," *Proceedings. Biological sciences*, vol. 287, no. 1927, p. 20 200 508, 2020.

[89] M. Visbal, T. O. Yilmaz, and D. Rockwell, "Three-dimensional vortex formation on a heaving low-aspect-ratio wing: Computations and experiments," *Journal of Fluids and Structures*, vol. 38, pp. 58–76, 2013.

[90] A. Brandenburg, C. Kuhlemeier, and R. Bshary, "Hawkmoth pollinators decrease seed set of a low-nectar petunia axillaris line through reduced probing time," *Current Biology*, vol. 22, no. 17, pp. 1635–1639, 2012.

[91] S. Watkins, J. Milbank, B. J. Loxton, and W. H. Melbourne, "Atmospheric winds and their implications for microair vehicles," *AIAA Journal*, vol. 44, no. 11, pp. 2591–2600, 2006.

[92] A. T. Conlisk, "Modern helicopter aerodynamics," *Annual Review of Fluid Mechanics*, vol. 29, pp. 515–567, 1997.

[93] J. P. Dyhr, K. A. Morgansen, T. L. Daniel, and N. J. Cowan, "Flexible strategies for flight control: an active role for the abdomen," *Journal of Experimental Biology*, vol. 216, pp. 1523–1536, 2013.

[94] L. A. Miller, A. Santhanakrishnan, S. Jones, C. Hamlet, K. Mertens, and L. Zhu, "Reconfiguration and the reduction of vortex-induced vibrations in broad leaves," *Journal of Experimental Biology*, vol. 215, no. 15, pp. 2716–2727, 2012.

[95] S. P. Graham, "Visitors to Southeastern Hawkmoth Flowers," *Southeastern Naturalist*, vol. 9, no. 3, pp. 413–426, 2010.

[96] K. M. Laurent, B. Fogg, T. Ginsburg, C. Halverson, M. J. Lanzone, T. A. Miller, D. W. Winkler, and G. P. Bewley, "Turbulence explains the accelerations of an eagle in natural flight," *Proceedings of the National Academy of Sciences of the United States of America*, vol. 118, no. 23, 2021. arXiv: 2102.12374.

[97] J. L. Fox, A. L. Fairhall, and T. L. Daniel, "Encoding properties of haltere neurons enable motion feature detection in a biological gyroscope," *Proceedings of the National Academy of Sciences*, vol. 107, no. 8, pp. 3840–3845, 2010.

[98] J. Urzay, S. G. Llewellyn Smith, E. Thompson, and B. J. Glover, "Wind gusts and plant aeroelasticity effects on the aerodynamics of pollen shedding: A hypothetical turbulence-initiated wind-pollination mechanism," *Journal of Theoretical Biology*, vol. 259, no. 4, pp. 785–792, 2009.

[99] R. Alarcón, G. Davidowitz, and J. L. Bronstein, "Nectar usage in a southern Arizona hawkmoth community," *Ecological Entomology*, vol. 33, no. 4, pp. 503–509, 2008.

[100] J. F. Louf, L. Nelson, H. Kang, P. N. Song, T. Zehnbauer, and S. Jung, "How wind drives the correlation between leaf shape and mechanical properties," *Scientific Reports*, vol. 8, no. 1, pp. 1–7, 2018.

[101] R. J. Bomphrey, "Insects in flight: direct visualization and flow measurements," *Bioinspiration & Biomimetics*, vol. 1, S1–S9, 2006.

[102] J. J. Chang, J. D. Crall, and S. A. Combes, "Wind alters landing dynamics in bumblebees," *Journal of Experimental Biology*, no. July, 2016.

[103] T. Nakata and H. Liu, "Aerodynamic performance of a hovering hawkmoth with flexible wings: a computational approach," *Proceedings of the Royal Society B: Biological Sciences*, vol. 279, no. 1729, pp. 722–731, 2012.

[104] S. A. Combes and T. L. Daniel, "Into thin air: Contributions of aerodynamic and inertial-elastic forces to wing bending in the hawkmoth Manduca sexta.," *The Journal of experimental biology*, vol. 206, no. Pt 17, pp. 2999–3006, 2003.

[105] K. Y. Ma, P. Chirarattananon, S. B. Fuller, and R. J. Wood, "Controlled Flight of a Biologically Inspired, Insect-Scale Robot," *Science*, vol. 340, pp. 603–607, 2013.

[106] M. S. Melius, K. Mulleners, and R. B. Cal, "Coherent Structure Interaction During Unsteady Separation," *AIAA Journal*, vol. 57, no. 8, pp. 3239–3249, 2019.

[107] T. L. Hedrick and T. L. Daniel, "Flight control in the hawkmoth Manduca sexta: the inverse problem of hovering," *The Journal of Experimental Biology*, vol. 209, pp. 3114–3130, 2006.

[108] N. Hempel De Ibarra, K. V. Langridge, and M. Vorobyev, "More than colour attraction: behavioural functions of flower patterns," *Current Opinion in Insect Science*, vol. 12, no. Figure 1, pp. 64–70, 2015.

[109] G. T. Broadhead, T. Basu, M. von Arx, and R. A. Raguso, "Diel rhythms and sex differences in the locomotor activity of hawkmoths," *Journal of Experimental Biology*, vol. 220, pp. 1472–1480, 2017.

[110] E. Limacher, C. Morton, and D. Wood, "On the trajectory of leading-edge vortices under the influence of Coriolis acceleration," *Journal of Fluid Mechanics*, vol. 800, no. 2016, 2016.

[111] W. Thielicke and R. Sonntag, "Particle Image Velocimetry for MATLAB: Accuracy and enhanced algorithms in PIVlab," *Journal of Open Research Software*, vol. 9, pp. 1–14, 2021.

[112] T. J. Popic, G. M. Wardle, and Y. C. Davila, "Flower-visitor networks only partially predict the function of pollen transport by bees," *Austral Ecology*, vol. 38, no. 1, pp. 76–86, 2013.

[113] A. Fisher, S. Ravi, S. Watkins, J. Watmuff, C. Wang, H. Liu, and P. Petersen, "The gust-mitigating potential of flapping wings," *Bioinspiration & Biomimetics*, vol. 11, no. 4, p. 046 010, 2016.

[114] S. A. Combes and R. Dudley, "Turbulence-driven instabilities limit insect flight performance.," *Proceedings of the National Academy of Sciences of the United States of America*, vol. 106, no. 22, pp. 9105–8, 2009.

[115] R. J. Bomphrey, G. K. Taylor, and A. L. R. Thomas, "Smoke visualization of free-flying bumblebees indicates independent leading-edge vortices on each wing pair," *Experiments in Fluids*, vol. 46, pp. 811–821, 2009.

[116] J. M. Birch and M. H. Dickinson, "Spanwise flow and the attachment of the leading-edge vortex on insect wings," *Nature*, vol. 412, pp. 729–733, 2001.

[117] P. G. Kevan and H. G. Baker, "Insects as Flower Visitors and Pollinators," *Annual Review of Entomology*, vol. 28, no. 1, pp. 407–453, 1983.

[118] J. S. Han, J. W. Chang, and H. K. Cho, "Vortices behavior depending on the aspect ratio of an insect-like flapping wing in hover," *Experiments in Fluids*, vol. 56, no. 9, pp. 1–16, 2015.

[119] Y. Chen, N. Gravish, A. L. Desbiens, R. Malka, and R. J. Wood, "Experimental and computational studies of the aerodynamic performance of a flapping and passively rotating insect wing," *Journal of Fluid Mechanics*, vol. 791, no. 2016, pp. 1–33, 2016.

[120] J. Warren and P. James, "Do flowers wave to attract pollinators? A case study with Silene maritima," *Journal of Evolutionary Biology*, vol. 21, pp. 1024–1029, 2008.

[121] R. A. Raguso, A. R. LeClere, and B. O. Schlumpberger, "Sensory flexibility in hawkmoth foraging behavior: Lessons from Manduca sexta and other species," *Chemical Senses*, vol. 30 SUPPL. No. suppl 1, pp. 295–296, 2005.

[122] E. Virot, A. Ponomarenko, Dehandschoewercker, D. Quéré, and C. Clanet, "Critical wind speed at which trees break," *Physical Review E*, vol. 93, no. 2, pp. 1–7, 2016.

[123] D. Schanz, S. Gesemann, and A. Schröder, "Shake - The - Box : Lagrangian particle tracking at high particle image densities," *Experiments in Fluids*, vol. 57, no. 5, pp. 1–27, 2016.

[124] C. van den Berg and C. P. Ellington, "The three-dimensional leading-edge vortex of a 'hovering' model hawkmoth," *Philosophical Transactions of the Royal Society B: Biological Sciences*, vol. 352, pp. 329–340, 1997.

[125] D. L. Harder, O. Speck, C. L. Hurd, and T. Speck, "Reconfiguration as a prerequisite for survival in highly unstable flow-dominated habitats," *Journal of Plant Growth Regulation*, vol. 23, no. 2, pp. 98–107, 2004.

[126] J. D. Crall, J. J. Chang, R. L. Oppenheimer, and S. A. Combes, "Foraging in an unsteady world: bumblebee flight performance in field- realistic turbulence," *Interface Focus*, vol. 7, 2017.

[127] W. Thielicke, *The Flapping Flight of Birds Analysis and Application*. 2014, ISBN: 9789036772419.

[128] I. Beyaert and M. Hilker, "Plant odour plumes as mediators of plant-insect interactions," *Biological Reviews*, vol. 89, no. 1, pp. 68–81, 2014.

[129] A. Miri, D. Dragovich, and Z. Dong, "The response of live plants to airflow – Implication for reducing erosion," *Aeolian Research*, vol. 33, no. December 2017, pp. 93–105, 2018.

[130] B. Martínez Gallar, B. W. van Oudheusden, A. Sciacchitano, and M. Karásek, "Large-scale volumetric flow visualization of the unsteady wake of a flapping-wing micro air vehicle," *Experiments in Fluids*, vol. 61, no. 1, pp. 1–21, 2020.

[131] C. Koenig, A. Bretschneider, D. G. Heckel, E. Grosse-Wilde, B. S. Hansson, and H. Vogel, "The plastic response of Manduca sexta to host and non-host plants," *Insect Biochemistry and Molecular Biology*, vol. 63, pp. 72–85, 2015.

[132] F. P. Schiestl and S. D. Johnson, "Pollinator-mediated evolution of floral signals," *Trends in Ecology and Evolution*, vol. 28, no. 5, pp. 307–315, 2013.

[133] J. R. Usherwood, J. A. Cheney, J. Song, S. P. Windsor, J. P. J. Stevenson, U. Dierksheide, A. Nila, and R. J. Bomphrey, "High aerodynamic lift from the tail reduces drag in gliding raptors," *The Journal of Experimental Biology*, vol. 223, no. 3, jeb214809, 2020.

[134] R. W. Cruden, "Hawkmoth Pollination of Mirabilis (Nyctaginaceae)," *Bulletin of the Torrey Botanical Club*, vol. 97, no. 2, p. 89, 1970.

[135] P. Chirarattananon, Y. Chen, E. F. Helbling, K. Y. Ma, R. Cheng, and R. J. Wood, "Dynamics and flight control of a flapping- wing robotic insect in the presence of wind gusts," 2017.

[136] M. Aoki, T. Mizuno, H. Aono, and H. Ishikawa, "Vortex Structure Extraction from Circular Disk Wake by POD and PIV Processing," in *Springer Proceedings in Physics*, vol. 185, 2016, pp. 139–145, ISBN: 9783319306001.

[137] S. Sponberg, J. P. Dyhr, R. W. Hall, and T. L. Daniel, "Luminance-dependent visual processing enables moth flight in low light," *Science*, vol. 348, pp. 1245–1248, 2015.

[138] Y. Liu, J. Roll, S. V. Kooten, and X. Deng, "Schlieren photography on freely flying hawkmoth," *Biology Letters*, vol. 14, 2018.

[139] T. Deora, M. A. Ahmed, T. L. Daniel, and B. W. Brunton, "Tactile active sensing in an insect plant pollinator," *Journal of Experimental Biology*, vol. 224, no. 4, 2021.

[140] A. R. Jones, A. Medina, H. Spooner, and K. Mulleners, "Characterizing a burst leading-edge vortex on a rotating flat plate wing," *Experiments in Fluids*, vol. 57, no. 4, p. 52, Apr. 2016.

[141] V. M. Ortega-Jimenez, M. Badger, H. Wang, and R. Dudley, "Into rude air: hummingbird flight performance in variable aerial environments," *Philosophical transactions of the Royal Society of London B: Biological Sciences*, vol. 371, no. 1704, p. 20 150 387, 2016.

[142] M. P. Fenske, L. A. P. Nguyen, E. K. Horn, J. A. Riffell, and T. Imaizumi, "Circadian clocks of both plants and pollinators influence flower seeking behavior of the

pollinator hawkmoth Manduca sexta," *Scientific Reports*, vol. 8, no. 1, pp. 1–13, 2018.

[143] D. Adhikari and E. K. Longmire, "Visual hull method for tomographic PIV measurement of flow around moving objects," *Experiments in Fluids*, vol. 53, no. 4, pp. 943–964, 2012.

[144] A. Stöckl, J. Smolka, D. O'Carroll, and E. Warrant, "Resolving the trade-off between visual sensitivity and spatial acuity – lessons from hawkmoths," *Integrative And Comparative Biology*, vol. 57, no. 5, pp. 1093–1103, 2017.

[145] T. Jardin, "Coriolis effect and the attachment of the leading edge vortex," *Journal of Fluid Mechanics*, vol. 820, pp. 312–340, 2017.

[146] M. Badger, V. M. Ortega-Jimenez, L. Von Rabenau, A. Smiley, R. Dudley, and A. Gruverman, "Electrostatic charge on flying hummingbirds and its potential role in pollination," *PLoS ONE*, vol. 10, no. 9, pp. 1–11, 2015.

[147] W. F. Towne, A. E. Ritrovato, A. Esposto, and D. F. Brown, "Honeybees use the skyline in orientation," *Journal of Experimental Biology*, pp. 2476–2485, 2017.

[148] M. García, S. Benítez-Vieyra, A. N. Sérsic, A. Pauw, A. A. Cocucci, A. Traveset, F. Sazatornil, and V. Paiaro, "Is variation in flower shape and length among native and non-native populations of Nicotiana glauca a product of pollinator-mediated selection?" *Evolutionary Ecology*, vol. 34, no. 6, pp. 893–913, 2020.

[149] J. E. Armstrong, "Fringe science: Are the corollas of Nymphoides (Menyanthaceae) flowers adapted for surface tension interactions?" *American Journal of Botany*, vol. 89, no. 2, pp. 362–365, 2002.

[150] T. Jardin, A. Farcy, and L. David, "Three-dimensional effects in hovering flapping flight," *Journal of Fluid Mechanics*, vol. 702, pp. 102–125, 2012.

[151] S. P. Sane, A. Dieudonne, M. A. Willis, and T. L. Daniel, "Antennal Mechanosensors Mediate Flight Control in Moths," *Science*, vol. 315, pp. 863–866, 2007.

[152] R. M. Waldman and K. S. Breuer, "Camber and aerodynamic performance of compliant membrane wings," *Journal of Fluids and Structures*, vol. 68, no. June 2016, pp. 390–402, 2017.

[153] D. Lentink and M. H. Dickinson, "Rotational accelerations stabilize leading edge vortices on revolving fly wings," *Journal of Experimental Biology*, vol. 212, pp. 2705–2719, 2009.

[154] A. M. Mountcastle, S. Ravi, and S. A. Combes, "Nectar vs. pollen loading affects the tradeoff between flight stability and maneuverability in bumblebees," *Proceedings of the National Academy of Sciences*, vol. 112, no. 33, pp. 10 527–10 532, 2015.

[155] L. Comba, "Patch use by bumblebees (hymenoptera apidae): Temperature, wind, flower density and traplining," *Ethology Ecology and Evolution*, vol. 11, no. 3, pp. 243–264, 1999.

[156] C. A. Ozen and D. Rockwell, "Flow structure on a rotating plate," *Experiments in Fluids*, vol. 52, no. 1, pp. 207–223, 2012.

[157] R. L. Kaczorowski, A. R. Seliger, A. C. Gaskett, S. K. Wigsten, and R. A. Raguso, "Corolla shape vs. size in flower choice by a nocturnal hawkmoth pollinator," *Functional Ecology*, vol. 26, no. 3, pp. 577–587, 2012.

[158] C. Cummins, M. Seale, A. Macente, D. Certini, E. Mastropaolo, I. M. Viola, and N. Nakayama, "A separated vortex ring underlies the flight of the dandelion," *Nature*, vol. 562, no. 7727, pp. 414–418, 2018.

[159] L. Ristroph, G. Ristroph, S. Morozova, A. J. Bergou, S. Chang, J. Guckenheimer, Z. J. Wang, and I. Cohen, "Active and passive stabilization of body pitch in insect flight," *Journal of the Royal Society Interface*, vol. 10, 2013.

[160] G. K. Taylor, R. L. Nudds, and A. L. R. Thomas, "Flying and swimming animals cruise at a Strouhal number tuned for high power efficiency," *Nature*, pp. 707–711, 2003.

[161] B. Wieneke, "Iterative reconstruction of volumetric particle distribution," *Measurement Science and Technology*, vol. 24, no. 2, 2013.

[162] P. Liu and B. Cheng, "Limitations of rotational manoeuvrability in insects and hummingbirds: evaluating the effects of neuro-biomechanical delays and muscle mechanical power," *Journal of the Royal Society Interface*, vol. 14, 2017.

[163] U. Klahre, A. Gurba, K. Hermann, M. Saxenhofer, E. Bossolini, P. M. Guerin, and C. Kuhlemeier, "Pollinator choice in petunia depends on two major genetic loci for floral scent production," *Current Biology*, vol. 21, no. 9, pp. 730–739, 2011.

[164] H. H. Zakon, "Electric fields of flowers stimulate the sensory hairs of bumble bees," *Proceedings of the National Academy of Sciences*, vol. 113, no. 26, pp. 7020–7021, 2016.

[165] R. Hillier and N. J. Cherry, "The effects of stream turbulence on separation bubbles," *Journal of Wind Engineering and Industrial Aerodynamics*, vol. 8, no. 1-2, pp. 49–58, 1981.

[166] M. R. A. Nabawy and W. J. Crowther, "The role of the leading edge vortex in lift augmentation of steadily revolving wings : a change in perspective," 2017.

[167] L. C. Johansson, S. Engel, A. Kelber, M. K. Heerenbrink, and A. Hedenström, "Multiple leading edge vortices of unexpected strength in freely flying hawkmoth," *Scientific Reports*, vol. 3, no. 3264, pp. 1–5, 2013.

[168] A. Gehke and K. Mulleners, "Phenomenology and scaling of optimal flapping wing kinematics," pp. 1–29, 2020. arXiv: 2007.15729.

[169] R. J. Bomphrey, N. J. Lawson, G. K. Taylor, and A. L. R. Thomas, "Application of digital particle image velocimetry to insect aerodynamics: Measurement of the leading-edge vortex and near wake of a hawkmoth," *Experiments in Fluids*, vol. 40, pp. 546–554, 2006.

[170] M. J. Lighthill, "On the Weis-Fogh mechanism of lift generation," *Journal of Fluid Mechanics*, vol. 60, pp. 1–17, 1973.

[171] T. Nakata and H. Liu, "A fluid-structure interaction model of insect flight with flexible wings," *Journal of Computational Physics*, vol. 231, no. 4, pp. 1822–1847, 2012.

[172] C. P. Ellington, C. van den Berg, A. P. Willmott, and A. L. R. Thomas, "Leading-edge vortices in insect flight," *Nature*, vol. 384, no. 6610, pp. 626–630, 1996.

[173] J. S. Han, J. W. Chang, J. K. Kim, and J. H. Han, "Role of Trailing-Edge Vortices on the Hawkmothlike Flapping Wing," *Journal of Aircraft*, vol. 52, no. 4, pp. 1256–1266, 2015.

[174] L. Tadrist, M. Saudreau, P. Hémon, X. Amandolese, A. Marquier, T. Leclercq, and E. de Langre, "Foliage motion under wind, from leaf flutter to branch buffeting," *Journal of the Royal Society Interface*, vol. 15, no. 142, 2018.

[175] D. J. Martins and S. D. Johnson, "Interactions between hawkmoths and flowering plants in east africa: Polyphagy and evolutionary specialization in an ecological context," *Biological Journal of the Linnean Society*, vol. 110, no. 1, pp. 199–213, 2013.

[176] M. F. M. Osborne, "Aerodynamics of Flapping Flight with Application to Insects," *The Journal of Experimental Biology*, vol. 28, no. 2, pp. 221–245, 1951.

[177] B. Martínez Gallar, B. W. van Oudheusden, A. Sciacchitano, and M. Karásek, "Large-scale volumetric flow visualization of the unsteady wake of a flapping-wing micro air vehicle," *Experiments in Fluids*, vol. 61, no. 1, pp. 1–21, 2020.

[178] E. Roth, K. Zhuang, S. A. Stamper, E. S. Fortune, and N. J. Cowan, "Stimulus predictability mediates a switch in locomotor smooth pursuit performance for Eigenmannia virescens," *Journal of Experimental Biology*, vol. 214, pp. 1170–1180, 2011.

[179] V. M. Ortega-Jimenez, J. S. M. Greeter, R. Mittal, and T. L. Hedrick, "Hawkmoth flight stability in turbulent vortex streets," *Journal of Experimental Biology*, vol. 216, pp. 4567–4579, 2013.

[180] A. P. Willmott and A. Búrquez, "The pollination of Merremia palmeri (Convolvulaceae): Can hawk moths be trusted?" *American Journal of Botany*, vol. 83, no. 8, pp. 1050–1056, 1996.

[181] S. A. Combes and T. L. Daniel, "Flexural stiffness in insect wings. II. Spatial distribution and dynamic wing bending," *Journal of Experimental Biology*, vol. 206, no. 17, pp. 2989–2997, 2003.

[182] H. E. Robinson, C. M. Finelli, and M. A. Koehl, "Interactions between benthic predators and zooplanktonic prey are affected by turbulent waves," *Integrative and Comparative Biology*, vol. 53, no. 5, pp. 810–820, 2013.

[183] R. J. Gegear, R. Burns, and K. A. Swoboda-Bhattarai, "Hummingbird floral traits interact synergistically to discourage visitation by bumble bee foragers," *Ecology*, vol. 98, no. 2, pp. 489–499, 2017.

[184] F. P. Schiestl and P. M. Schluter, "Floral isolation, specialized pollination, and pollinator behavior in orchids," *Annual Review of Entomology*, vol. 54, pp. 425–446, 2009.

[185] S. Alben, M. Shelley, and J. Zhang, "How flexibility induces streamlining in a two-dimensional flow," *Physics of Fluids*, vol. 16, no. 5, pp. 1694–1713, 2004.

[186] G. H. Koopmann, "The vortex wakes of vibrating cylinders at low Reynolds numbers," *Journal of Fluid Mechanics*, vol. 28, pp. 501–512, 1967.

[187] S. A. Combes and T. L. Daniel, "Flexural stiffness in insect wings I. Scaling and the influence of wing venation," *Journal of Experimental Biology*, vol. 206, no. 17, pp. 2979–2987, 2003.

[188] K. J. Niklas, *Plant biomechanics: An engineering approach to plant form and function*. 1992, ISBN: 9780470015902.

[189] D. Adhikari and E. K. Longmire, "Infrared tomographic PIV and 3D motion tracking system applied to aquatic predator-prey interaction," *Measurement Science and Technology*, vol. 24, no. 2, 2013.

[190] F. T. Muijres, N. A. Iwasaki, M. J. Elzinga, J. M. Melis, and M. H. Dickinson, "Flies compensate for unilateral wing damage through modular adjustments of wing and body kinematics," *Interface Focus*, vol. 7, 2017.

[191] J. C. Liao, "A review of fish swimming mechanics and behaviour in altered flows," *Philosophical Transactions of the Royal Society B: Biological Sciences*, vol. 362, pp. 1973–1993, 2007.

[192] B. Pratt, T. Deora, T. Mohren, and T. L. Daniel, "Neural evidence supports a dual sensory-motor role for insect wings," *Proceedings of the Royal Society B: Biological Sciences*, vol. 284, 2017.

[193] A. P. Willmott and C. P. Ellington, "The mechanics of flight in the hawkmoth Manduca sexta. I. Kinematics of hovering and forward flight," *Journal of Experimental Biology*, vol. 200, pp. 2723–2745, 1997.

[194] C. Galliot, M. E. Hoballah, C. Kuhlemeier, and J. Stuurman, "Genetics of flower size and nectar volume in Petunia pollination syndromes," *Planta*, vol. 225, no. 1, pp. 203–212, 2006.

[195] M. Devoto, S. Bailey, and J. Memmott, "The 'night shift': Nocturnal pollen-transport networks in a boreal pine forest," *Ecological Entomology*, vol. 36, no. 1, pp. 25–35, 2011.

[196] J. R. Usherwood and C. P. Ellington, "The aerodynamics of revolving wings I. Model hawkmoth wings.," *The Journal of experimental biology*, vol. 205, no. Pt 11, pp. 1547–1564, 2002.

[197] C. P. Shao, Y. J. Chen, and J. Z. Lin, "Wind induced deformation and vibration of a Platanus acerifolia leaf," *Acta Mechanica Sinica/Lixue Xuebao*, vol. 28, no. 3, pp. 583–594, 2012.

[198] C. Coutand, "Biomechanical study of the effect of a controlled bending on tomato stem elongation: local strain sensing and spatial integration of the signal," *Journal of Experimental Botany*, vol. 51, no. 352, pp. 1825–1842, 2000.

[199] A. M. Mountcastle and T. L. Daniel, "Aerodynamic and functional consequences of wing compliance," *Experiments in Fluids*, pp. 311–320, 2009.

[200] D. D. Chin and D. Lentink, "Flapping wing aerodynamics: from insects to vertebrates," *Journal of Experimental Biology*, vol. 219, pp. 920–932, 2016.

[201] C. Lahondère, C. Vinauger, R. P. Okubo, G. H. Wolff, J. K. Chan, O. S. Akbari, and J. A. Riffell, "The olfactory basis of orchid pollination by mosquitoes," *Proceedings of the National Academy of Sciences of the United States of America*, vol. 117, no. 1, pp. 708–716, 2020.

[202] J. C. Liao, D. N. Beal, G. V. Lauder, and M. S. Triantafyllou, "Fish Exploiting Vortices Decrease Muscle Activity," *Science*, vol. 302, pp. 1566–1569, 2003.

[203] B. Cheng, X. Deng, and T. L. Hedrick, "The mechanics and control of pitching manoeuvres in a freely flying hawkmoth (Manduca sexta)," *Journal of Experimental Biology*, vol. 214, pp. 4092–4106, 2011.

[204] J. Tank, L. Smith, and G. R. Spedding, "On the possibility (or lack thereof) of agreement between experiment and computation of flows over wings at moderate Reynolds number," 2017.

[205] A. Etnier and S. Vogel, "Reorientation of Daffodil (Narcissus : Amaryllidaceae) Flowers in Wind : Drag Reduction and Torsional Flexibility Author (s): Shelley A . Etnier and Steven Vogel Source : American Journal of Botany , Vol . 87 , No . 1 (Jan ., 2000), pp . 29-32 Publi," vol. 87, no. 1, pp. 29–32, 2000.

[206] S. Vogel, "Living in a physical world," vol. 29, no. June, pp. 391–397, 2004.

[207] E. O. Campos, H. D. Bradshaw, and T. L. Daniel, "Shape matters: Corolla curvature improves nectar discovery in the hawkmoth Manduca sexta," *Functional Ecology*, vol. 29, no. 4, pp. 462–468, 2015.

[208] L. T. Wasserthal, "Evolution of Long-Tongued Hawkmoths and Pollination of Long-Spurred Angraecum Orchids," in *Proceedings of the 20th World Orchid Conference*, 2011.

[209] B. Harter, C. Leistikow, W. Wilms, B. Truylio, and W. Engels, "Bees collecting pollen from flowers with poricidal anthers in a south Brazilian Araucaria forest: A community study," *Journal of Apicultural Research*, vol. 41, no. 1-2, pp. 9–16, 2002.

[210] D. J. Groom, M. C. B. Toledo, D. R. Powers, B. W. Tobalske, and K. C. Welch, "Integrating morphology and kinematics in the scaling of hummingbird hovering metabolic rate and efficiency," *Proceedings of the Royal Society B: Biological Sciences*, vol. 285, no. 1873, 2018.

[211] P. Wester and K. Lunau, "Plant–Pollinator Communication," in *Advances in Botanical Research*, vol. 82, Elsevier Ltd, 2017, pp. 225–257, ISBN: 9780128014318.

[212]   G. V. Lauder, "Fish Locomotion: Recent Advances and New Directions," *Dx.Doi.Org*, vol. 7, no. 1, pp. 521–545, 2015.

[213]   Y. Zhao, X. Deng, and S. P. Sane, "Modulation of leading edge vorticity and aerodynamic forces in flexible flapping wings," *Bioinspiration & Biomimetics*, vol. 6, no. 3, p. 036 007, 2011.

[214]   J. S. M. Greeter and T. L. Hedrick, "Direct lateral maneuvers in hawkmoths," *Biology Open*, vol. 0, pp. 1–11, 2016.

[215]   L. Zheng, T. L. Hedrick, and R. Mittal, "Time-Varying Wing-Twist Improves Aerodynamic Efficiency of Forward Flight in Butterflies," *PLoS ONE*, vol. 8, no. 1, pp. 1–10, 2013.

[216]   M. A. Selosse, "Letters to the twenty-first century botanist: "what is a flower?" (3) the flower as an evolutionary arms race: Was Linnaeuss choice misleading?" *Botany Letters*, vol. 163, no. 3, pp. 231–235, 2016.

[217]   W. M. Farina, D. Kramer, and D. Varjú, "The response of the hovering hawk moth Macroglossum stellatarum to translatory pattern motion," *Journal of Comparative Physiology A*, vol. 176, pp. 551–562, 1995.

[218]   E. De Langre, "Plant vibrations at all scales: A review," *Journal of Experimental Botany*, vol. 70, no. 14, pp. 3521–3531, 2019.

[219]   K. Toyoda and R. Hiramoto, "Manipulation of vortex rings for flow control," *Fluid Dynamics Research*, vol. 41, no. 5, 2009.

[220]   H. F. Wang, H. L. Cao, and Y. Zhou, "POD analysis of a finite-length cylinder near wake," *Experiments in Fluids*, vol. 55, no. 8, 2014.

[221]   T. L. Hedrick, "Damping in flapping flight and its implications for manoeuvring, scaling and evolution," *Journal of Experimental Biology*, vol. 214, pp. 4073–4081, 2011.

[222]   M. S. Madhav, S. A. Stamper, E. S. Fortune, and N. J. Cowan, "Closed-loop stabilization of the Jamming Avoidance Response reveals its locally unstable and globally nonlinear dynamics.," *The Journal of experimental biology*, vol. 216, no. Pt 22, pp. 4272–84, 2013.

[223]   D. W. Snow and D. L. Teixeira, "Hummingbirds and their flowers in the coastal mountains of southeastern Brazil," *Journal of Ornithology*, vol. 123, no. 4, pp. 446–450, 1982.

[224] B. R. Aiello, M. Tan, U. B. Sikandar, and A. J. Alvey, "Adaptive shifts underlie the divergence in wing morphology in bombycoid moths Corresponding Author : Author contributions :," 2021.

[225] L. T. Wasserthal, "The Pollinators of the Malagasy Star Orchids Angruecum sesguipedule, A. sororium and A. compuctum and the Evolution of Extremely long Spurs by Pollinator Shift," *Botanica Acta*, vol. 110, no. 5, pp. 343–359, 1997.

[226] D. Adhikari, D. R. Webster, and J. Yen, "Portable tomographic PIV measurements of swimming shelled Antarctic pteropods," *Experiments in Fluids*, vol. 57, no. 12, pp. 1–17, 2016.

[227] M. a. Rodríguez-Gironés and L. Santamaría, "Resource competition, character displacement, and the evolution of deep corolla tubes.," *The American naturalist*, vol. 170, no. 3, pp. 455–464, 2007.

[228] A. P. Willmott and C. P. Ellington, "Measuring the angle of attack of beating insect wings: robust three-dimensional reconstruction from two-dimensional images," *Journal of Experimental Biology*, vol. 200, pp. 2693–704, 1997.

[229] M. Fathi-Moghadam, *Physical properties of tall vegetation for resistance to flow*, 2007.

[230] T. Engels, D. Kolomenskiy, K. Schneider, F. .-O. Lehmann, and J. Sesterhenn, "Bumblebee Flight in Heavy Turbulence," *Physical Review Letters*, vol. 028103, pp. 1–5, 2016.

[231] D. Francescangeli, G. De Guyon, and K. Mulleners, "Lagrangian analysis of the formation of a vortex pair on a rotating flat plate," *19th Symposium on the Applications of Laser and Imaging Techniques to Fluid Mechanics, Lisbon, Portugal*, pp. 1–6, 2018.

[232] A. S. Barfod, "Letter to the twenty-first century botanist - What is a flower? 4. Heterochrony - Still an overlooked source of rapid morphological change in flowers?" *Botany Letters*, vol. 164, no. 2, pp. 105–109, 2017.

[233] S. Ravi, D. Kolomenskiy, T. Engels, K. Schneider, C. Wang, J. Sesterhenn, and H. Liu, "Bumblebees minimize control challenges by combining active and passive modes in unsteady winds," *Scientific Reports*, vol. 6, no. April, p. 35 043, 2016. arXiv: 1603.00221.

[234] T. L. Daniel, A. Dieudonne, J. Fox, C. Myhrvold, S. Sane, and B. Wark, "Inertial guidance systems in insects: from the neurobiology to the structural mechanics of biological gyroscopes," *Navigation*, vol. 55, no. 4, pp. 235–240, 2008.

[235] J. M. Birch, "The influence of wing-wake interactions on the production of aerodynamic forces in flapping flight," *Journal of Experimental Biology*, vol. 206, no. 13, pp. 2257–2272, 2003.

[236] M. Veits, I. Khait, U. Obolski, E. Zinger, A. Boonman, A. Goldshtein, K. Saban, R. Seltzer, U. Ben-Dor, P. Estlein, A. Kabat, D. Peretz, I. Ratzersdorfer, S. Krylov, D. Chamovitz, Y. Sapir, Y. Yovel, and L. Hadany, "Flowers respond to pollinator sound within minutes by increasing nectar sugar concentration," *Ecology Letters*, vol. 22, no. 9, pp. 1483–1492, 2019.

[237] E. C. Polhamus, "Predictions of vortex-lift characteristics by a leading-edge suction analogy," *Journal of Aircraft*, vol. 8, no. 4, pp. 193–199, 1971.

[238] T. L. Daniel and S. A. Combes, "Flexible wings and fins: bending by inertial or fluid-dynamic forces?" *Integrative and comparative biology*, vol. 42, no. 5, pp. 1044–1049, 2002.

[239] B. H. Dickerson, Z. N. Aldworth, and T. L. Daniel, "Control of moth flight posture is mediated by wing mechanosensory feedback," *Journal of Experimental Biology*, vol. 217, pp. 2301–2308, 2014.

[240] S. K. Ghosh, C. L. Dora, and D. Das, "Unsteady Wake Characteristics of a Flapping Wing through 3D TR-PIV," *Journal of Aerospace Engineering*, vol. 25, no. 4, pp. 547–558, 2012.

[241] W. M. Farina, D. Varjú, and Y. Zhou, "The regulation of distance to dummy flowers during hovering flight in the hawk moth Macroglossum stellatarum," *Journal of Comparative Physiology A*, vol. 174, pp. 239–247, 1994.

[242] R. R. Harbig, J. Sheridan, and M. C. Thompson, "Relationship between aerodynamic forces , flow structures and wing camber for rotating insect wing planforms," *J. Fluid Mech*, pp. 52–75, 2013.

[243] L. A. Nilsson, "Deep flowers for long tongues," *Trends in Ecology and Evolution*, vol. 13, no. 7, pp. 259–260, 1998.

[244] A. M. Mountcastle and T. L. Daniel, "Vortexlet models of flapping flexible wings show tuning for force production and control," *Bioinspiration and Biomimetics*, vol. 5, no. 4, 2010.

[245] N. Beals and A. R. Jones, "Lift Production by a Passively Flexible Rotating Wing," vol. 53, no. 10, 2015.

[246] R. Dudley, "Mechanisms and Implications of Animal Flight Maneuverability," *Integrative and Comparative Biology*, vol. 42, pp. 135–140, 2002.

[247] C.-k. Kang and W. Shyy, "Analytical model for instantaneous lift and shape deformation of an insect-scale flapping wing in hover," *Journal of Royal Society Interface*, vol. 11, p. 20 140 933, 2014.

[248] A. Ippolito, G. W. Fernandes, and T. P. Holtsford, "Pollinator preferences for Nicotiana alata, N. forgetiana, and their F 1 hybrids," *Evolution*, vol. 58, no. 12, pp. 2634–2644, 2004.

[249] W. Merzkirch, "Techniques of Flow Visualization," Advisory Group for Aerospace Research & Development, Tech. Rep., 1987, pp. 1689–1699. arXiv: arXiv:1011.1669v3.

[250] E. Dodinet, "Letter to the 21st century botanist: "what is a flower?" the social science perspective," *Botany Letters*, vol. 163, no. 2, pp. 155–158, 2016.

[251] R. A. Raguso, "Flowers as sensory billboards: Progress towards an integrated understanding of floral advertisement," *Current Opinion in Plant Biology*, vol. 7, no. 4, pp. 434–440, 2004.

[252] J. Nattero, A. N. Sérsic, and A. A. Cocucci, "Patterns of contemporary phenotypic selection and flower integration in the hummingbird-pollinated Nicotiana glauca between populations with different flower-pollinator combinations," *Oikos*, vol. 119, no. 5, pp. 852–863, 2010.

[253] J. C. Theobald, E. J. Warrant, and D. C. O'Carroll, "Wide-field motion tuning in nocturnal hawkmoths.," *Proceedings of the Royal Society B: Biological Sciences*, vol. 277, pp. 853–860, 2009.

[254] Y. L. Zhang and M. Sun, "Dynamic flight stability of hovering model insects: Theory versus simulation using equations of motion coupled with Navier-Stokes equations," *Acta Mechanica Sinica*, vol. 26, pp. 175–190, 2010.

[255] L. Graftieaux, M. Michard, and G. Nathalie, "Combining PIV, POD and vortex identification algorithms for the study of unsteady turbulent swirling flows," *Measurement Science and Technology*, vol. 12, no. 9, pp. 1422–1429, 2001.

[256] R. Dudley, *The Biomechanics of Insect Flight: Form, Function, Evolution*. Princeton, 2002, p. 223, ISBN: 0691094918.

[257] J. A. Riffell, R. Alarcón, and L. Abrell, "Floral trait associations in hawkmoth-specialized and mixed pollination systems," *Communicative & Integrative Biology*, vol. 1, no. 1, pp. 6–8, 2008.

[258] J. S. Han, A. T. Nguyen, and J. H. Han, "Aerodynamic characteristics of flapping wings under steady lateral inflow," *Journal of Fluid Mechanics*, vol. 870, pp. 735–759, 2019.

[259] C. Cummins, M. Seale, A. Macente, D. Certini, E. Mastropaolo, I. M. Viola, and N. Nakayama, "A separated vortex ring underlies the flight of the dandelion," *Nature*, vol. 562, no. 7727, pp. 414–418, 2018.

[260] L. Tadrist, M. Saudreau, and E. de Langre, "Wind and gravity mechanical effects on leaf inclination angles," *Journal of Theoretical Biology*, vol. 341, pp. 9–16, 2014.

[261] T. L. Hedrick, "Software techniques for two- and three-dimensional kinematic measurements of biological and biomimetic systems," *Bioinspiration & Biomimetics*, vol. 3, 2008.

[262] A. Gehrke and K. Mulleners, "Phenomenology and scaling of optimal flapping wing kinematics," *Bioinspiration and Biomimetics*, vol. 16, no. 2, 2021. arXiv: 2007.15729.

[263] J. A. Riffell, E. Shlizerman, E. Sanders, L. Abrell, B. Medina, A. J. Hinterwirth, and J. N. Kutz, "Flower discrimination by pollinators in a dynamic chemical environment," *Science*, vol. 344, no. 6191, pp. 1515–1518, 2014.

[264] S. Ravi, J. D. Crall, A. Fisher, and S. A. Combes, "Rolling with the flow: bumblebees flying in unsteady wakes," *Journal of Experimental Biology*, vol. 216, pp. 4299–4309, 2013.

[265] K. S. Mead, M. B. Wiley, M. A. Koehl, and J. R. Koseff, "Fine-scale patterns of odor encounter by the antennules of mantis shrimp tracking turbulent plumes in wave-affected and unidirectional flow," *Journal of Experimental Biology*, vol. 206, no. 1, pp. 181–193, 2003.

[266] J. A. Riffell, R. Alarcón, L. Abrell, G. Davidowitz, J. L. Bronstein, and J. G. Hildebrand, "Behavioral consequences of innate preferences and olfactory learning in hawkmoth-flower interactions.," *Proceedings of the National Academy of Sciences of the United States of America*, vol. 105, no. 9, pp. 3404–9, 2008.

[267] E. W. McCarthy, M. W. Chase, S. Knapp, A. Litt, A. R. Leitch, and S. C. Le Comber, *Transgressive phenotypes and generalist pollination in the floral evolution of Nicotiana polyploids*, 2016.

[268] M. E. Hoballah, J. Stuurman, T. C. Turlings, P. M. Guerin, S. Connétable, and C. Kuhlemeier, "The composition and timing of flower odour emission by wild Petunia axillaris coincide with the antennal perception and nocturnal activity of the pollinator Manduca sexta," *Planta*, vol. 222, no. 1, pp. 141–150, 2005.

[269] A. Ushimaru and F. Hyodo, "Why do bilaterally symmetrical flowers orient vertically? Flower orientation influences pollinator landing behaviour," *Evolutionary Ecology Research*, vol. 7, no. 1, pp. 151–160, 2005.

[270] C. H. K. Williamson, "Vortex Dynamics in the Cylinder Wake," *Annual Review of Fluid Mechanics*, vol. 28, pp. 477–539, 1996.

[271] J. Weiss, "A tutorial on the proper orthogonal decomposition," *AIAA Aviation 2019 Forum*, no. June, pp. 1–21, 2019.

[272] K. Alcorn, H. Whitney, and B. Glover, "Flower movement increases pollinator preference for flowers with better grip," *Functional Ecology*, vol. 26, no. 4, pp. 941–947, 2012.

[273] S. Sefati, I. D. Neveln, E. Roth, T. R. T. Mitchell, J. B. Snyder, M. A. MacIver, E. S. Fortune, and N. J. Cowan, "Mutually opposing forces during locomotion can eliminate the tradeoff between maneuverability and stability," *Proceedings of the National Academy of Sciences*, vol. 110, no. 47, pp. 18 798–18 803, 2013.

[274] J. Goyret, M. Pfaff, R. A. Raguso, and A. Kelber, "Why do Manduca sexta feed from white flowers? Innate and learnt colour preferences in a hawkmoth," *Naturwissenschaften*, vol. 95, no. 6, pp. 569–576, 2008.

[275] J. Choi, W. P. Jeon, and H. Choi, "Mechanism of drag reduction by dimples on a sphere," *Physics of Fluids*, vol. 18, no. 4, pp. 16–19, 2006.

[276] K. Taira, S. L. Brunton, S. T. Dawson, C. W. Rowley, T. Colonius, B. J. McKeon, O. T. Schmidt, S. Gordeyev, V. Theofilis, and L. S. Ukeiley, "Modal analysis of fluid flows: An overview," *AIAA Journal*, vol. 55, no. 12, pp. 4013–4041, 2017. arXiv: 1702.01453.

[277] S. P. Sane, "The aerodynamics of insect flight," *Journal of Experimental Biology*, vol. 206, pp. 4191–4208, 2003.

[278] E. de Langre, A. Gutierrez, and J. Cossé, "On the scaling of drag reduction by reconfiguration in plants," *Comptes Rendus - Mecanique*, vol. 340, no. 1-2, pp. 35–40, 2012.

[279] C. Damerval and S. Nadot, "Letter to the 21st century botanist: "what is a flower?" 6. the evo-devo of floral symmetry," *Botany Letters*, vol. 164, no. 3, pp. 193–196, 2017.

[280] S. D. Johnson, M. Moré, F. W. Amorim, W. A. Haber, G. W. Frankie, D. A. Stanley, A. A. Cocucci, and R. A. Raguso, "The long and the short of it: a global analysis

of hawkmoth pollination niches and interaction networks," *Functional Ecology*, vol. 31, no. 1, pp. 101–115, 2017.

[281] K. J. Niklas, "Responses of hollow, septate stems to vibrations: Bidmechanical evidence that nodes can act mechanically as spring-like joints," *Annals of Botany*, vol. 80, no. 4, pp. 437–448, 1997.

[282] G. Reddy, A. Celani, T. J. Sejnowski, and M. Vergassola, "Learning to soar in turbulent environments," *Proceedings of the National Academy of Sciences*, vol. 113, no. 33, E4877–E4884, 2016.

[283] E. C. Polhamus, "SHARP-EDGE DELTA WINGS BASED O N A LEADING-EDGE-SUCTION ANALOGY," NASA, Langley Research Center, Tech. Rep., 1966.

[284] R. Goulard, J. L. Vercher, and S. Viollet, "To crash or not to crash: How do hoverflies cope with free-fall situations and weightlessness?" *Journal of Experimental Biology*, vol. 219, no. 16, pp. 2497–2503, 2016.

[285] A. Haverkamp, B. S. Hansson, I. T. Baldwin, M. Knaden, and F. Yon, "Floral trait variations among wild tobacco populations influence the foraging behavior of hawkmoth pollinators," *Frontiers in Ecology and Evolution*, vol. 6, no. FEB, pp. 1–10, 2018.

[286] D. Timerman and S. C. H. Barrett, "Divergent selection on the biomechanical properties of stamens under wind and insect pollination," *Proceedings of the Royal Society B: Biological Sciences*, vol. 285, no. 1893, p. 20 182 251, 2018.

[287] E. de Langre, "Effects of Wind on Plants," *Annual Review of Fluid Mechanics*, vol. 40, no. 1, pp. 141–168, 2008.

[288] K. B. Lua, T. T. Lim, and K. S. Yeo, "Effect of wing-wake interaction on aerodynamic force generation on a 2D flapping wing," *Experiments in Fluids*, vol. 51, pp. 177–195, 2011.

[289] J. H. Kang, E. J. Lee, and S. J. Lee, "Wind tunnel experiment for wind breakage of Actinidia deliciosa P. shoots," *Journal of Mechanical Science and Technology*, vol. 27, no. 10, pp. 3113–3121, 2013.

[290] R. A. Fisher, "Tests of significance in harmonic analysis," *Proc. R. Soc. London Ser. A Contain. Pap. Math. Phys. Character*, vol. 125, 1929.

[291] R. B. Srygley and A. L. R. Thomas, "Unconventional lift-generating mechanisms in free-flying butterflies," *Nature*, vol. 420, pp. 660–664, 2002.

[292] A. L. Stöckl, K. Kihlstrom, S. Chandler, and S. Sponberg, "Comparative system identification of flower tracking performance in three hawkmoth species reveals adaptations for dim light vision," *Philosophical Transactions of the Royal Society B: Biological Sciences*, vol. 372, 2017.

[293] M. Matthews and S. Sponberg, "Hawkmoth flight in the unsteady wakes of flowers," *Journal of Experimental Biology*, vol. 221, no. 22, 2018.

[294] T. R. Neil, Z. Shen, D. Robert, B. W. Drinkwater, and M. W. Holderied, "Thoracic scales of moths as a stealth coating against bat biosonar.," *Journal of the Royal Society, Interface*, vol. 17, no. 163, p. 20 190 692, 2020.

[295] Y. Lou and I. T. Baldwin, "Manduca sexta recognition and resistance among allopolyploid Nicotiana host plants," *Proceedings of the National Academy of Sciences of the United States of America*, vol. 100, no. 24, pp. 14 581–14 586, 2003.

[296] J. G. Wong and D. E. Rival, "Determining the relative stability of leading-edge vortices on nominally two-dimensional flapping profiles," *Journal of Fluid Mechanics*, vol. 766, pp. 611–625, 2015.

[297] S. Sponberg and T. L. Daniel, "Abdicating power for control: a precision timing strategy to modulate function of flight power muscles," *Proceedings of the Royal Society B: Biological Sciences*, vol. 279, pp. 3958–3966, 2012.

[298] A. Maia, A. P. Sheltzer, and E. D. Tytell, "Streamwise vortices destabilize swimming bluegill sunfish (Lepomis macrochirus)," *Journal of Experimental Biology*, vol. 218, pp. 786–792, 2015.

[299] B. J. Knörlein, D. B. Baier, S. M. Gatesy, J. D. Laurence-Chasen, and E. L. Brainerd, "Validation of XMALab software for marker-based XROMM," *The Journal of Experimental Biology*, vol. 219, no. 23, pp. 3701–3711, 2016.

[300] J. C. Caissard and S. Baudino, "Letters to the twenty-first century botanist: "what is a flower?" (4) the flower as a scent factory," *Botany Letters*, vol. 163, no. 4, pp. 355–358, 2016.

[301] F.-O. Lehmann, "When wings touch wakes: understanding locomotor force control by wake wing interference in insect wings," *Journal of Experimental Biology*, vol. 211, no. 2, pp. 224–233, 2008.

[302] Y. Vaknin, S. Gan-Mor, A. Bechar, B. Ronen, and D. Eisikowitch, "The role of electrostatic forces in pollination," *Plant Systematics and Evolution*, vol. 222, no. 1-4, pp. 133–142, 2000.

[303] Y. Pan, E. Follett, M. Chamecki, and H. Nepf, "Strong and weak, unsteady recon-figuration and its impact on turbulence structure within plant canopies," *Physics of Fluids*, vol. 26, no. 10, 2014.

[304] W. L. Mechaber and J. G. Hildebrand, "Novel , Non-Solanaceous Hostplant Record for Manduca sexta (Lepidoptera : Sphingidae) in the Southwestern United States Novel , Non-Solanaceous Hostplant Record for Manduca sexta (Lepidoptera : Sphingidae) in the Southwestern United States," *Ecology and Population Biology*, vol. 93, no. 3, pp. 447–451, 2000.

[305] C. H. K. Williamson and A. Roshko, "Vortex formation in the wake of an oscillating cylinder," *Journal of Fluids and Structures*, vol. 2, pp. 355–381, 1988.

[306] R. A. Raguso and M. A. Willis, "Hawkmoth pollination in Arizona's Sonoran desert: behavioral responses to floral traits," in *Evolution and ecology taking flight: butterflies as model systems*, 2003, pp. 43–65.

[307] D. Lentink, W. B. Dickson, J. L. van Leeuwen, and M. H. Dickinson, "Leading-Edge Vortices Elevate Lift of Autorotating Plant Seeds," *Science*, vol. 324, no. 5933, pp. 1438–1440, 2009.

[308] S. A. Córdoba and A. A. Cocucci, "Does hardness make flower love less promiscu-ous? Effect of biomechanical floral traits on visitation rates and pollination assem-blages," *Arthropod-Plant Interactions*, vol. 11, pp. 299–305, 2017.

[309] A. R. Shenoy and C. Kleinstreuer, "Flow over a thin circular disk at low to moderate Reynolds numbers," *Journal of Fluid Mechanics*, vol. 605, pp. 253–262, 2008.

[310] A. R. Kothari and N. P. Burnett, "Herbivores alter plant–wind interactions by acting as a point mass on leaves and by removing leaf tissue," *Ecology and Evolution*, vol. 7, no. 17, pp. 6884–6893, 2017.

[311] R. R. Harbig, J. Sheridan, and M. C. Thompson, "Reynolds number and aspect ratio effects on the leading-edge vortex for rotating insect wing planforms," *Journal of Fluid Mechanics*, vol. 730, pp. 52–75, 2013.

[312] R. A. Cordero, "Ecophysiology of Cecropia schreberiana saplings in two wind regimes in an elfin cloud forest: Growth, gas exchange, architecture and stem biome-chanics," *Tree Physiology*, vol. 19, pp. 153–163, 1999.

[313] T. Jardin and L. David, "Coriolis effects enhance lift on revolving wings," *Physical Review E - Statistical, Nonlinear, and Soft Matter Physics*, vol. 91, no. 3, pp. 2–5, 2015.

[314] N. Phillips, K. Knowles, and R. J. Bomphrey, "The effect of aspect ratio on the leading-edge vortex over an insect-like flapping wing.," *Bioinspiration & Biomimetics*, vol. 10, no. 5, p. 056 020, 2015.

[315] W. Thielicke and E. J. Stamhuis, "PIVlab – Towards User-friendly, Affordable and Accurate Digital Particle Image Velocimetry in MATLAB," *Journal of Open Research Software*, vol. 2, 2014.

[316] F. F. De Araujo, R. Oliveira, T. Mota, J. R. Stehmann, and C. Schlindwein, "Solitary bee pollinators adjust pollen foraging to the unpredictable flower opening of a species of Petunia (Solanaceae)," *Biological Journal of the Linnean Society*, vol. 129, no. 2, pp. 273–287, 2020.

[317] C. Tur, B. Vigalondo, K. Trøjelsgaard, J. M. Olesen, and A. Traveset, "Downscaling pollen-transport networks to the level of individuals," *Journal of Animal Ecology*, vol. 83, no. 1, pp. 306–317, 2014.

[318] D. Lentink, G. F. Van Heijst, F. T. Muijres, and J. L. Van Leeuwen, "Vortex interactions with flapping wings and fins can be unpredictable," *Biology Letters*, vol. 6, no. 3, pp. 394–397, 2010.

[319] J. R. Usherwood, J. A. Cheney, J. Song, S. P. Windsor, J. P. J. Stevenson, U. Dierksheide, A. Nila, and R. J. Bomphrey, "High aerodynamic lift from the tail reduces drag in gliding raptors," *The Journal of Experimental Biology*, vol. 223, no. 3, jeb214809, 2020.

[320] D. L. Whitaker, L. A. Webster, and J. Edwards, "The biomechanics of Cornus canadensis stamens are ideal for catapulting pollen vertically," *Functional Ecology*, vol. 21, pp. 219–225, 2007.

[321] K. Warfvinge, M. KleinHeerenbrink, and A. Hedenström, "The power-speed relationship is U-shaped in two free-flying hawkmoths (Manduca sexta)," *Journal of the Royal Society Interface*, vol. 14, no. 134, 2017.

[322] C. J. Barnes, M. R. Visbal, and P. G. Huang, "On the effects of vertical offset and core structure in streamwise-oriented vortex–wing interactions," *Journal of Fluid Mechanics*, vol. 799, pp. 128–158, 2016.

[323] N. Slegers, M. Heilman, J. Cranford, A. Lang, J. Yoder, and M. L. Habegger, "Beneficial aerodynamic effect of wing scales on the climbing flight of butterflies," *Bioinspiration and Biomimetics*, vol. 12, no. 1, 2017.

[324] J. Yang, M. Liu, G. Wu, W. Zhong, and X. Zhang, "Numerical study on coherent structure behind a circular disk," *Journal of Fluids and Structures*, vol. 51, pp. 172–188, 2014.

[325] S. P. Windsor, R. J. Bomphrey, and G. K. Taylor, "Vision-based flight control in the hawkmoth Hyles lineata," *Journal of the Royal Society Interface*, vol. 11, 2014.

[326] A. Lang, P. Motta, M. L. Habegger, R. Hueter, and F. Afroz, "Shark skin separation control mechanisms," *Marine Technology Society Journal*, vol. 45, no. 4, pp. 208–215, 2011.

[327] M. A. R. Koehl, *Koehl_1986.pdf*, 1986.

[328] N. J. Cowan, M. M. Ankarali, J. P. Dyhr, M. S. Madhav, E. Roth, S. Sefati, S. Sponberg, S. A. Stamper, E. S. Fortune, and T. L. Daniel, "Feedback control as a framework for understanding tradeoffs in biology," *Integrative and Comparative Biology*, vol. 54, no. 2, pp. 223–237, 2014. arXiv: 1402.5702.